HEAT PUMP AGGREGATION, OPTIMIZATION AND CONTROL

A Cornell University doctoral thesis by Kevin James Kircher

August 2019

HEAT PUMP AGGREGATION, OPTIMIZATION AND CONTROL

Kevin James Kircher, Ph.D.

Cornell University 2019

One tenth of anthropogenic greenhouse gas emissions are caused by heating and cooling buildings. Efficient electric heat pumps could significantly reduce these emissions, but face barriers to adoption related to costs, equipment selection and installation, and other factors. The goal of this thesis is to reduce emissions by lowering barriers to heat pump adoption.

To this end, we investigate *heat purchase agreements (HPAs),* a new model of heat pump ownership, and develop supporting methods. In an HPA, users host heat pumps owned by an aggregator. The aggregator buys the heat pumps' electricity and sells their heat or cooling output to the users. We show that HPAs can lower barriers to adoption and benefit both the aggregator and the users. We also develop a method for fairly pricing heat and cooling.

An HPA aggregator is responsible for selecting an appropriate heat pump for each user under uncertainty. We develop a data-driven selection method that provides probabilistic feasibility and optimality guarantees, and illustrate the method through simulations.

An HPA aggregator operates a fleet of heat pumps. If the aggregator invests in sensing, communication and control capabilities, then they can provide services to the electricity grid by perturbing the heat pumps' power use. We develop methods for co-optimizing day-ahead capacity offers for the two highest-priced services, regulation and spinning reserve. In simulations, each heat pump offers 285–325 W of combined annual-average capacity and earns \$25–75 of annual revenue. Providing these services could help grid operators integrate more renewable power, and thereby reduce emissions from electricity generation.

Acknowledgments

The form and intent of this thesis are somewhat idiosyncratic relative to today's academic culture in mechanical engineering. In this culture, a doctoral thesis often consists of a number of loosely-related publications. My thesis is not a collection of my published work, but an attempt to explore one new, narrow issue in depth and detail. While I published papers during my doctoral studies, that work is not reported here.

I am grateful to my advisor, Professor K. Max Zhang, for allowing me to follow this path. Max also accommodated my idiosyncrasies at other points during my doctoral studies. He both gave me the freedom to follow my curiosity, and grounded my ideas in practical applications. This balance was not always easy to strike. I thank Max for his patience, kindness and guidance.

I am also grateful to Dr. Marcia Sawyer of the mechanical engineering department. I had health problems during my doctoral studies that I feel lucky to have survived. Marcia was unfailingly supportive in these hard times. I am also grateful to Max and the department leadership, who gave me leave when I needed it and helped me reintegrate when I returned.

The work described in this dissertation was in part supported by the National Science Foundation under grant 1711546. In addition, portions of my doctoral studies were supported by the New York State Energy Research and Development Authority, the Hydro Fellowship Program of the Hydropower Foundation, and the Consortium for Electric Reliability Technology Solutions. I am grateful to these agencies for their support.

Many people helped shape this thesis. I thank my committee members, Professors Bob Thomas and Eilyan Bitar, for their formative input. Professor Andy Ruina asked many insightful questions along the way. I am grateful to Ian Shapiro, P.E., who provided the much-needed perspective of an industry expert. My groupmates, particularly Zach Lee, offered valuable feedback and suggestions. I thank Professors Les Norford and Shane Henderson for thought-provoking conversations.

Throughout my education, I have benefitted from advantages that are essentially accidents of birth. I am lucky to have parents who had the means to invest in my education. It has never been hard for me to find role models in science and engineering who look and sound like me. I have had many teachers and mentors who encouraged my interests in these fields. These privileges have made me feel welcome in science and engineering in a way that many people do not. I hope to be an ally to these people as we work to make science and engineering as welcoming to everyone as they have been to me.

This thesis is dedicated with love and gratitude to my partner, Katrina Moraine.

Biographical sketch

Kevin J. Kircher grew up in Milwaukee, Wisconsin. He graduated with high honors from the University of Wisconsin-Milwaukee, where he majored in applied mathematics and physics. He then earned a Master of Engineering degree from Cornell University in engineering physics, worked as a building technologies researcher at the Lawrence Berkeley National Laboratory, and returned to Cornell for his doctoral studies in mechanical engineering. After graduation, Kevin will begin postdoctoral research in electrical engineering at the Massachusetts Institute of Technology.

Contents

Chapter 1

Introduction

1.1 Motivations

One tenth of anthropogenic greenhouse gas emissions are caused by heating and cooling buildings. [1–3] These emissions could increase sharply in the coming decades, as global demand for heating and cooling is projected to double by 2050. [2, 4] To avoid the worst consequences of global climate change, deep reductions in greenhouse gas emissions from all economic sectors, including heating and cooling, will likely be necessary. [5, 6] In this thesis, we explore one approach to reducing the emissions from heating and cooling: replacing fossil-fueled or inefficient heating and cooling equipment by efficient electric heat pumps.

As illustrated in Figure 1.2, electric heat pumps use electricity to move heat. In winter, they provide heating by moving heat from outdoors to indoors. In summer, they provide cooling by moving heat in the opposite direction. Two broad categories of heat pumps are *air-source* heat pumps, which exchange heat with the outdoor air, and *ground-source* or *geothermal* heat pumps, which exchange heat with the ground. Ground-source heat pumps are typically more efficient, while air-source heat pumps are typically less expensive to install. In this thesis, we focus primarily on air-source heat pumps, particularly those with variable-

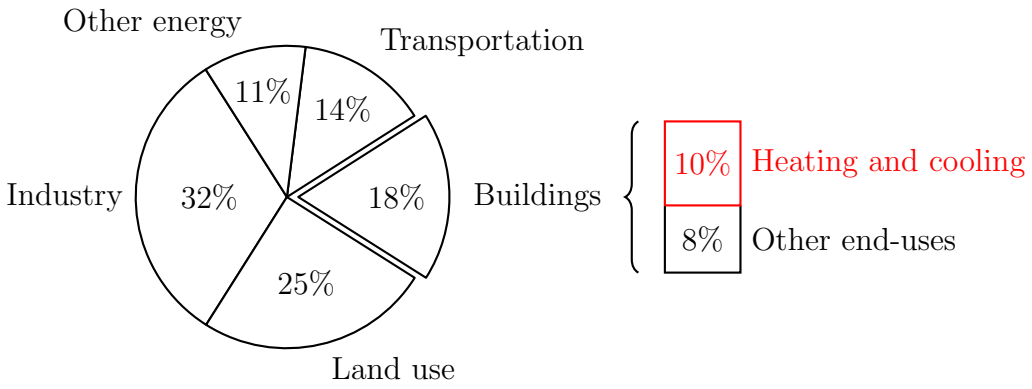

Figure 1.1: 2010 anthropogenic greenhouse gas emission shares by economic sector. [1] Total: 49 Gt CO_2-equivalent. One tenth of emissions are caused by heating and cooling buildings. This includes both direct emissions from on-site combustion and indirect emissions from electricity use. 'Land use' refers primarily to agriculture, deforestation and biomass burning. 'Other energy' refers to all energy sector activities other than producing electricity and heat.

speed drives, and their use for space heating and cooling in homes and small businesses. We note, however, that our methods and results extend to many other contexts.

Heat pump technology has advanced significantly in the last decade, in terms of both efficiency and of heating capacity in cold weather. [7–9] Meanwhile, the greenhouse gas intensity of electricity has decreased in much of the world, driven by fuel transitions and rising power plant efficiencies. [10] Due to these technological advances, heat pumps now have the potential to reduce emissions from heating and cooling by half or more. [8, 11, 12]

While heat pumps can reduce emissions in many applications, they face several barriers to widespread adoption. Their lifetime costs are not always competitive with incumbent technologies such as natural gas furnaces. [11] Even when lifetime heat pump costs are competitive, the initial costs of procuring and installing them can be prohibitive. [13–17] Additional barriers include finding skilled installers, selecting appropriate heat pump models and sizes, and identifying and applying for rebates, tax credits or other incentives. [13–15]

The goal of this thesis is to reduce emissions by lowering barriers to heat pump adoption.

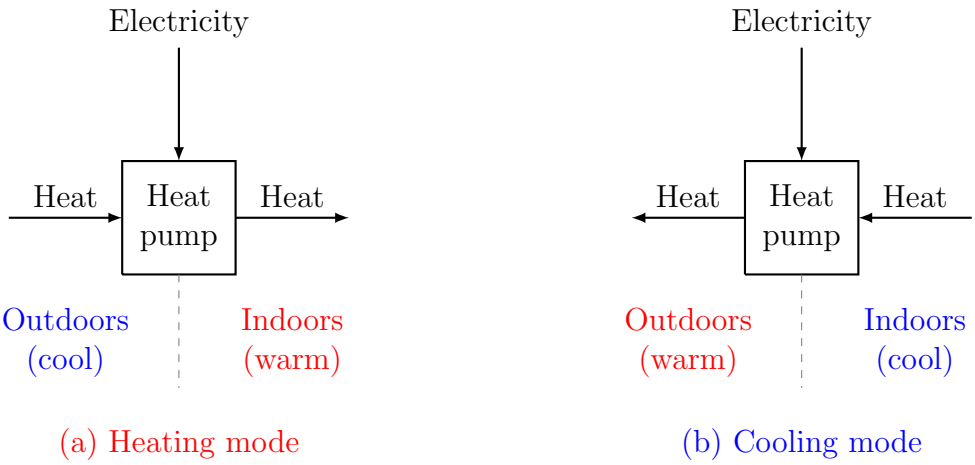

(a) Heating mode (b) Cooling mode

Figure 1.2: Electric heat pumps provide heating or cooling by using electricity to move heat.

1.2 Heat purchase agreements

In the traditional model of heat pump ownership, a *user* (such as the owner of a home or business) pays an installer to procure and install a heat pump. The user's initial capital cost includes the heat pump, the installation labor, and the installer's overhead and profit. The user is responsible for identifying and applying for any rebates, tax credits or other incentives for heat pump adoption. Over the heat pump's lifetime, the user also pays for the electricity the heat pump consumes and any maintenance it requires.

As an alternative to the traditional heat pump ownership model, we investigate a model of third-party ownership based on *heat purchase agreements (HPAs)*. Figure 1.3 illustrates this model. Users host heat pumps that are owned and operated by an *aggregator*, such as a for-profit or nonprofit business, a utility, a heat pump manufacturer, or a local government agency. The aggregator buys the electricity the heat pumps consume. Each user pays the aggregator an agreed-upon price per unit of heat or cooling they use. The aggregator can also sell the collective flexibility of its heat pump fleet to the power system operator for ancillary services; we discuss this further in §1.3.

HPAs could lower the barriers to heat pump adoption discussed in §1.1. The aggregator

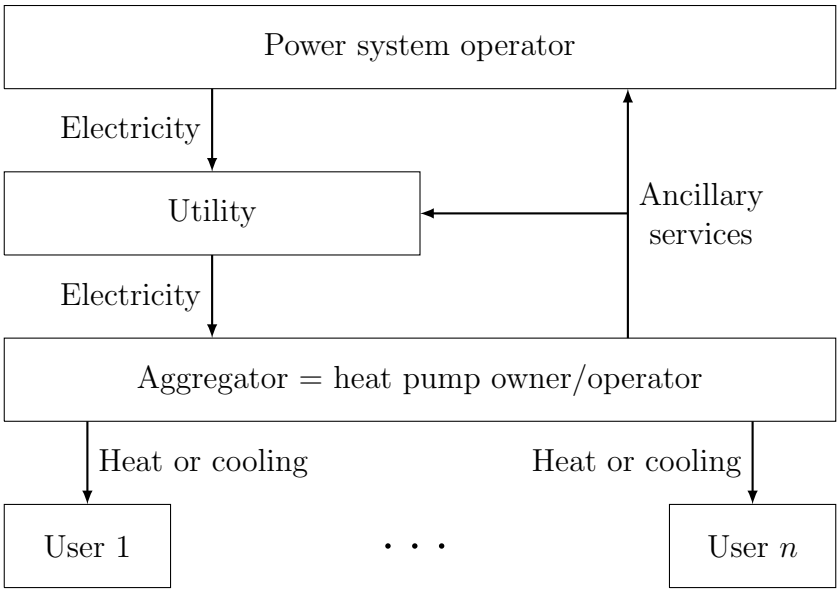

Figure 1.3: Commodity flows in the HPA model of third-party heat pump ownership.

owns and installs the heat pumps, eliminating the users' initial capital costs. The aggregator also assumes responsibility for sizing the heat pumps appropriately and installing them correctly. As the heat pump owner, the aggregator is the party eligible for any rebates or tax credits; the aggregator therefore takes on the related burdens and benefits.

HPAs provide the user and aggregator with rational incentives. Because the user pays for the heat or cooling they use, they are incentivized to maintain an efficient building envelope and to choose moderate temperature setpoints. Because the aggregator's profits are tied to their heat pumps' lifetime performance, the aggregator is incentivized to invest in quality heat pumps, size them appropriately, install them correctly, operate them efficiently, and maintain them well.

When entering into an HPA, the aggregator makes an initial investment in the heat pump. They expect to recover this investment over time through heat or cooling sales. The returns on the aggregator's investment depend on how much heat or cooling is used. If the user chooses milder temperature setpoints than expected, or makes efficiency improvements to their building envelope, then the aggregator's returns could be smaller than expected.

For this reason, the aggregator might add some form of minimum-use clause to the HPA. A minimum-use clause could weaken the user's efficiency incentives; to mitigate this, the aggregator could offer the user an energy audit and envelope efficiency upgrades before negotiating the HPA. This could reduce emissions, provide the aggregator with another revenue stream, and reduce the risk associated with the heat pump investment.

Who should aggregate heat pumps? Two candidates with significant economic advantages are heat pump manufacturers and electricity distribution utilities. An HPA aggregator's business model involves buying heat pumps, buying electricity, and selling heat and cooling. Initial investments in heat pumps and instrumentation are likely to be smallest for heat pump manufacturers. Utilities buy electricity wholesale, rather than retail, so their electricity costs would likely be lowest. Utilities also have existing relationships with energy end-users, and are experienced with raising capital and investing in energy infrastructure. Of course, social or political arguments could be made in favor of other entities.

1.2.1 Related ideas

HPAs can be found in the marketing materials of several energy companies [18–20], and in a small number of academic papers [21, 22]. In both cases, the model arises in the context of district heating systems, where heat is produced at a central plant and circulated through a distribution network to many users. To our knowledge, this thesis is the first academic investigation of HPAs in the context of stand-alone heat pumps serving individual users.

HPAs are closely related to *power purchase agreements*, a third-party ownership model prevalent in the United States rooftop solar market. [23, 24] In the solar power purchase agreement model, a firm owns solar panels hosted by users; the users buy the power that the panels produce. The primary distinction between HPAs and power purchase agreements is that in the former, the aggregator draws electricity from the grid and uses it to move heat,

while in the latter, the firm generates electricity from sunlight on site.

Other models of third-party heat pump ownership could reduce some of the barriers to adoption discussed in §1.1. For example, users could *lease* heat pumps from the aggregator. We focus on HPAs, rather than leases, for two reasons. First, HPAs incentivize efficiency by tying the aggregator's profits to the heat pumps' performance. Under a lease, by contrast, the aggregator would likely receive fixed monthly payments whether the heat pumps perform poorly or well. Second, leases are well-understood, while HPAs raise new research questions. Under what conditions are HPAs mutually beneficial to the user, the aggregator and (by reducing emissions) society? How should heat and cooling be priced? Chapter 2 of this thesis addresses these questions.

Another relevant ownership model is *property-assessed clean energy financing*. [25–27] In this model, a user borrows money, typically from a local government or a nonprofit agency, and uses it to buy solar panels, windows, insulation, or other clean energy technologies. The loan is repaid through the user's property taxes. If the user moves before the loan is repaid, the debt transfers with the property to the next owner. Property-assessed clean energy financing has accelerated adoption of clean energy technologies in California [26, 27] and Colorado [25]. Adapting this model to heat pumps could lower barriers to adoption, as it would provide users with a source of capital and reduce risks associated with moving. An HPA aggregator could likely benefit from a similar contract mechanism tying revenues to properties, rather than to individual users.

Another innovative ownership model is *community purchasing*. [28] This model involves a number of users who want to purchase heat pumps. Rather than purchasing the heat pumps individually from various installers at full retail prices, the users combine their purchases into one large order with a single installer. Community purchasing can lower the users' capital costs by enabling bulk discounts on hardware and installation. It can also lower other barriers to adoption by, *e.g.*, streamlining the processes of finding installers, selecting

appropriate heat pumps and applying for rebates, tax credits or other incentives. The primary difference between community purchasing and HPAs is that community purchasing can lower users' capital costs, while HPAs can eliminate them.

In summary, there is a range of innovative models of third-party heat pump ownership that can lower barriers to heat pump adoption. HPAs are one option. While we argue that HPAs have certain advantages, we also acknowledge that different options may appeal to different users, and that all of the options mentioned above have the potential to reduce greenhouse gas emissions from heating and cooling.

1.3 Heat pumps, renewables and the grid

The central task of power system operation is to continuously balance electricity supply and demand. This task grows more challenging as power systems integrate more wind and solar generation, which are intermittent and uncertain. [29] To maintain reliability with increasing shares of renewable generation, power system operators will likely need more *ancillary services*. [30–32]

Ancillary services are commodities that are traded in power system markets and facilitate the balancing of electricity supply and demand. [33] The adjective 'ancillary' indicates that these services are not directly related to meeting energy demand, but support this activity. Most ancillary services involve perturbing real power (as opposed to reactive power) at the system operator's request. Different system operators define different real-power ancillary services, but these services can be broadly categorized as *regulation* and *reserve*. [33, 34]

Regulation involves perturbing power to track a reference signal with a time step on the order of one second. System operators use regulation continuously during normal operations. Some system operators run separate markets for upward regulation (increasing generation or decreasing load) and downward regulation (decreasing generation or increasing load). Other

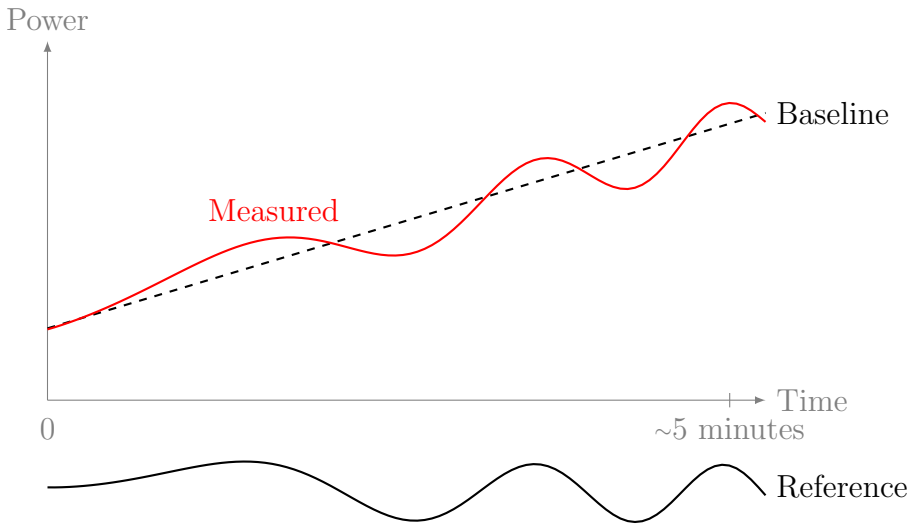

Figure 1.4: Regulation involves perturbing measured power (red curve) away from a baseline (dashed black line). The power perturbation should track the reference signal (solid black curve) sent by the power system operator.

system operators run a single market and require symmetric regulation capacity. Regulation is typically the highest-priced ancillary service. [34]

Figure 1.4 illustrates a resource providing symmetric regulation. In this figure, the dashed black line is the resource's power baseline, *i.e.*, the power they would generate or consume if they were not providing regulation. The red curve is the resource's measured power. The power perturbation is the difference between the measured power and the baseline. The power perturbation should track the reference signal, drawn in solid black beneath the plot.

Reserve is capacity held in reserve in case of a contingency, such as a generator outage, a power line failure, or a sudden drop in the power output of a wind or solar farm. Unlike regulation, reserve is not dispatched during normal operations. When a contingency occurs and reserve is dispatched, resources must deliver a predetermined power perturbation within a given response time: ~10 minutes for spinning reserve and ~30 minutes for non-spinning reserve. Spinning reserve is typically the next highest-priced ancillary service after regulation. [34]

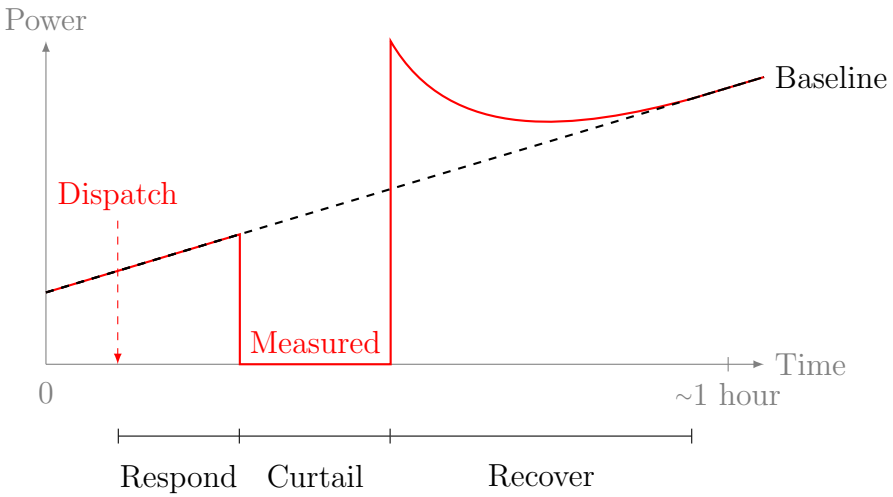

Figure 1.5: To provide spinning reserve, a load must be able to curtail within ~10 minutes of dispatch. Spinning reserves are dispatched in response to infrequent contingencies such as generator outages or power line failures.

Figure 1.5 illustrates a load providing spinning reserve. As in Figure 1.4, the dashed black line and red curve in Figure 1.5 are the load's baseline and measured power, respectively. After receiving a dispatch signal, the load turns off within ~10 minutes. This curtailment is sustained for ~15 minutes, at which point non-spinning reserves come online and the system operator relieves the load. The load then recovers, *e.g.*, by bringing indoor air temperatures back to desired levels.

Ancillary services have traditionally been provided by generators, but controllable loads can also provide them. [35–41] In particular, recent experiments have demonstrated that individual heat pumps equipped with variable-speed electric motors can rapidly and accurately track requested power perturbations. [42–47]

Despite variable-speed heat pumps' technical capabilities, they face a significant barrier to ancillary service market entry. This barrier is a matter of scale. Total power system capacities are typically tens to hundreds of GW. To keep operations manageable, power system operators require a minimum capacity, typically 100 kW or 1 MW, to participate in ancillary service markets. [34] Most heat pumps, by contrast, have electric power capacities

on the order of one to ten kW. To participate in ancillary service markets, therefore, heat pumps likely need to be aggregated by the hundreds or thousands.

The HPA model discussed in §1.2 can overcome this barrier to entry. In this model, the aggregator owns and operates a fleet of heat pumps. If this fleet is sufficiently large, and has the necessary sensing, communication and control capabilities, then the aggregator can sell its collective flexibility in ancillary service markets. The aggregator has an economic incentive to meet these criteria, as ancillary service markets offer new revenue opportunities.

1.3.1 Related ideas

The idea of loads providing power system services dates back at least to the energy crisis of the 1970s. [48–53] Throughout the last four decades, utilities have used price signals or direct load control to reduce peak load, shift load to low-price times, and curtail load in emergencies. [52, 54–57] Thermal loads such as air conditioners and water heaters have consistently played a central role in these efforts.

For most of the 20th century, the United States electricity industry involved a small number of government-sanctioned monopolies that owned the generation, transmission and distribution infrastructure in their respective service areas. [58] In the late 1990s, the industry was restructured to allow competition at the wholesale level. [59, 60] Restructuring paved the way for loads to participate in energy and ancillary service markets. [61, 62] Meanwhile, due to the proliferation of sensing, communication and computing technologies, loads became increasingly capable of reliably providing ancillary services. [36, 63, 64]

Recently, two research threads have made significant progress toward controlling heating and cooling loads for ancillary services. The first focuses on aggregating thermostatically-controlled loads such as air conditioners, refrigerators and water heaters in residential and small commercial buildings. [37, 65–70] The second focuses on individual variable-speed

fans, pumps and compressors in large commercial and industrial buildings. [38–43, 71–74]

In this thesis, we explore a third and complementary thread: aggregating variable-speed heat pumps in residential and small commercial buildings. Other contributions in this thread include [44–47]. Our primary contributions are (1) regulation control at the aggregate scale, rather than the scale of an individual heat pump; (2) co-optimization of regulation and reserve offers in day-ahead markets; and (3) quantifying the regulation and reserve capacities and revenues of a heat pump aggregation. We discuss this further in Chapter 5.

1.4 Research contributions

The primary research contributions of this thesis include analysis of the HPA model and development of methods to support its implementation. More specifically, we claim the following original and substantial research contributions.

1. In Chapter 2, we analyze the economics of HPAs. In particular, we derive necessary and sufficient conditions for an HPA to mutually benefit the aggregator and the user. We also provide a method for fairly pricing heat and cooling.

2. In Chapter 4, we develop a method for selecting an appropriate heat pump for a given application. The method is data-driven, provides probabilistic feasibility and optimality guarantees, and applies to both HPAs and traditional ownership.

3. In Chapter 5, we demonstrate the feasibility of providing regulation and spinning reserve from aggregated variable-speed heat pumps. In particular, we develop a regulation controller at the aggregate scale and quantify its tracking performance. We also show that the indoor air temperature perturbations caused by providing regulation and spinning reserve are small.

4. Also in Chapter 5, we develop new methods for co-optimizing day-ahead regulation and reserve capacity offers for an aggregation of variable-speed heat pumps under uncertainty. In simulations, each heat pump can offer 285–325 W of annual-average capacity and earn $25–75 of annual revenue. These are combined figures from providing both regulation and spinning reserve in the PJM Interconnection, the largest power system in the United States.

1.5 Potential impact

The potential impact of this thesis is the self-reinforcing cycle illustrated in Figure 1.6. We now walk through this cycle, beginning at the top.

1. HPAs could encourage adoption of more heat pumps.
2. An HPA aggregator could use these heat pumps to provide ancillary services, helping power system operators integrate more renewable generation.
3. New renewables could drive down the prices and greenhouse gas intensities of electricity. (These effects have been observed in regions with high shares of renewable generation, such as Germany [75, 76] and Texas [77].)
4. Lower electricity prices and greenhouse gas intensities could make heat pumps more economically and environmentally attractive, encouraging further heat pump adoption.

This cycle could reduce emissions directly, by replacing fossil-fueled or inefficient heating and cooling equipment with efficient heat pumps powered by clean electricity. It could also reduce emissions indirectly, by enabling wind and solar power to displace fossil-fueled generation.

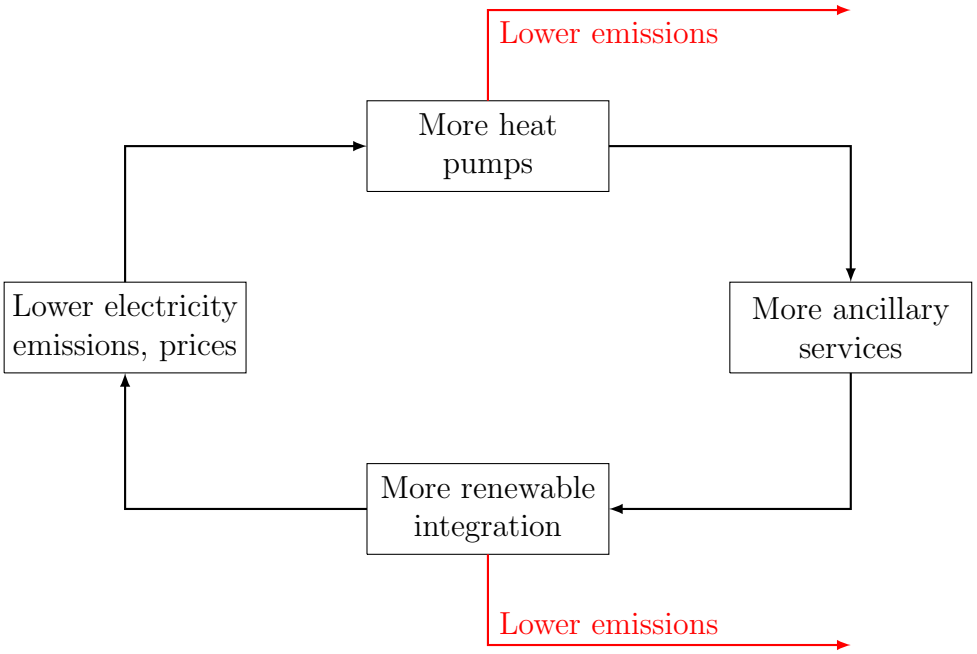

Figure 1.6: Renewables and heat pumps could form a self-reinforcing cycle, reducing emissions from heating, cooling and electricity generation.

1.6 Organization of this thesis

This thesis is organized into four chapters and two appendices, plus this introductory chapter and the conclusion in Chapter 6. Chapters 2–5 are intended to be read sequentially, but readers who are familiar with the emissions and economics of heating and cooling systems can safely skip Chapter 2. Chapter 3 lays the foundation for Chapters 4–5. Some methodology discussion in Chapter 5 assumes familiarity with the methods employed in Chapter 4. The appendices are supplemental.

In Chapter 2, we analyze the emissions and economics of heat pumps and incumbent heating and cooling technologies. We conduct this analysis at a high level in order to highlight the important ideas and parameters with a minimum of conceptual and notational overhead. A particular focus of Chapter 2 is the economics of third-party heat pump ownership under HPAs. Notably, the analysis includes (a) conditions under which HPAs are mutually beneficial to the aggregator and user, and (b) methods for fairly pricing heat and

cooling.

In Chapter 3, we present mathematical models of heat pumps and thermal loads. By contrast to the high-level models in Chapter 2, the models in Chapter 3 are sufficiently accurate to be used for optimization and control of real heat pumps, and we use them for these purposes in Chapters 4–5. The heat pump discussion starts from basic physics and builds up to a data-driven heat pump model. The thermal load discussion presents a thermal circuit model that is simple, accurate, and broadly applicable. We discuss the history of this model, its recent use in research on optimization and control of heating and cooling systems, and how its parameters can be fit to high-level energy consumption data.

In Chapter 4, we develop a data-driven method for selecting an appropriate heat pump for a given application. We discuss existing approaches to this problem in industry and in the research literature. We then develop a new method, position it relative to a subfield of Monte Carlo simulation called ranking and selection, and simulate its use in a realistic heat pump selection example. The new selection method comes with a robustness guarantee that we prove in Appendix A.

Chapter 5 covers the technical feasibility and economic viability of providing regulation and spinning reserve from aggregated variable-speed heat pumps. The technical feasibility sections focus on quantifying the impacts of ancillary service provision on building occupants. For regulation, this entails the design of a real-time controller at the aggregate level; we discuss our controller and simulate its performance under historical regulation signal data. The economic viability section of Chapter 5 focuses on estimating the regulation and spinning reserve capacity that a heat pump aggregator could offer and the revenue that they could earn. The estimation procedure involves long-term stochastic simulation of a large heat pump aggregation.

Chapter 2

Emissions and economics

In this chapter, we analyze the emissions and economics of heat pumps and competing technologies. We conduct this analysis at a high level in order to emphasize the key parameters and relationships between them. Later chapters of this thesis will provide more detailed analyses and more concrete interpretations of the high-level parameters.

2.1 Emission reductions from heat pumps

We consider a user whose annual heating and cooling loads are Q_h (kWh_t) and Q_c (kWh_t), respectively. Here the subscript t denotes thermal, rather than electrical, energy. We allow for the cases where either $Q_h = 0$ or $Q_c = 0$, but we assume that $Q_h + Q_c > 0$, meaning at least one of the annual thermal loads is strictly positive. We compare the emissions of two scenarios:

1. A reversible electric heat pump with seasonal heating and cooling coefficients of performance (COPs) η_h and η_c, respectively.

2. An incumbent heating and cooling system with seasonal COPs $\tilde{\eta}_h$ and $\tilde{\eta}_c$.

By COP, we simply mean the ratio of the output thermal energy (heating or cooling) to the energy supplied by the input electricity or fuel. For some equipment, such as fossil-fueled furnaces and boilers, this ratio is typically called an *efficiency*, and is always between zero and one. For heat pumps, by contrast, COPs can be greater than one, and are often in the range of three to five. [7–9]

The annual electrical energy consumed by the heat pump is

$$\frac{Q_h}{\eta_h} + \frac{Q_c}{\eta_c}.$$

Similarly, the incumbent system consumes input energy

$$\frac{Q_h}{\tilde{\eta}_h} + \frac{Q_c}{\tilde{\eta}_c}.$$

For the incumbent system, the input heating energy could come from natural gas, propane, heating oil, electricity, *etc.* We assume that the input cooling energy is electricity.

We define the greenhouse gas intensity of electricity, μ (kg/kWh), as the equivalent mass of CO_2 (in terms of warming potential) emitted per unit of electrical energy. Similarly, we define the greenhouse gas intensity of the incumbent heating fuel, $\tilde{\mu}$ (kg/kWh), as the mass of CO_2-equivalent emitted per unit of chemical potential energy in the heating fuel. With these definitions, the annual greenhouse gas emission reduction due to the heat pump is

$$\left(\frac{\tilde{\mu}}{\tilde{\eta}_h} - \frac{\mu}{\eta_h}\right) Q_h + \mu \left(\frac{1}{\tilde{\eta}_c} - \frac{1}{\eta_c}\right) Q_c. \tag{2.1}$$

2.1.1 Typical parameter values

In field studies in cold climates, ductless air-source heat pumps typically achieve seasonal heating COPs of 2.6 to 2.9. [78–80] Seasonal average cooling COPs are significantly higher:

typically 3.7 to 4.3. [80] Cooling COPs exceed heating COPs because air-source heat pumps are more efficient when the temperature difference between the indoor and outdoor air is smaller. In cold climates, temperature differences are significantly smaller over the cooling season than the heating season.

Typical fossil-fueled furnace and boiler efficiencies range from 55% for old, propane- or oil-fueled units to 95% for new natural gas units. [81] By contrast to ductless heat pumps, most fossil-fueled furnaces and boilers produce heat centrally and distribute it through a network of ducts or pipes. Distribution entails additional losses. Distribution efficiencies range from 65% for old steam systems, which operate at high temperatures and pressures, to 95% for new ducts or pipes in conditioned space. [81, 82] Therefore, the combined efficiency of a fossil-fueled heating system, including the central plant and the distribution network, ranges from 35% to 90%. A recommended nominal value of the efficiency of a ducted natural gas furnace in an existing United States home is 70%. [81]

Central air conditioners' seasonal COPs typically range from 1.9 for old units to 4 for new units. [81] Like fossil-fueled furnaces, central air conditioners distribute cool air through ducts, typically with 70% to 95% efficiency. [81, 82] Therefore, the combined seasonal COPs of ducted central air conditioning systems, including the central plant and the distribution network, range from 1.3 for old units to 3.8 for new units. Room air conditioners provide cooling directly to conditioned space, so avoid distribution losses. Room air conditioners' seasonal COPs typically range from 1.6 for old units to 2.9 for new units. [81]

The greenhouse gas intensities of natural gas, propane and heating oil are 0.18, 0.22 and 0.25 kg/kWh, respectively. [83] The greenhouse gas intensity of electricity depends on the efficiencies and input fuels of the power plants that generate the electricity. The generation mix varies over both space and time, so the greenhouse gas intensity of electricity does too. In the United States, the average greenhouse gas intensity, defined as the ratio of the total mass of CO_2-equivalent emitted to the total electrical energy generated, was 0.46 kg/kWh in

2017. [84] This metric varied from 0.03 kg/kWh in Vermont to 0.93 kg/kWh in Wyoming.

2.1.2 Data sources

The sources [78–80] are technical reports of field-monitoring studies of cold-climate air-source heat pumps. The COP values reported in these studies are compiled from long-term measurements of actual heat pumps serving residential buildings in several dozen locations, primarily in the Northeastern United States. These data include measurements of the specific line of heat pumps we discuss and model in §3.1.3. These studies are conducted by independent researchers, rather than heat pump manufacturers, and the data show fair agreement across studies. For these reasons, we consider the COP values reported in [78–80] to be quite robust.

We use the source [81] primarily for the efficiencies of incumbent heating and cooling equipment. This source is a technical report that specifies protocols for simulating the energy consumption of heating and cooling equipment for purposes such as predicting emission and cost reductions from building retrofits. This report is an official document from the United States Department of Energy's Building America program, an industry/government collaboration aimed at improving the energy efficiency of residential buildings. The efficiency values reported in [81] were compiled by a team of independent researchers at national laboratories based on field measurements, review of research literature, and discussion with industry practitioners. We note that efficiencies vary widely depending on equipment age and quality; the efficiency ranges in §2.1.1 reflect this variety.

We use the source [84] for greenhouse gas intensities of electricity. This source is a product of the United States Environmental Protection Agency's Emissions & Generation Resource Integrated Database. It contains (among other data) the total equivalent greenhouse gas intensities of electricity, including emissions of CO_2, NO_x, SO_2 and CH_4, for each state. We use the data from 2016, the most recent year available. The annual greenhouse gas intensities

Table 2.1: State-independent parameter values used in Figure 2.1.

Parameter	η_h	η_c	$\tilde{\eta}_h$	$\tilde{\eta}_c$	$\tilde{\mu}$
Value	2.75	4	0.7	2.7	0.18 kg/kWh

in [84] are computed by dividing the total equivalent mass of CO_2 emitted by all power plants in each state by the total electrical energy those plants produce. These greenhouse gas intensities can therefore be viewed as averages over both time and generators. For a discussion of other greenhouse gas accounting methods, we refer the interested reader to pages 23–25 of [11].

2.1.3 United States emission reduction potential

Figure 2.1 shows a map of the United States, color-coded by the estimated percent emission reduction,

$$100\left(1-\frac{\lambda/\eta_h+1/\eta_c}{\lambda\tilde{\mu}/(\mu\tilde{\eta}_h)+1/\tilde{\eta}_c}\right)\%,$$

where

$$\lambda := \frac{Q_h}{Q_c}.$$

To color-code this figure, we used the parameter values in Table 2.1. In this table, the values of $\tilde{\eta}_h$ and $\tilde{\mu}$ represent a ducted natural gas furnace of typical age and efficiency. The value of $\tilde{\eta}_c$ represents a ducted central air conditioner of typical age and efficiency. We adjusted the heat pump and air conditioner COPs linearly based on the seasonal average temperature in each state. The heating adjustment was 100% at 0 °C with a slope of 1%/°C. The cooling adjustment was 100% at 20 °C with a slope of −3%/°C. These values were based on the manufacturer COP data discussed in §3.1.3.

The parameters λ and μ used in Figure 2.1 vary by state. For each state's value of λ, we used the ratio of the average heating load to cooling load from the 2015 survey data in

[85] for a single-family home in the relevant climate zones. For μ, we used each state's 2017 electricity greenhouse gas intensity from [84].

With these input data, the percent emission reductions range from -18% (an 18% *increase*) in Wyoming, the state with $\mu = 0.93$ kg/kWh, to a 95% reduction in Vermont, the state with $\mu = 0.03$ kg/kWh. The average emission reduction is 38%. The standard deviation is 25%.

We note that Figure 2.1 shows the estimated emission reduction that could likely be achieved in each state by replacing a typical natural gas furnace and central air conditioner with a typical cold-climate air-source heat pump. Actual emission reductions will, of course, vary with the age, quality and fuel sources of the replaced equipment, the heat pump quality, and exogenous factors related to weather and occupant behavior. The numerical emission reductions reported here should be viewed as high-level, ballpark estimates. The main value of Figure 2.1 is to highlight regions where the emission reduction potential of heat pumps is particularly strong, such as the Northeast and the Pacific Northwest.

2.1.4 Sensitivity analysis

We now consider the influence of each parameter on the absolute emission reduction in Equation[1] (2.1). To quantify this influence, we first introduce the notion of *sensitivity*.

Sensitivity definition

We consider a generic output $y \in \mathbf{R}$ that is a function $f : \mathbf{R}^n \to \mathbf{R}$ of a vector $p \in \mathbf{R}^n$ of parameters. We are interested in the change Δy caused by a small change Δp_i to a particular parameter p_i. In the neighborhood of the nominal parameter values $\bar{p} \in \mathbf{R}^n$, Δy

[1] In this thesis, only equations that are referred to in the text are numbered.

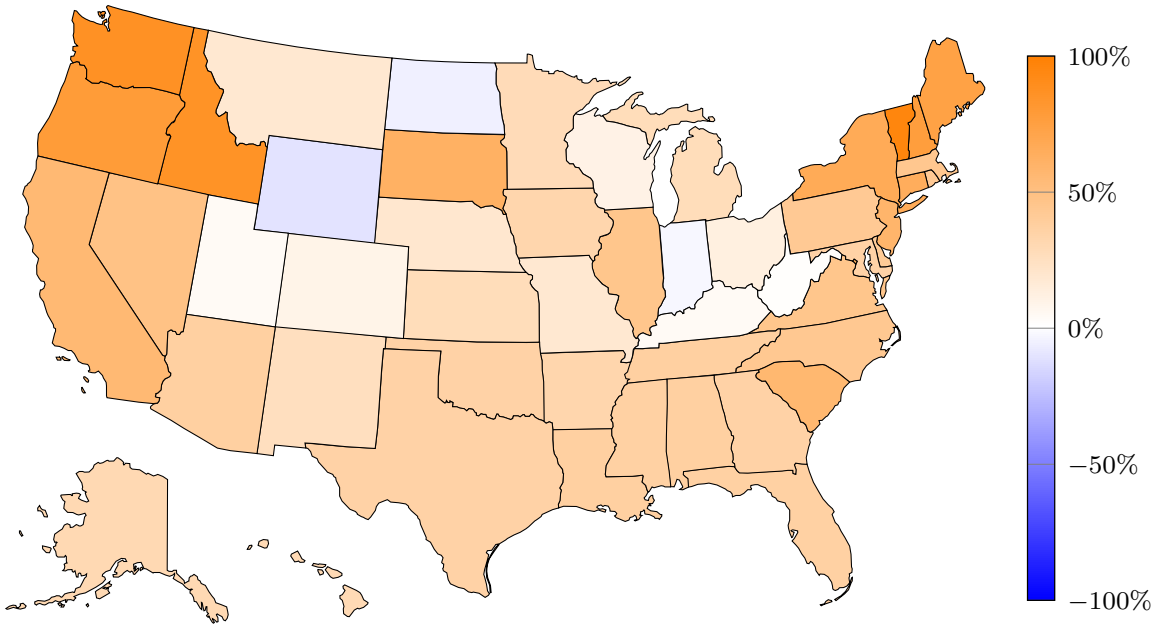

Figure 2.1: Estimated percent emission reductions from replacing a typical natural gas furnace and air conditioner by an efficient electric heat pump. Darker orange shades indicate larger reductions; blue shades indicate emission increases. Estimates range from an 18% increase in Wyoming to a 95% reduction in Vermont. The national average is a 38% reduction.

is well-approximated by

$$\Delta y \approx \left.\frac{\partial f}{\partial p_i}\right|_{\bar{p}} \Delta p_i.$$

To allow direct comparison between different parameters' influences on y, we define the sensitivity of y to p_i in terms of the *relative* change in y caused by a small *relative* change in p_i:

$$\text{sensitivity of } y \text{ to } p_i := \frac{\Delta y/\bar{y}}{\Delta p_i/\bar{p}_i} \approx \left.\frac{\partial f}{\partial p_i}\right|_{\bar{p}} \frac{\bar{p}_i}{\bar{y}}.$$

Here $\bar{y} = f(\bar{p})$ is the value of y at the nominal parameter values. The sensitivity of y to p_i can be interpreted as the percent change in y caused by a 1% change in p_i, with all other parameters held constant at their nominal values.

Table 2.2: Emission reduction sensitivities.

Parameter	η_h	η_c	$\tilde{\eta}_h$	$\tilde{\eta}_c$	μ	$\tilde{\mu}$
Sensitivity	1.50	0.79	-2.34	-1.18	-1.10	2.34

Emission reduction sensitivities

Table 2.2 shows the sensitivities[2] of the absolute emission reduction to the relevant parameters. To compute these sensitivities, we used the nominal parameter values in Table 2.1. We also used the 2017 United States average greenhouse gas intensity of electricity, $\mu = 0.455$ kg/kWh, and the United States average heating and cooling loads for single-family homes from [85].

The emission reduction is increasing in η_h, η_c and $\tilde{\mu}$ and decreasing in $\tilde{\eta}_h$, $\tilde{\eta}_c$ and μ. To maximize the emission reduction, therefore, we should target inefficient air conditioners and inefficient heating systems powered by fuels with high greenhouse gas intensities. We should replace these systems with efficient heat pumps powered by clean electricity.

In the neighborhood of the nominal parameter values, the emission reduction is most sensitive to $\tilde{\eta}_h$ and $\tilde{\mu}$. This suggests that the characteristics of the incumbent heating system have the greatest influence on the potential emission reductions.

2.1.5 Average and marginal greenhouse gas intensities

The emissions analysis above uses greenhouse gas intensity data from [84]. These greenhouse gas intensity data are averaged over both time and generators. Another approach to quantifying the emissions of electrical devices uses the *marginal* greenhouse gas intensity of electricity, *i.e.*, the greenhouse gas intensity of electricity generated by the power plant or plants whose real-time power output changes in response to changes in system load. We

[2]Sensitivities, as defined in §2.1.4, are dimensionless quantities. They are directly comparable between variables; each sensitivity can be viewed as the percent change in the output caused by a one percent change in the input.

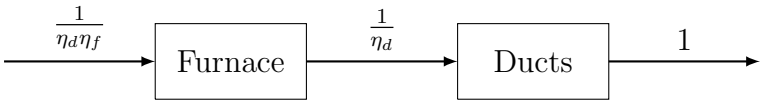

Figure 2.2: A forced-air natural gas heating system. To produce one unit of heat, the ducted furnace consumes $1/(\eta_d \eta_f)$ units of chemical potential energy.

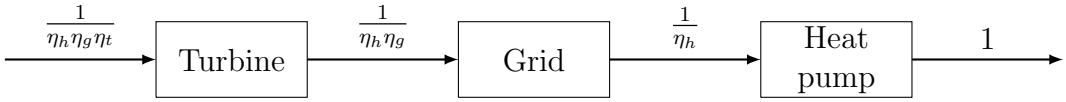

Figure 2.3: A point-source heat pump system powered by gas-fueled electricity. To produce one unit of heat (which is delivered directly to the space, rather than distributed through ducts), the system consumes $1/(\eta_h \eta_g \eta_t)$ units of chemical potential energy.

now illustrate the marginal approach in the case where marginal electricity is generated from natural gas. For a fuller comparison of different approaches to greenhouse gas accounting, see pages 23–25 of [11].

To illustrate the marginal approach to greenhouse gas accounting, we consider the two cases depicted in Figures 2.2–2.3. Figure 2.2 depicts the case where heating is provided by a ducted natural gas furnace. To produce one unit of heat, this system consumes $1/(\eta_d \eta_f)$ units of input chemical potential energy from natural gas. Here η_d is the duct efficiency and η_f is the furnace efficiency. Figure 2.3 depicts a heat pump powered by gas-fueled electricity. This case represents a *point-source* heat pump, such as a ductless mini-split, that delivers heat directly to the space rather than distributing hot air through ducts. The heat pump system in Figure 2.3 consumes $1/(\eta_h \eta_g \eta_t)$ units of chemical potential energy to produce one unit of heat. Here η_t is the natural gas turbine efficiency and η_g is the combined efficiency of transmitting, transforming and distributing electricity over the grid.

The United States Environmental Protection Agency's Emissions & Generation Resource Integrated Database [84] contains estimates of η_g for 26 regions in the United States. The 2016 estimates range from 94.7% to 95.8%, with a national average of 95.5%. According to the United States Energy Information Agency's Office of Independent Statistics & Analysis,

the average operating efficiency of United States natural gas turbines in 2016 was 43.4%. [86] (Modern combined-cycle natural gas turbines can exceed 60% operating efficiencies, but the United States natural gas fleet also includes many older or single-cycle units.) With $\eta_t = 0.434$, $\eta_g = 0.955$ and $\eta_h = 2.75$ (*cf.* the cold-climate heat pump field studies [78–80]), the heat pump system in Figure 2.3 consumes $1/(\eta_h \eta_g \eta_t) = 0.87$ units of chemical potential energy to produce one unit of heat. Therefore, this system reduces greenhouse gas emissions relative to the natural gas heating system in Figure 2.2 whenever $1/(\eta_d \eta_f) > 0.87$, or, equivalently, $\eta_d \eta_f < 1.15$. As η_d and η_f are both less than one, this inequality always holds. Assuming $\eta_d \eta_f = 0.7$, a typical value for an existing forced-air natural gas furnace and ducts in a United States home [81], the relative emission reduction from the heat pump system is $1 - \eta_d \eta_f / (\eta_h \eta_g \eta_t) = 0.39$. In other words, replacing the natural gas heating system in Figure 2.2 by the heat pump system in Figure 2.3 powered by gas-fueled electricity can be expected to reduce the greenhouse gas emissions from heating by about 39%. The percent emission reduction is increasing in η_t, η_g and η_h and decreasing in η_f and η_d.

2.2 Economics of traditional heat pump ownership

In the traditional model of heat pump ownership, the user pays an installer to procure and install a heat pump. Over the heat pump's lifetime, the user pays for the electricity the heat pump consumes and any maintenance it requires. In this ownership model, the net present cost of the user's heat pump investment is

$$c + \gamma \left[\pi \left(\frac{Q_h}{\eta_h} + \frac{Q_c}{\eta_c} \right) + m \right],$$

where

$$\gamma := \sum_{i=1}^{Y} \frac{1}{(1+\rho)^i} = \frac{1-(1+\rho)^{-Y}}{\rho}.$$

In these expressions,

- c (\$) is the user's installed cost, including the heat pump, the installation labor, the installer's overhead and profit, and any available rebates, tax credits or other incentives.
- π (\$/kWh) is the annual average electricity price.
- m (\$) is the annual maintenance cost.
- Y is the number of years in the heat pump's lifetime.
- ρ is the user's annual cash flow discount rate.

In deriving these expressions, we assume that the heat pump's salvage value at the end of its life is negligible. We also assume that the annual heating and cooling loads, seasonal COPs, annual average electricity and fuel prices, and annual maintenance costs are constant over the heat pump's lifetime. These assumptions can be relaxed (see §2.5); we make them mainly to keep notation light.

As in §2.1, we compare the heat pump to an incumbent heating and cooling system. Assuming the lifetime of the incumbent system is equal to the heat pump lifetime, the net present cost of the incumbent system is

$$\tilde{c} + \gamma \left(\frac{\tilde{\pi} Q_h}{\tilde{\eta}_h} + \frac{\pi Q_c}{\tilde{\eta}_c} + \tilde{m} \right).$$

Here $\tilde{c}$ (\$), $\tilde{m}$ (\$), and $\tilde{\pi}$ (\$/kWh) are the incumbent system's installed cost, annual maintenance cost, and heating fuel price, respectively. The net present value of the user's heat

pump investment is the net present cost reduction, relative to the incumbent system:

$$\tilde{c} - c + \gamma \left[\left(\frac{\tilde{\pi}}{\tilde{\eta}_h} - \frac{\pi}{\eta_h} \right) Q_h + \pi \left(\frac{1}{\tilde{\eta}_c} - \frac{1}{\eta_c} \right) Q_c + \tilde{m} - m \right].$$

The heat pump investment is attractive if its net present value is nonnegative. This occurs if and only if

$$\left(\frac{\tilde{\pi}}{\tilde{\eta}_h} - \frac{\pi}{\eta_h} \right) Q_h + \pi \left(\frac{1}{\tilde{\eta}_c} - \frac{1}{\eta_c} \right) Q_c \geq \frac{c - \tilde{c}}{\gamma} + m - \tilde{m}. \tag{2.2}$$

The left-hand side of this inequality is the annual energy cost reduction. The right-hand side is a weighted sum of the increases in the initial capital cost and the annual maintenance cost. Thus, the investment is attractive if the energy cost savings outweigh the (potentially) increased capital and maintenance costs.

2.2.1 Typical parameter values

Heating and cooling equipment lifetimes typically range from 10 to 20 years; air-source heat pump manufacturers typically provide 10 or 12 year equipment warranties. Users' annual cash flow discount rates generally depend on their source of capital and the rate of return they expect from their other investments. Typical discount rates range from 5% to 15%. Therefore, typical values of the capital-operating cost trade-off parameter γ range from 5 to 12.5.

Electricity prices vary over space and time. In 2016, the United States average residential electricity price was 0.13 \$/kWh. [87] The minimum and maximum 2016 prices were 0.075 \$/kWh in Louisiana and 0.239 \$/kWh in Hawaii.

The prices of incumbent heating fuels, such as natural gas, propane and heating oil, also vary over space and time. Between 2015 and 2019, the United States winter average natural

gas retail price was 0.033 $/kWh. [88] The minimum 2015–2019 winter average natural gas retail price was 0.023 $/kWh in North Dakota; the maximum was 0.129 $/kWh in Hawaii. United States 2015–2019 winter average propane and heating oil prices were 0.09 and 0.078 $/kWh, respectively. In other words, propane and heating oil were 2.7 and 2.3 times more expensive than natural gas, on average.

A heat pump's installed cost depends on the type and size of the unit; the installer's labor costs, overhead and profit margin; and any rebates, tax credits or other incentives for which the user or installer is eligible. Installed costs are therefore highly variable. As one point of reference, the unsubsidized installed cost of a high-quality ductless heat pump with one ton (3.5 kW_t) of nameplate cooling capacity typically ranges from $4,000 to $5,000. Installed costs of incumbent heating and cooling systems also vary substantially across technologies, capacities, efficiencies, installers, incentives, *etc.*

Annual heat pump maintenance costs vary from year to year. Some years may involve only maintenance that can be done by the user at no cost, such as cleaning air filters and washing outdoor unit coils. Other maintenance, such as periodically checking refrigerant charge, requires a technician. Warranties typically cover damaged hardware, but not technician labor for maintenance or repairs. A plausible range of annual maintenance costs, on average over a heat pump's lifetime, is $50 to $100. Typical maintenance costs of incumbent technologies are comparable.

2.2.2 Data sources

We use the source [87] for electricity prices. This source is a product of the United States Energy Information Administration's Office of Independent Statistics & Analysis. This source contains (among other data) the weighted-average residential retail price of electricity in each state, averaged over that state's utilities and other electricity providers, weighted by

the total electrical energy produced by each provider. We use the data from 2018, the most recent year available.

For fossil fuel prices, we use the database [88]. These data are also compiled by the United States Energy Information Administration's Office of Independent Statistics & Analysis, and compiled using similar methods to the electricity price data. Because fossil fuel prices are significantly more volatile than electricity prices, we average the 2015–2019 prices. We use the winter residential retail prices for each fuel (natural gas, propane and heating oil).

2.2.3 United States energy cost reduction potential

Figure 2.4 shows a map of the United States, color-coded by the estimated percent energy cost reduction,

$$100\left(1-\frac{\lambda/\eta_h+1/\eta_c}{\lambda\tilde{\pi}/(\pi\tilde{\eta}_h)+1/\tilde{\eta}_c}\right)\%.$$

To color-code this figure, we used the efficiency parameter values in Table 2.1, adjusted based on state temperatures. We used the same values to color-code the emission reduction map in Figure 2.1. These parameters represent replacing a typical ducted natural gas furnace and central air conditioner in existing construction.

The parameters λ, π and $\tilde{\pi}$ vary by state. As in the emissions map, for each state's value of λ, we used the ratio of the average heating load to cooling load from the 2015 survey data in [85] for a single-family home in the relevant climate. For π, we used the 2016 state averages from [87]. For $\tilde{\pi}$, we used the 2015–2019 state winter average natural gas retail prices from [88].

With these input data, the percent energy cost reductions range from a 41% increase in Alaska to a 47% reduction in Arkansas. The average energy cost reduction is 24%. The standard deviation is 17%.

We emphasize that energy cost reduction is only part of the story. The net present value

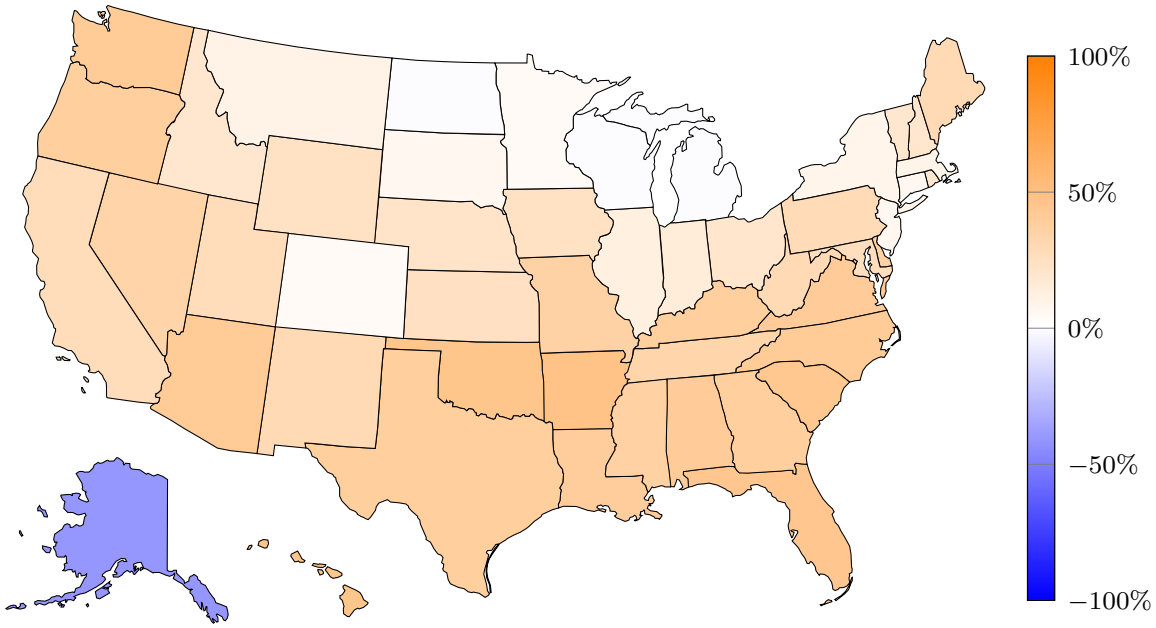

Figure 2.4: Estimated energy cost reductions from replacing a typical natural gas furnace and central air conditioner by an efficient electric heat pump. Darker orange shades indicate larger reductions; blue shades indicate cost increases. Estimates range from a 41% increase in Alaska to a 47% reduction in Arkansas. The national average is a 24% reduction.

of a heat pump investment also depends on the installed costs and maintenance costs of the heat pump and the incumbent system. As with Figure 2.1, we note that Figure 2.4 shows the estimated cost reduction that could likely be achieved in each state by replacing a typical natural gas furnace and central air conditioner with a typical cold-climate air-source heat pump. Actual cost reductions will vary with the age, quality and fuel sources of the replaced equipment, heat pump quality, weather, occupant behavior, *etc.* The numerical cost reductions reported here should be viewed as high-level, ballpark estimates. The main value of Figure 2.4 is to highlight that (1) compared to the emission reductions in Figure 2.1, the cost reductions in Figure 2.4 are significantly smaller, and (2) the regions with high emission reduction potential, such as the Northeast and Pacific Northwest, are not the same as the regions with high cost reduction potential, such as the Southeast.

Table 2.3: Energy cost reduction sensitivities.

Parameter	η_h	η_c	$\tilde{\eta}_h$	$\tilde{\eta}_c$	π	$\tilde{\pi}$
Sensitivity	1.87	0.98	-2.37	-1.47	-1.37	2.37

2.2.4 Sensitivity analysis

We now analyze the sensitivity of the energy cost reduction (the left-hand side of Inequality (2.2)) to each parameter. Table 2.3 shows the sensitivities. To compute them, we used the approach discussed in §2.1.4. We used the nominal efficiencies in Table 2.1. We also used the 2016 United States average residential electricity price, $\pi = 0.103$ \$/kWh, the 2015–2019 United States average winter natural gas price, $\tilde{\pi} = 0.033$ \$/kWh, and the United States average heating and cooling loads for single-family homes from [85].

The energy cost reduction is increasing in η_h, η_c and $\tilde{\pi}$ and decreasing in $\tilde{\eta}_h$, $\tilde{\eta}_c$ and π. To maximize the energy cost reduction, therefore, we should target inefficient air conditioners and inefficient heating systems powered by expensive fuels. We should replace these systems with efficient heat pumps powered by cheap electricity.

In the neighborhood of the nominal parameter values, the energy cost reduction is most sensitive to $\tilde{\eta}_h$, $\tilde{\pi}$ and, to a lesser extent, η_h. This suggests that the characteristics of the incumbent heating system have the greatest influence on the energy cost reductions. The heat pump's heating COP is also influential.

2.2.5 Internalizing the cost of emissions

The economic analysis in this section includes the costs of hardware, installation, energy and maintenance, but leaves out the societal cost of greenhouse gas emissions. The cost of emissions can be internalized by penalizing emissions at a price π_g (\$/kg). The economic

analysis remains the same, with the energy prices redefined:

$$\pi \leftarrow \pi + \pi_{\mathrm{g}} \mu$$

$$\tilde{\pi} \leftarrow \tilde{\pi} + \pi_{\mathrm{g}} \tilde{\mu}.$$

There are also embodied emissions in the heat pump and the incumbent system due to manufacturing, shipping, *etc.* These can be internalized by redefining the capital costs:

$$c \leftarrow c + \pi_{\mathrm{g}} M$$

$$\tilde{c} \leftarrow \tilde{c} + \pi_{\mathrm{g}} \tilde{M}.$$

Here M (kg) and $\tilde{M}$ (kg) are the masses of CO_2-equivalent embodied in the heat pump and the incumbent system, respectively.

2.3 Economics of heat purchase agreements

In the previous section, we compared an incumbent heating and cooling system to a heat pump under the traditional ownership model. In this section, we compare the traditional ownership model to an HPA for the same heat pump.

Under an HPA, the user hosts a heat pump owned by an aggregator. The aggregator pays for the heat pump and installation labor, and receives any rebates, tax credits or other incentives. The aggregator also pays for the electricity the heat pump consumes. The user pays the aggregator an agreed-upon price for each unit of heating or cooling the heat pump produces, under the user's chosen temperature setpoints. The aggregator also absorbs the heat pump maintenance costs and sells the heat pump's flexibility in ancillary service markets.

2.3.1 User benefit

Under the traditional ownership model, the user's net present cost is

$$c + \gamma \left[\pi \left(\frac{Q_h}{\eta_h} + \frac{Q_c}{\eta_c} \right) + m \right].$$

Under an HPA, the user's net present cost is

$$\gamma \left(\pi_h Q_h + \pi_c Q_c \right).$$

Here π_h (\$/kWh$_t$) and π_c (\$/kWh$_t$) are the heating and cooling prices that the user and aggregator agree upon. The net present value of the HPA to the user is the net present cost reduction:

$$v_u := c + \gamma \left[\left(\frac{\pi}{\eta_h} - \pi_h \right) Q_h + \left(\frac{\pi}{\eta_c} - \pi_c \right) Q_c + m \right].$$

The HPA benefits the user if and only if $v_u \geq 0$, or, equivalently,

$$\frac{\pi_h Q_h + \pi_c Q_c}{Q_h + Q_c} \leq \overline{\pi}, \tag{2.3}$$

where

$$\begin{aligned} \overline{\pi} &:= \frac{1}{Q_h + Q_c} \left(\pi_h Q_h + \pi_c Q_c + \frac{v_u}{\gamma} \right) \\ &= \frac{1}{Q_h + Q_c} \left[\frac{c}{\gamma} + \pi \left(\frac{Q_h}{\eta_h} + \frac{Q_c}{\eta_c} \right) + m \right]. \end{aligned}$$

2.3.2 Aggregator benefit

We assume, for the sake of simplicity, that the aggregator discounts future cash flows at the same rate ρ as the user. Under this assumption, the aggregator's net present cost is

$$c_a + \gamma \left[\pi \left(\frac{Q_h}{\eta_h} + \frac{Q_c}{\eta_c} \right) + m_a \right],$$

where c_a (\$) and m_a (\$) are the aggregator's total installed cost and annual maintenance cost, respectively. The aggregator's net present revenue is

$$\gamma(\pi_h Q_h + \pi_c Q_c + r),$$

where r is the aggregator's annual ancillary service revenue for this heat pump. The net present value of the HPA to the aggregator is the net present profit:

$$v_a = -c_a + \gamma \left[\left(\pi_h - \frac{\pi}{\eta_h} \right) Q_h + \left(\pi_c - \frac{\pi}{\eta_c} \right) Q_c + r - m_a \right].$$

The HPA benefits the aggregator if and only if $v_a \geq 0$, or, equivalently,

$$\frac{\pi_h Q_h + \pi_c Q_c}{Q_h + Q_c} \geq \underline{\pi}, \tag{2.4}$$

where

$$\begin{aligned} \underline{\pi} &:= \frac{1}{Q_h + Q_c} \left(\pi_h Q_h + \pi_c Q_c - \frac{v_a}{\gamma} \right) \\ &= \frac{1}{Q_h + Q_c} \left[\frac{c_a}{\gamma} + \pi \left(\frac{Q_h}{\eta_h} + \frac{Q_c}{\eta_c} \right) + m_a - r \right]. \end{aligned}$$

2.3.3 Mutual benefit

The HPA is mutually beneficial to the user and the aggregator if and only if the inequalities (2.3) and (2.4) both hold:

$$\underline{\pi} \leq \frac{\pi_h Q_h + \pi_c Q_c}{Q_h + Q_c} \leq \overline{\pi}.$$

A necessary condition is that $\overline{\pi} \geq \underline{\pi}$. It is straightforward to show that

$$\overline{\pi} - \underline{\pi} = \frac{v_u + v_a}{\gamma(Q_h + Q_c)}.$$

Thus, $\overline{\pi} \geq \underline{\pi}$ if and only if $v \geq 0$, where

$$\begin{aligned} v &:= v_u + v_a \\ &= c - c_a + \gamma\,(m - m_a + r) \end{aligned}$$

is the total value of the HPA. We note that v is a weighted sum of three terms: the capital cost reduction $c - c_a$, the maintenance cost reduction $m - m_a$, and the ancillary service revenue r. Therefore, the value of the HPA is highest when the aggregator minimizes their installed and maintenance costs (for example, by buying heat pumps in bulk, hiring efficient installation and maintenance teams, and minimizing overhead) and maximizes their ancillary service revenue.

The following theorem summarizes these results.

Theorem 1 (Mutual benefit). *The HPA is mutually beneficial if and only if both of the following conditions hold:*

1. $v \geq 0$ *(or, equivalently,* $\underline{\pi} \leq \overline{\pi}$*), and*

2. π_h *and* π_c *are chosen such that*

$$\underline{\pi} \leq \frac{\pi_h Q_h + \pi_c Q_c}{Q_h + Q_c} \leq \overline{\pi}.$$

2.3.4 Pricing heat and cooling

We suppose that the total value of the HPA is nonnegative ($v \geq 0$), and that the aggregator and user negotiate the user's share $\phi \in [0, 1]$ of the value:

$$v_u = \phi v, \quad v_a = (1 - \phi)v.$$

To ensure mutual benefit, it follows that π_h and π_c must satisfy

$$\frac{\pi_h Q_h + \pi_c Q_c}{Q_h + Q_c} = \phi\underline{\pi} + (1-\phi)\overline{\pi}.$$

This is one linear equation in the two prices π_h and π_c. A second equation is needed to resolve the prices. A simple choice is to make the heating and cooling prices equal:

$$\pi_h = \pi_c = \phi\underline{\pi} + (1-\phi)\overline{\pi}.$$

Of course, infinitely many other price choices could guarantee mutual benefit. For example, π_h and π_c could be chosen such that the aggregator's revenue from heating and cooling are equal:

$$\pi_h Q_h = \pi_c Q_c = \frac{(Q_h + Q_c)\left[\phi\underline{\pi} + (1-\phi)\overline{\pi}\right]}{2}.$$

In cold climates, this results in a much lower price of heating than cooling.

The following corollary summarizes these results.

Corollary 2 (Thermal prices). *Suppose $v \geq 0$ and the user and aggregator negotiate the user's share $\phi \in [0,1]$ of v. Then the HPA is mutually beneficial if and only if π_h and π_c satisfy*

$$\frac{\pi_h Q_h + \pi_c Q_c}{Q_h + Q_c} = \phi\underline{\pi} + (1-\phi)\overline{\pi}.$$

2.3.5 Comparison to incumbent systems

So far in this section, we have considered the case where the user compares an HPA to the traditional ownership model for the same heat pump. We now consider the case where the user compares an HPA for a heat pump to a traditionally-owned incumbent heating and cooling system.

Theorem 1 and Corollary 2 apply directly to this case; we only need to update the user's net present value v_u and the terms that depend on it. The user's net present cost under the incumbent system is

$$\tilde{c} + \gamma \left(\frac{\tilde{\pi} Q_h}{\tilde{\eta}_h} + \frac{\pi Q_c}{\tilde{\eta}_c} + \tilde{m} \right).$$

The user's net present value of the HPA is the net present cost reduction:

$$v_u = \tilde{c} + \gamma \left[\left(\frac{\tilde{\pi}}{\tilde{\eta}_h} - \pi_h \right) Q_h + \left(\frac{\pi}{\tilde{\eta}_c} - \pi_c \right) Q_c + \tilde{m} \right].$$

Therefore, the upper price threshold is

$$\begin{aligned} \overline{\pi} &:= \frac{1}{Q_h + Q_c} \left(\pi_h Q_h + \pi_c Q_c + \frac{v_u}{\gamma} \right) \\ &= \frac{1}{Q_h + Q_c} \left(\frac{\tilde{c}}{\gamma} + \frac{\tilde{\pi} Q_h}{\tilde{\eta}_h} + \frac{\pi Q_c}{\tilde{\eta}_c} + \tilde{m} \right). \end{aligned}$$

Similarly, the value of the HPA is

$$\begin{aligned} v &:= v_u + v_a \\ &= \tilde{c} - c_a + \gamma \left[\left(\frac{\tilde{\pi}}{\tilde{\eta}_h} - \frac{\pi}{\eta_h} \right) Q_h + \pi \left(\frac{1}{\tilde{\eta}_c} - \frac{1}{\eta_c} \right) Q_c + \tilde{m} - m_a + r \right]. \end{aligned} \tag{2.5}$$

Thus, the HPA is mutually beneficial if and only if

$$\left(\frac{\tilde{\pi}}{\tilde{\eta}_h} - \frac{\pi}{\eta_h} \right) Q_h + \pi \left(\frac{1}{\tilde{\eta}_c} - \frac{1}{\eta_c} \right) Q_c + r \geq \frac{c_a - \tilde{c}}{\gamma} + m_a - \tilde{m} \tag{2.6}$$

and π_h and π_c satisfy condition 2 of Theorem 1.

Inequality (2.6) holds if the energy cost reduction and ancillary service revenue outweigh the (potentially) increased capital and maintenance costs. This is analogous to Inequality

(2.2), which covers the case where the user compares a traditionally-owned heat pump to an incumbent system. The differences are the following.

1. The left-hand side of (2.6) includes the aggregator's ancillary service revenue r.

2. The right-hand side of (2.6) includes the aggregator's installed and maintenance costs, c_a and m_a, rather than the user's costs c and m as in (2.2).

Thus, the additional value of the HPA, above and beyond the value of a traditionally-owned heat pump, is maximized under the same conditions discussed in §2.3.3. Namely, when the aggregator minimizes their installed and maintenance costs and maximizes their ancillary service revenue.

2.4 Numerical examples

In this section, we analyze the emissions and economics of a heat pump and an incumbent heating and cooling system through Monte Carlo simulation. We consider an unfavorable state (Colorado), a typical state (Pennsylvania), and a favorable state (Washington). By 'favorable', we mean that the price and greenhouse gas intensity of electricity are relatively low, while the natural gas price is relatively high.

The basic purpose of this section is to illustrate the analysis developed above. While the input data reflect our best efforts at accuracy, we acknowledge that there is significant uncertainty in some parameters, such as the user's installed and maintenance costs. These parameters include the contractor's internal equipment costs, which may differ substantially from the retail equipment costs available online, as well as their labor costs, overhead and profit. Installers tend not to share these data, so we resort to Internet sources and conversations with practitioners. This approach is fairly common in similar research; see, *e.g.*, [11, 12]. We discuss the input data further in §2.4.2.

2.4.1 Scenarios

In all states, we consider a typical two-story home with 200 m^2 of conditioned floor area. We assume that the home has a functioning forced-air natural gas furnace with distribution ducts in unconditioned space. The heating system is of typical age and efficiency for existing construction. The user wants to add cooling to their building.

The incumbent cooling system is a new central air conditioner. In the incumbent scenario, the existing natural gas furnace meets all of the heating load. The new central air conditioner meets all of the cooling load.

As an alternative, the user also considers installing two ductless mini-split heat pumps, one per story. Each heat pump consists of one indoor unit and one outdoor unit. In the heat pump scenarios, the heat pumps meet all of the cooling load and 90% of the heating load. The remaining 10% of the heating load is met by the natural gas furnace.

2.4.2 Parameter values

We model the parameters as independent, uniform random variables whose distributions are supported on the intervals discussed in §2.1.1 and §2.2.1. Uniform distributions are considered appropriate for cases such as this, where the true parameter distributions are unknown but plausible ranges are available. [89] We base uniform distribution supports on the sources discussed in §2.1.1–2.1.2 and §2.2.1–2.2.2.

Heating and cooling loads

Colorado, Pennsylvania and Washington all lie primarily in the Cold/Very Cold climate zone. [90] In all states, therefore, the heating and cooling loads match survey data for single-family homes in this climate zone. [85] The nominal heating and cooling loads are 11450 kWh_t and 3500 kWh_t, respectively. In simulations, we assume that the heating and cooling loads are

uniformly distributed within ±15% of these nominal values.

The source [85] is a product of the United States Energy Information Agency's Office of Independent Statistics & Analysis. The data are obtained from the Residential Energy Consumption Survey, which periodically collects energy-usage data and related building characteristics from a nationally-representative sample of United States homes. We use data from 2015, the most recent year available. In [85], heating and cooling load data are reported by climate zone; as discussed above, we use the Cold/Very Cold data. The survey data in [85] are fairly high-fidelity, as they represent the actual usage of existing homes. However, the only survey data statistics reported are the sample means; no further distributional information is available. For this reason, we resort to assuming uniform distributions centered on the sample means with ±15% variation.

Greenhouse gas intensities and prices

We treat the greenhouse gas intensity of natural gas from [83], $\tilde{\mu} = 0.181$ kg/kWh, as deterministic. The greenhouse gas intensities of electricity vary within ±10% of the nominal values of 0.67 kg/kWh in Colorado, 0.39 kg/kWh in Pennsylvania, and 0.085 kg/kWh in Washington. [84] The natural gas prices vary within ±10% of the nominal values of 0.025 $/kWh in Colorado, 0.0396 $/kWh in Pennsylvania, and 0.039 $/kWh in Washington. [88] The electricity prices vary within ±10% of the nominal values of 0.098 $/kWh in Colorado, 0.102 $/kWh in Pennsylvania, and 0.077 $/kWh in Washington. [87] For more discussion on the price and greenhouse gas intensity data sources, see §2.1.2 and §2.2.2.

Incumbent system

The installed and maintenance costs of the incumbent system cover the central air conditioner only, as the heat pumps would displace natural gas fuel use rather than replacing the furnace outright. The central air conditioner installed cost ranges from $4000–6000. The annual

maintenance cost ranges from \$50–100. The heating system efficiency, including the existing furnace and ducts, ranges from 60% to 80%. The seasonal cooling COP, including the new central air conditioner and the existing ducts, ranges from 2.5 to 3.8. The central air conditioner lifetime ranges from 10 to 20 years, while the user's discount rate ranges from 5% to 15%; the value of γ, therefore, ranges from 5 to 12.5.

While the incumbent system lifetimes and COPs are based on the fairly rigorous research underlying [81], we acknowledge that there is significant uncertainty in the cost data. We estimate the installed and maintenance costs based on homeowner and installer testimony on websites such as greenbuildingadvisor.com and homewyze.com and our conversations with practitioners. This approach is consistent with the Rocky Mountain Institute study [11] (see page 65), which considers heat pump economics and emissions. We resort to this approach because accurate installer cost data is difficult to find. This difficulty is likely due to installers' preference for keeping such data private, as it could adversely affect their market competitiveness.

Heat pumps

The heat pumps' seasonal heating COP ranges from 2.6 to 2.9. Their seasonal cooling COP ranges from 3.7 to 4.3. We assume that the heat pumps' lifetime equals that of the central air conditioner. The user's installed cost c ranges from \$8000 to \$10000. The aggregator's installed cost c_a ranges from \$6000 to \$7500. The user's annual heat pump maintenance cost m ranges from \$75 to \$125. The aggregator's annual maintenance cost ranges from \$50 to \$100. (We recall that c and m include the installer's profit, while c_a and m_a do not.) The aggregator's annual ancillary service revenue, from the two heat pumps combined, ranges from \$50 to \$100. The ancillary service revenue range is based on [68].

We emphasize that, as with the incumbent system costs, there is significant uncertainty in the heat pump installed and maintenance cost estimates. Following [11], we base these

estimates on homeowner and installer testimony in websites such as greenbuildingadvisor.com and homewyze.com and our own conversations with practitioners.

Heat purchase agreement

We assume that the benefit of the HPA is shared equally between the user and aggregator ($\phi = 0.5$), and that the heat and cooling prices are chosen to be equal. Under these assumptions, the heat and cooling prices are $\pi_h = \pi_c = (\overline{\pi} - \underline{\pi})/2$. We emphasize that the choice of $\phi = 0.5$ models a case where the value of the heat purchase agreement – which includes the incumbent installer's profit margin – is shared equally between the user and the aggregator. In practice, a nonprofit aggregator would likely set $\phi = 1$, allocating all value to the user, while an aggregator charging as much as the market can bear would set $\phi = 0$, allocating all value to the aggregator. We also assume that the aggregator's discount rate equals the user's.

2.4.3 Results

We now present the results of 10^6 Monte Carlo simulations. With this sample size, the estimated means and quantiles are accurate to within 0.1%. For each state and simulation, we calculate the annual emission reduction, the net present value of a traditionally-owned heat pump, and the user's net present value under a heat pump HPA.

Figure 2.5 shows histograms of the annual emission reduction in each state. The mean annual emission reductions are 451 kg (11.7%) in Colorado, 1507 kg (43.8%) in Pennsylvania, and 2659 kg (86.3%) in Washington. For reference, a typical car emits about 400 kg per thousand miles driven.

Figure 2.6 shows histograms of the net present value of the user's heat pump investment in each state, under both the traditional ownership model (top row) and an HPA (bottom

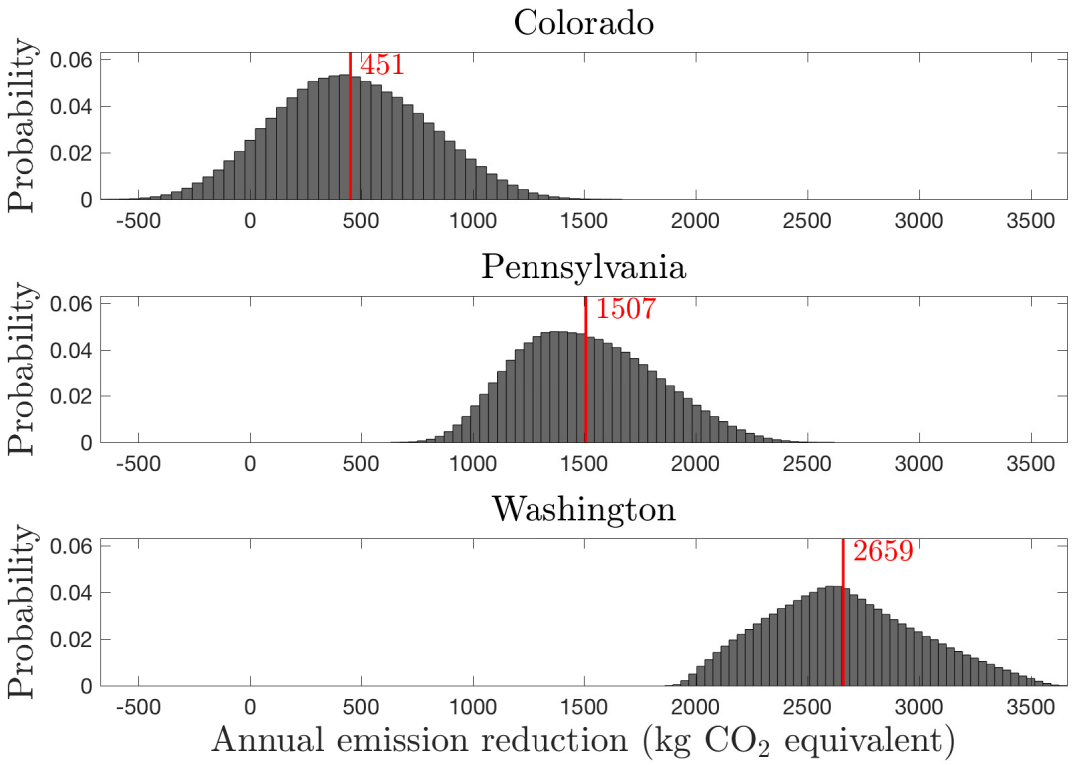

Figure 2.5: Histograms of the annual mass of greenhouse gas emission reduction from adopting a heat pump instead of the incumbent heating and cooling system. Red lines indicate mean values.

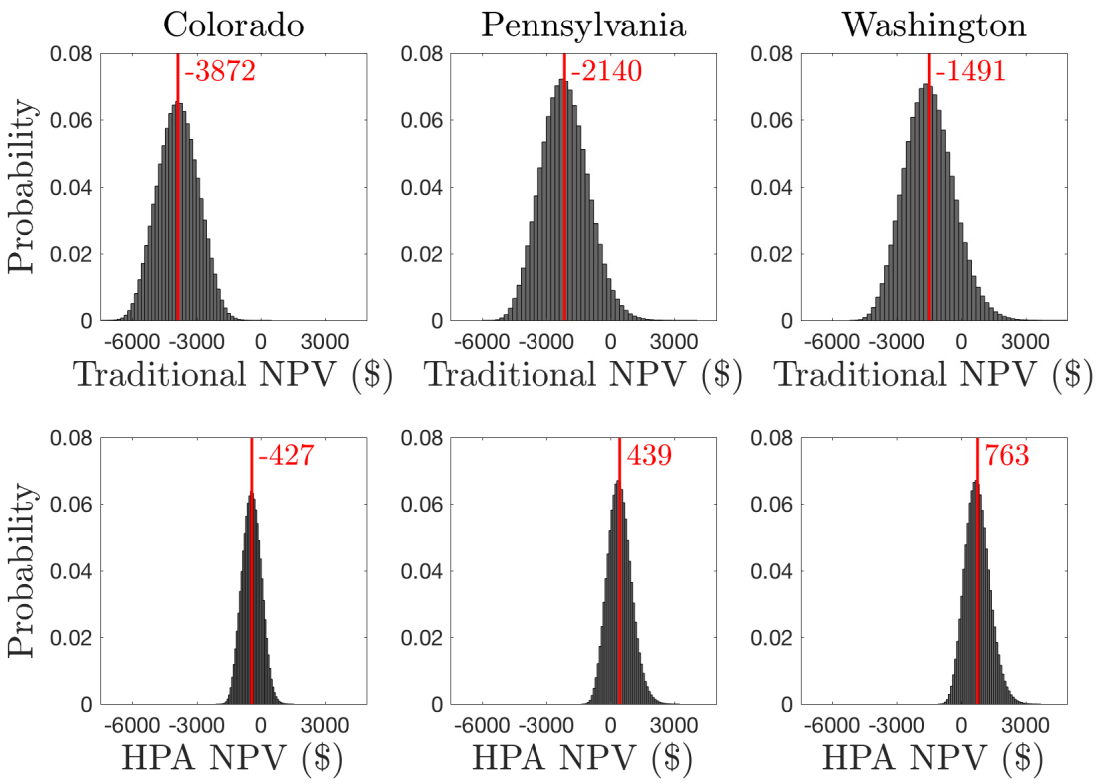

Figure 2.6: Histograms of the net present value of the user's heat pump investment under the traditional ownership model (top row) and an HPA (bottom row). Red lines indicate mean values.

row). The key message of this figure is that in the typical and favorable states, the HPA brings the user's heat pump investment into the black. In Pennsylvania and Washington, the HPA increases the net present value of the user's heat pump investment from −$2,140 and −$1,491 to $439 and $763, respectively.

A second message of Figure 2.6 is that the HPA reduces the risk associated with the user's investment. This can be seen from the narrowing of the empirical distributions from the top row to the bottom row. In Colorado, Pennsylvania and Washington, the HPA decreases the probability that the user loses money on the heat pump investment from 100%, 97% and 90% to 83%, 22%, and 8%, respectively.

The value of the ancillary service revenue is small but not insignificant. Without the ancillary service revenue, the user's expected net present value of the HPA decreases by \$288. On average, the ancillary service revenue γr makes up 20.2% of the value

$$v = c - c_a + \gamma(m - m_a + r)$$

of the HPA. The majority of the value (73.4%) is due to the capital cost reduction, $c - c_a$. The remaining 6.4% of the value is due to the maintenance cost reduction, $\gamma(m - m_a)$. These values are essentially constant across the three states.

2.5 Generalization of economic analyses

The economic analyses in §2.2–2.3 entail the following simplifying assumptions:

1. The salvage values of the heat pump and incumbent system are negligible.
2. The annual heating and cooling loads, COPs, prices and maintenance costs and ancillary service revenues are constant over the project lifetime.
3. The user and aggregator discount future cash flows at the same rate.

In this section, we relax these assumptions and revisit the economic analyses. We keep discussion to a minimum, as the definitions and arguments in this section parallel those in §2.2–2.3. To keep notation light, we still assume that the lifetimes of the heat pump and the incumbent system are equal, and that efficiencies are constant over the equipment lifetime. These assumptions can also be relaxed.

2.5.1 Traditional heat pump ownership

In the general setting, the net present heat pump cost is

$$c + \sum_{i=1}^{Y} \frac{1}{(1+\rho)^i} \left[\pi_i \left(\frac{Q_{hi}}{\eta_h} + \frac{Q_{ci}}{\eta_c} \right) + m_i \right] - \frac{v_s}{(1+\rho)^Y}.$$

Here $i = 1, \ldots, Y$ indexes the years of the heat pump's life. In year i, Q_{hi} (kWh_t) and Q_{ci} (kWh_t) are the total heating and cooling loads, π_i (\$/kWh) is the electricity price and m_i (\$) is the maintenance cost. The salvage value v_s (\$) is the remaining value of the heat pump after year Y. In vector-matrix form, the net present heat pump cost can be written as

$$c + \gamma^\top \left[\left(\frac{1}{\eta_h} Q_h + \frac{1}{\eta_c} Q_c \right) \pi + m \right] - s,$$

where

$$\gamma := \begin{bmatrix} (1+\rho)^{-1} \\ \vdots \\ (1+\rho)^{-Y} \end{bmatrix}, \quad \pi := \begin{bmatrix} \pi_1 \\ \vdots \\ \pi_Y \end{bmatrix}, \quad m := \begin{bmatrix} m_1 \\ \vdots \\ m_Y \end{bmatrix}, \quad s := \frac{v_s}{(1+\rho)^Y}$$

$$Q_h := \begin{bmatrix} Q_{h1} & & \\ & \ddots & \\ & & Q_{hY} \end{bmatrix}, \quad Q_c := \begin{bmatrix} Q_{c1} & & \\ & \ddots & \\ & & Q_{cY} \end{bmatrix}.$$

Similarly, the net present cost of the incumbent system is

$$\tilde{c} + \sum_{i=1}^{Y} \frac{1}{(1+\rho)^i} \left[\left(\frac{\tilde{\pi}_i Q_{hi}}{\tilde{\eta}_h} + \frac{\pi_i Q_{ci}}{\tilde{\eta}_c} \right) + \tilde{m}_i \right] - \frac{\tilde{v}_s}{(1+\rho)^Y}.$$

Here $\tilde{\pi}_i$ (\$/kWh) and $\tilde{m}_i$ (\$) are the incumbent heating fuel price and maintenance cost in year i, respectively. In vector-matrix form, the net present incumbent system cost can be

written as

$$\tilde{c} + \gamma^\top \left(\frac{1}{\tilde{\eta}_h} Q_h \tilde{\pi} + \frac{1}{\tilde{\eta}_c} Q_c \pi + \tilde{m} \right) - \tilde{s},$$

where

$$\tilde{\pi} := \begin{bmatrix} \tilde{\pi}_1 \\ \vdots \\ \tilde{\pi}_Y \end{bmatrix}, \quad \tilde{m} := \begin{bmatrix} \tilde{m}_1 \\ \vdots \\ \tilde{m}_Y \end{bmatrix}, \quad \tilde{s} := \frac{\tilde{v}_s}{(1+\rho)^Y}.$$

The net present value of the user's heat pump investment under the traditional ownership model is the net present cost reduction:

$$\tilde{c} - c + \gamma^\top \left[Q_h \left(\frac{1}{\tilde{\eta}_h} \tilde{\pi} - \frac{1}{\eta_h} \pi \right) + Q_c \left(\frac{1}{\tilde{\eta}_c} - \frac{1}{\eta_c} \right) \pi + \tilde{m} - m \right] - \tilde{s} + s.$$

The traditional heat pump investment is attractive if the net present value is nonnegative. This occurs if and only if the energy cost reductions outweigh the (potentially) increased installed cost, increased maintenance costs, and decreased salvage value:

$$\gamma^\top \left[Q_h \left(\frac{1}{\tilde{\eta}_h} \tilde{\pi} - \frac{1}{\eta_h} \pi \right) + Q_c \left(\frac{1}{\tilde{\eta}_c} - \frac{1}{\eta_c} \right) \pi \right] \geq c - \tilde{c} + \gamma^\top (m - \tilde{m}) + \tilde{s} - s.$$

2.5.2 Heat purchase agreements vs. traditional ownership

User benefit

The user's net present cost under the HPA is

$$\gamma^\top (Q_h \pi_h + Q_c \pi_c) - s,$$

where

$$\pi_h := \begin{bmatrix} \pi_{hi} \\ \vdots \\ \pi_{hY} \end{bmatrix}, \quad \pi_c := \begin{bmatrix} \pi_{ci} \\ \vdots \\ \pi_{cY} \end{bmatrix}.$$

Here π_{hi} and π_{ci} are the heating and cooling prices in year i. We assume that ownership of the heat pump transfers from the aggregator to the user at the end of year Y, so the discounted salvage value s goes to the user.

The net present value of the HPA to the user is the net present cost reduction, with respect to traditional heat pump ownership:

$$c + \gamma^\top \left[Q_h \left(\frac{1}{\eta_h} \pi - \pi_h \right) + Q_c \left(\frac{1}{\eta_c} \pi - \pi_c \right) + m \right].$$

The HPA is attractive to the user if the net present value is nonnegative. This occurs if and only if the heat and cooling prices are not too high:

$$\gamma^\top \left(Q_h \pi_h + Q_c \pi_c \right) \leq c + \gamma^\top \left[\left(\frac{1}{\eta_h} Q_h + \frac{1}{\eta_c} Q_c \right) \pi + m \right]. \tag{2.7}$$

Aggregator benefit

The net present value of the HPA to the aggregator is their net present profit:

$$-c_a + \gamma_a^\top \left[Q_h \left(\pi_h - \frac{1}{\eta_h} \pi \right) + Q_c \left(\pi_c - \frac{1}{\eta_c} \pi \right) + r - m_a \right],$$

where

$$\gamma_a := \begin{bmatrix} (1+\rho_a)^{-1} \\ \vdots \\ (1+\rho_a)^{-Y} \end{bmatrix}, \quad r := \begin{bmatrix} r_1 \\ \vdots \\ r_Y \end{bmatrix}, \quad m_a := \begin{bmatrix} m_{a1} \\ \vdots \\ m_{aY} \end{bmatrix}.$$

The parameters ρ_a, r_{ai}, and m_{ai} are the aggregator's discount rate, ancillary service revenue in year i, and maintenance cost in year i, respectively. The HPA is attractive to the aggregator if and only if the heat and cooling prices are not too low:

$$\gamma_a^\top \left(Q_h \pi_h + Q_c \pi_c\right) \geq c_a + \gamma_a^\top \left[\left(\frac{1}{\eta_h} Q_h + \frac{1}{\eta_c} Q_c\right) \pi + m_a - r\right]. \tag{2.8}$$

Mutual benefit

The HPA is mutually beneficial to the user and the aggregator if and only if Inequalities (2.7) and (2.8) both hold. This condition can be simplified further under some additional assumptions, such as the inequalities holding component-wise, but we do not pursue these simplifications here. We note only that the mutual benefit condition is structurally similar to that discussed in Theorem 1. The thermal prices must be chosen to lie in certain polyhedral sets determined by the user's and aggregator's requirements, and these sets must be nonempty.

2.5.3 Heat purchase agreements vs. incumbent systems

When comparing an HPA for a heat pump to a traditionally-owned incumbent system, the net present value of the HPA to the user is the net present cost reduction:

$$\tilde{c} + \gamma^\top \left[Q_h \left(\frac{1}{\tilde{\eta}_h} \tilde{\pi} - \pi_h\right) + Q_c \left(\frac{1}{\tilde{\eta}_c} \pi - \pi_c\right) + \tilde{m}\right] + s - \tilde{s}.$$

In this setting, the HPA is attractive to the user if and only if

$$\gamma^\top \left(Q_h \pi_h + Q_c \pi_c\right) \leq \tilde{c} + \gamma^\top \left(\frac{1}{\tilde{\eta}_h} Q_h \tilde{\pi} + \frac{1}{\tilde{\eta}_c} Q_c \pi + \tilde{m}\right) + s - \tilde{s}. \tag{2.9}$$

The HPA is mutually beneficial if and only if Inequalities (2.8) and (2.9) both hold.

Chapter 3

Physical modeling

In this chapter, we discuss physical modeling of heat pumps and thermal loads. This discussion is relevant to defining several parameters used in the high-level analyses of emissions and economics in Chapter 2. It is also relevant to Chapters 4 and 5, where we consider the problems of heat pump selection and control. The two purposes of this chapter are to provide background on the physics of heat pumps and thermal loads, and to develop heat pump and thermal load models for use in optimization and control in the sequel.

3.1 Heat pumps

As illustrated in Figure 3.1, a heat pump moves heat from a cold thermal reservoir at temperature T_{cold} (°K) to a hot one at temperature $T_{\text{hot}} > T_{\text{cold}}$ (°K). More specifically, a heat pump operates a thermodynamic cycle that uses work $W > 0$ (kWh) to extract heat $Q_{\text{cold}} > 0$ (kWh_t) from the cold reservoir and inject heat $Q_{\text{hot}} > 0$ (kWh_t) into the hot reservoir. The cold and hot thermal reservoirs have different interpretations depending on whether the heat pump is used for heating or cooling. Table 3.1 provides some concrete examples.

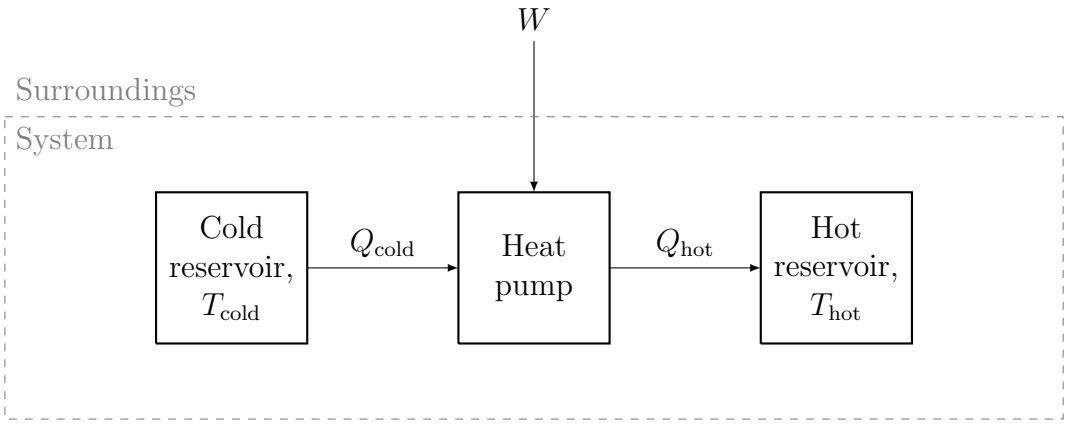

Figure 3.1: A heat pump uses work W to extract heat Q_{cold} from a cold thermal reservoir and inject heat Q_{hot} into a hot one.

Table 3.1: Interpretations of the cold and hot reservoirs for some common devices.

Heat pump device	Cold reservoir	Hot reservoir
Refrigerator	Refrigerator air	Kitchen air
Air-source heat pump (summer)	Indoor air	Outdoor air
Air-source heat pump (winter)	Outdoor air	Indoor air
Heat pump water heater	Outdoor air	Indoor water
Chiller	Indoor water	Outdoor air
Geothermal heat pump (winter)	Ground	Indoor air
Geothermal heat pump (summer)	Indoor air	Ground

3.1.1 Efficiency, capacity and temperature

A heat pump's energy efficiency is characterized by its *coefficient of performance* (COP) η, defined as the ratio of the output heating or cooling, $Q > 0$ (kWh_t), to the input work:

$$\eta = \frac{Q}{W}.$$

The COP is a dimensionless positive real number. The interpretation of Q depends on whether the heat pump is used for heating or cooling:

$$Q = \begin{cases} Q_{\text{hot}} & \text{for heating} \\ Q_{\text{cold}} & \text{for cooling.} \end{cases}$$

By the first law of thermodynamics,

$$Q_{\text{cold}} + W = Q_{\text{hot}}.$$

Since $W > 0$, we have $Q_{\text{hot}} - Q_{\text{cold}} > 0$, so the COP can be written as

$$\eta = \frac{Q}{Q_{\text{hot}} - Q_{\text{cold}}} = \begin{cases} Q_{\text{hot}}/(Q_{\text{hot}} - Q_{\text{cold}}) & \text{for heating} \\ Q_{\text{cold}}/(Q_{\text{hot}} - Q_{\text{cold}}) & \text{for cooling.} \end{cases} \tag{3.1}$$

The Carnot limit

A heat pump's COP depends fundamentally on the temperatures of the cold and hot thermal reservoirs. For any $(T_{\text{cold}}, T_{\text{hot}})$ pair, the theoretical upper limit on the COP, called the Carnot limit and denoted by $\eta^\star$, is given by an ideal heat pump. The Carnot limit is unattainable in practice, but provides useful intuition into the temperature dependence of a real heat pump's COP. An ideal heat pump generates no entropy, so by the second law of thermodynamics,

$$\frac{Q^\star_{\text{hot}}}{T_{\text{hot}}} - \frac{Q^\star_{\text{cold}}}{T_{\text{cold}}} = 0.$$

Substituting this expression into into Equation (3.1) gives the Carnot limit,

$$\eta^\star = \begin{cases} Q^\star_{\text{hot}}/(Q^\star_{\text{hot}} - Q^\star_{\text{cold}}) = T_{\text{hot}}/(T_{\text{hot}} - T_{\text{cold}}) & \text{for heating} \\ Q^\star_{\text{cold}}/(Q^\star_{\text{hot}} - Q^\star_{\text{cold}}) = T_{\text{cold}}/(T_{\text{hot}} - T_{\text{cold}}) & \text{for cooling.} \end{cases}$$

Temperature dependence in the Carnot limit

For both heating and cooling, $\eta^\star \to \infty$ as $|T_{\text{hot}} - T_{\text{cold}}| \to 0$. This means that an ideal heat pump is more efficient when the driving temperature difference is smaller. For both heating and cooling, we also have

$$\frac{\partial \eta^\star}{\partial T_{\text{cold}}} = \frac{T_{\text{hot}}}{(T_{\text{hot}} - T_{\text{cold}})^2} > 0$$
$$\frac{\partial \eta^\star}{\partial T_{\text{hot}}} = \frac{-T_{\text{cold}}}{(T_{\text{hot}} - T_{\text{cold}})^2} < 0.$$

Therefore, $\eta^\star$ is always increasing in T_{cold} and decreasing in T_{hot}. This implies, for example, that space heating with an (ideal) air-source heat pump is more efficient when the outdoor air is warmer ($T_{\text{cold}} \uparrow$), and when the indoor air temperature setpoint is lower ($T_{\text{hot}} \downarrow$). We will now show that the COPs of non-ideal heat pumps exhibit similar temperature dependence.

Temperature dependence of non-ideal heat pumps

Only an ideal heat pump attains the Carnot limit. Any real heat pump generates entropy $S > 0$ ($\text{kWh}_\text{t}/^\circ\text{K}$) in the system (*i.e.*, inside the dashed gray rectangle in Figure 3.1). By the second law of thermodynamics, for a non-ideal heat pump,

$$\frac{Q_{\text{hot}}}{T_{\text{hot}}} - \frac{Q_{\text{cold}}}{T_{\text{cold}}} = S.$$

Rearranging this equation gives

$$\frac{Q_{\text{cold}}}{Q_{\text{hot}}} = (1 + \gamma_{\text{hot}}) \frac{T_{\text{cold}}}{T_{\text{hot}}}$$

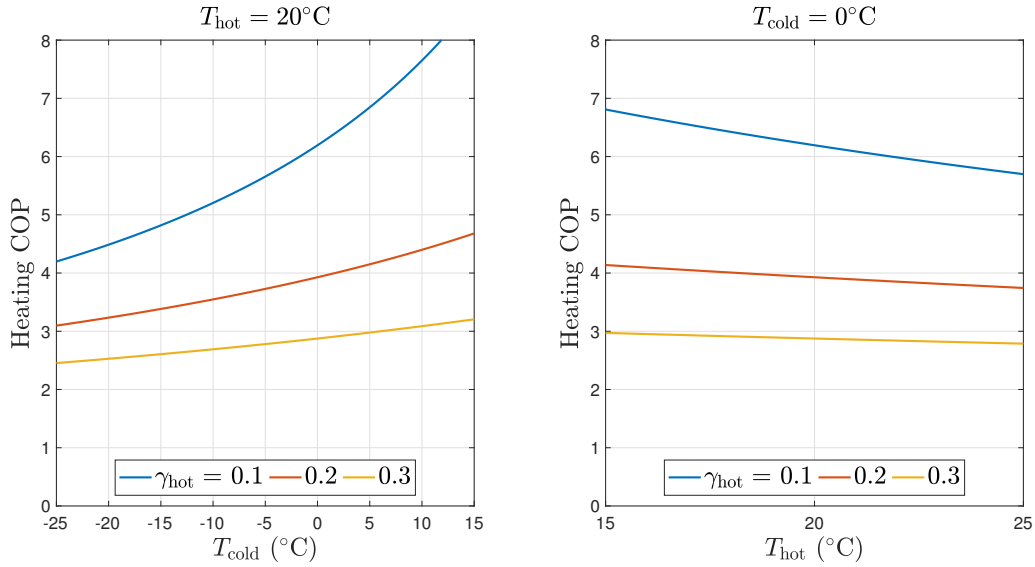

Figure 3.2: Heating COP of a hypothetical, non-ideal heat pump. Left: COP vs. cold reservoir (*e.g.*, indoor air) temperature. Right: COP vs. hot reservoir (*e.g.*, outdoor air) temperature. Performance approaches the Carnot limit as $\gamma_{\text{hot}} \to 0$.

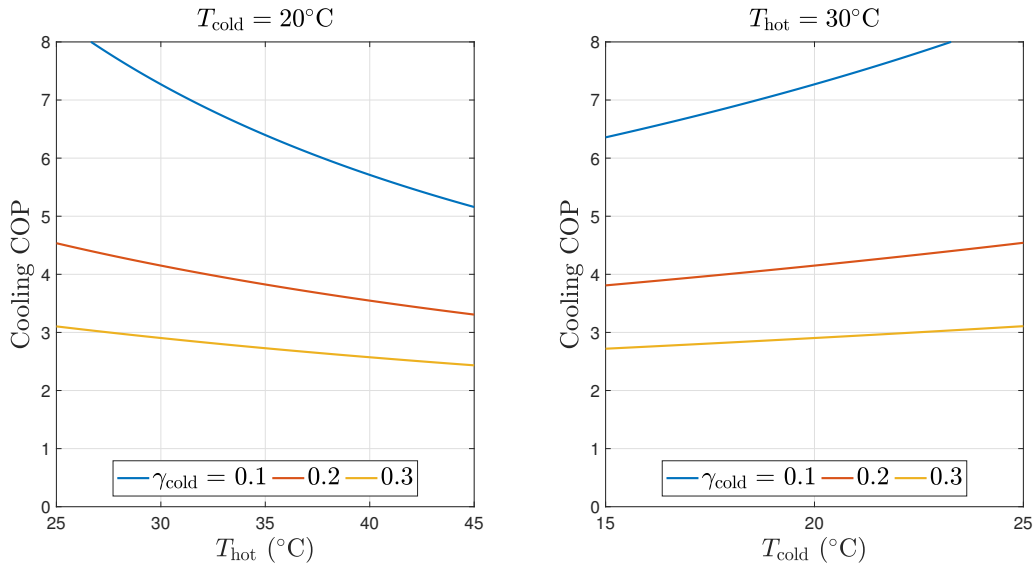

Figure 3.3: Cooling COP of a hypothetical, non-ideal heat pump. Left: COP vs. hot reservoir (*e.g.*, indoor air) temperature. Right: COP vs. cold reservoir (*e.g.*, outdoor air) temperature. Performance approaches the Carnot limit as $\gamma_{\text{cold}} \to 0$.

and

$$\frac{Q_{\text{hot}}}{Q_{\text{cold}}} = (1 - \gamma_{\text{cold}}) \frac{T_{\text{hot}}}{T_{\text{cold}}},$$

where

$$\gamma_{\text{hot}} = \frac{ST_{\text{hot}}}{Q_{\text{hot}}}, \quad \gamma_{\text{cold}} = \frac{ST_{\text{cold}}}{Q_{\text{cold}}}.$$

Substituting these expressions into Equation (3.1), we have

$$\eta = \begin{cases} T_{\text{hot}}/(T_{\text{hot}} - (1 - \gamma_{\text{hot}})T_{\text{cold}}) & \text{for heating} \\ T_{\text{cold}}/((1 + \gamma_{\text{cold}})T_{\text{hot}} - T_{\text{cold}}) & \text{for cooling.} \end{cases} \tag{3.2}$$

These formulas suggest that the COP η of a non-ideal heat pump exhibits similar temperature dependence to the Carnot limit.

The parameters γ_{hot} and γ_{cold} are always positive, since $S > 0$, and vanish as $S \to 0$. In this limit, the heating and cooling COPs in Equation (3.2) approach their respective Carnot limits. For a modern heat pump, γ_{hot} and γ_{cold} are typically on the order of 0.1. [91] Figures 3.2 and 3.3 illustrate the dependence of the heating and cooling COPs, respectively, on T_{hot}, T_{cold}, γ_{hot} and γ_{cold} over typical operating ranges. As the parameters γ_{hot} and γ_{cold} grow, the COPs become smaller and less sensitive to temperature changes.

Capacity

A heat pump's *capacity* $\dot{Q}$ (kW_t) is its thermal power output. Assuming the heat pump's thermodynamic cycle lasts a duration $\Delta t > 0$ (h), and that T_{cold}, T_{hot}, Q_{cold}, Q_{hot} and W are constant, the heat pump provides the (steady-state) thermal power

$$\dot{Q} = \frac{Q}{\Delta t} = \frac{\eta W}{\Delta t}.$$

This equation suggests that a heat pump's capacity should depend on the hot and cold reservoir temperatures through the COP η. Empirical data show that this is indeed the case, as we discuss in §3.1.3.

3.1.2 Heat pumps in practice: vapor compression

In the preceding discussion, we took an abstract view of heat pumps. We now discuss heat pumps in more concrete terms, with an eye toward implementation in hardware. We present empirical data from heat pump manufacturers in §3.1.3. As a prelude to the empirical data, we first briefly review the most common heat pump hardware implementation. This is the vapor compression cycle illustrated in Figure 3.4.

Vapor compression heat pumps move heat by circulating a refrigerant between the warmer and cooler thermal reservoirs. The main components of a vapor compression heat pump are the evaporator, compressor, condenser and expansion valve. In the evaporator, the refrigerant changes phase from liquid to gas. This phase change absorbs heat from the cooler reservoir, just as boiling water absorbs heat from a stove. The compressor increases the refrigerant's pressure and temperature. In the condenser, the refrigerant changes phase from gas to liquid, releasing heat to the warmer reservoir. The refrigerant then flows through an expansion valve, which decreases its pressure and temperature, and the cycle repeats.

Energy use

Vapor compression heat pumps use energy primarily in the compressor. They may also use energy in fans or pumps at the evaporator or condenser. These fans or pumps circulate air or water over the heat exchangers to accelerate transfer. In electric heat pumps, the compressors, fans and pumps are driven by electric motors.

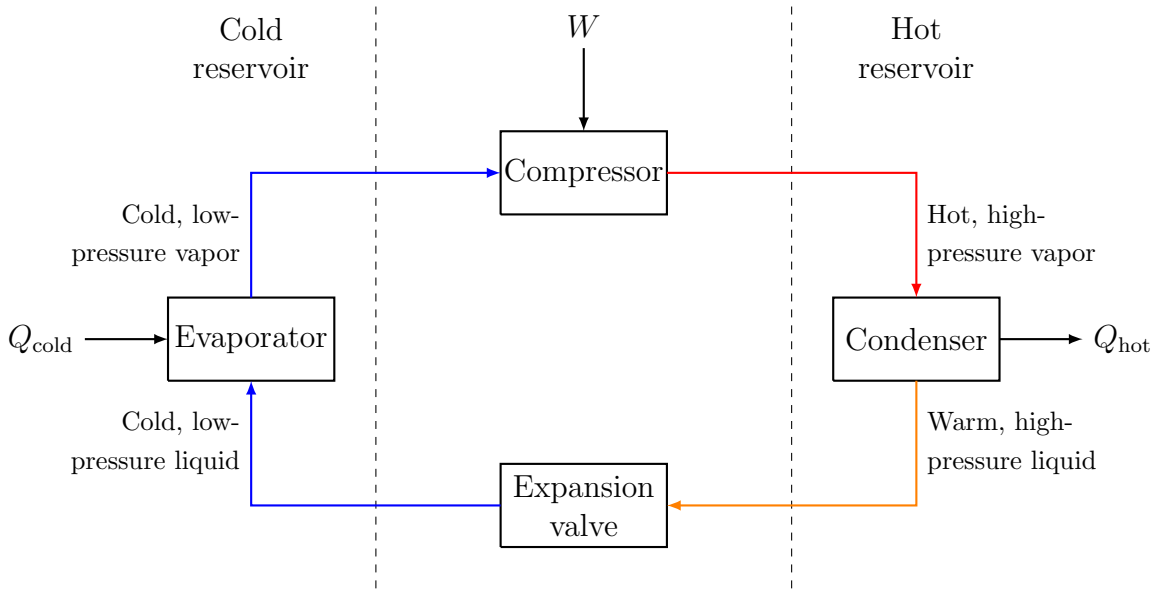

Figure 3.4: The vapor compression cycle of a typical heat pump.

3.1.3 Manufacturer data

In this section, we present empirical data published by the manufacturer of a popular line of heat pumps. [9, 92] We discuss the data primarily in the captions of Figures 3.7–3.12. First, we discuss the hardware scope, the relevant terminology, the input data, and the key take-away points.

Hardware scope

Each heat pump in the product line presented here can be described as follows.

- *Reversible.* The heat pump can provide both heating and cooling.
- *Air-to-air.* The heat pump moves heat between the indoor and outdoor air.
- *Electric.* The compressor and fan motors are powered by electricity.
- *Variable-speed.* The compressor and fan motors can modulate continuously, rather than operating in an on/off manner.

Figure 3.5: The indoor and outdoor units of a ductless mini-split heat pump. Refrigerant lines connect the units through a roughly 8 cm (in diameter) hole in the wall. Photo credit: greenbuildingadvisor.com.

- *Ductless.* The heat pump delivers conditioned air directly to the space, rather than to a network of distribution ducts.
- *Mini-split.* The heat pump consists of a small indoor unit and a small outdoor unit, connected by refrigerant lines through a roughly 8 cm (in diameter) hole in the wall.

Figure 3.5 shows the indoor and outdoor units.

Terminology

By *capacity*, we mean thermal power output. By *nameplate capacity* and *nameplate COP*, we mean the capacity and COP that the manufacturer reports at the standard test conditions of 16 °C indoor air temperature and 8 °C outdoor air temperature (for heating), and 27 °C indoor/35 °C outdoor (for cooling). By *size*, we mean the heat pump's nameplate cooling capacity. By *rated capacity*, we mean the capacity measured at a given pair of indoor and

outdoor air temperatures. Rated capacity depends on the boundary temperatures, and is typically 50–80% of *maximum capacity*. By *minimum capacity*, we mean the lowest capacity at which the heat pump can modulate continuously; if thermal load is below minimum capacity, the heat pump cycles off and on rather than modulating.

By *rated COP*, we mean the COP measured at rated capacity at given boundary temperatures. Rated COP is usually the highest COP the heat pump achieves at given boundary temperatures. In other words, rated capacity is an efficiency 'sweet spot'.

Input data

The input data in this section come from two sources. The first, [9], is a publicly-available spreadsheet containing cold-climate air-source heat pump data compiled by the Northeast Energy Efficiency Partnerships. For each heat pump model, the data in [9] include measurements of rated capacity, maximum capacity and minimum modulating capacity at a range of boundary temperatures. They also include the COP measurements at the same boundary temperatures and several part-load ratios. For reversible units, [9] includes both heating and cooling data. The measurements themselves are obtained from heat pump manufacturers.

The second data source is a set of manufacturer specification sheets downloadable at [92]. These data contain capacity and COP measurements at a more granular set of boundary temperatures and load levels, but are structurally similar to the data in [9]. To obtain the best possible statistical fits, we combined all available data from [9] and [92] on one popular manufacturer's full line of cold-climate single-zone units.

The heat pump data have two basic limitations. The first is that the data in both [9] and [92] are voluntarily reported by heat pump manufacturers. To our knowledge, these data have not been validated in an independent, third-party laboratory. The only such independent validation of heat pump manufacturer data that we are aware of is [93], which dates back to 2011. In [93], Winkler conducts a range of independent laboratory tests of the

2009 units from the same line of heat pumps considered in this thesis. Winkler concludes that "experimental test data aligned with manufacturer reported values." While this conclusion applies to the 2009 units, not the 2019 units studied in this thesis, it does build confidence in the fidelity of empirical data reported by the manufacturer whose units we study.

The second limitation of [9] and [92] is that they do not contain data on COP while cycling. This is significant because field and laboratory studies report that cycling can degrade COPs. [93, 94] In [93], Winkler conducts laboratory tests on COP while cycling for the same line of heat pumps considered in this thesis. He finds that cycling degrades COPs by 12–45% (see Table 4 of [93]). Winkler attributes this degradation to the transient behavior of the heat pump control systems, which "overshoot the minimum load by running the compressor at a higher speed than required for a short period of time" before settling into steady operation at minimum capacity.

COP and cycling

A fully-specified model of a variable-speed heat pump must define the heat pump's COP for all values of thermal load between zero and maximum capacity. To the best of our knowledge, no manufacturers report data on their variable-speed heat pumps' COPs for loads below minimum modulating capacity. Third-party laboratory data on COP below minimum modulating capacity is extremely sparse. Therefore, any fully-specified model of a variable-speed heat pump that is based on published empirical data must entail some assumption or assumptions about COP for loads below minimum modulating capacity.

To meet loads below their minimum modulating capacities, variable-speed heat pumps cycle off and on. Cycling is a qualitatively different behavior than continuous modulation. The limited laboratory data in [93] suggest that COPs can degrade significantly while cycling. To capture this degradation, we assume that cycling COP decreases with load below minimum modulating capacity. We further assume that this decrease is linear. The linear-

ity assumption is based on Occam's razor: a linear COP function is the simplest function that allows variation of COP with load. Among the family of polynomials, for example, a constant function is simpler than a linear function but does not allow for variation with load, while a quadratic function allows for variation with load but is more complex than a linear function. A quadratic model would entail an additional parameter and a curvature assumption.

To fix the slope and intercept of the COP line below minimum modulating capacity, we require two points. The first point follows naturally from continuity: the line should intersect the part-load curve at minimum modulating capacity. For a second point, we assume that the worst-case COP degradation (which necessarily occurs at the lowest nonzero load) is 25%, relative to rated COP. This assumption of 0-25% COP degradation while cycling is optimistic relative to the available empirical data, which include COP degradation measurements of 12-45% (see Table 4 of [93]).

In summary, the model of COP while cycling used in this thesis is our best effort at representing all available empirical data. Still, we acknowledge that there is significant uncertainty in these data. Further laboratory testing of the COPs of variable-speed heat pumps while cycling at low load is an important area for future research.

Take-aways

We now summarize the salient features of the manufacturer heat pump data considered in this section and illustrated in Figures 3.6–3.12.

1. Heating and cooling capacities are linearly related. (See Figure 3.6.)

2. Bigger models are less efficient. (See Figure 3.7.)

3. Capacity and efficiency depend on the indoor and outdoor air temperatures. Capacity and efficiency are higher in milder conditions. (See Figures 3.8 and 3.9.)

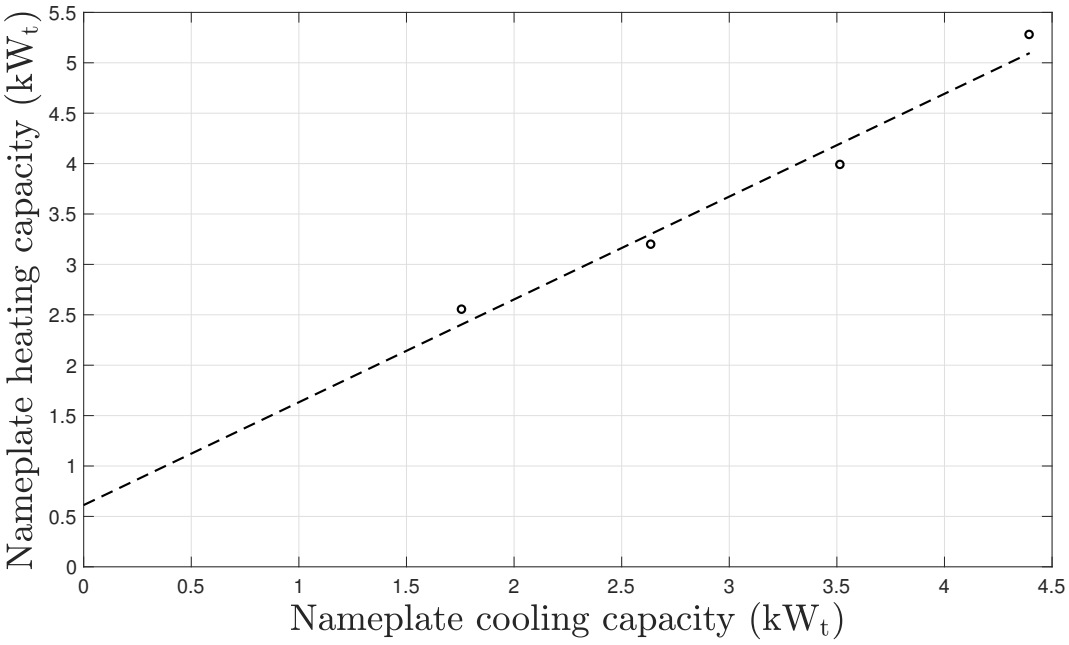

Figure 3.6: Nameplate heating and cooling capacities are linearly related. Data sources: [9, 92]. $R^2 = 0.97$.

4. Maximum capacity is significantly higher than rated capacity. For heating, maximum capacity is typically 150–185% of rated capacity; for cooling, 110–150%. (See Figure 3.10.)

5. Variable-speed heat pumps have minimum capacities, below which they start cycling off and on rather than modulating continuously. Minimum capacity varies by model. For heating, minimum capacity is typically 15–30% of rated capacity; for cooling, 20–40%. (See Figure 3.11.)

6. At any given boundary temperatures, efficiency depends on how hard the heat pump is working. Efficiency degrades at very low load, when the heat pump starts cycling, and at very high load. (See Figure 3.12.)

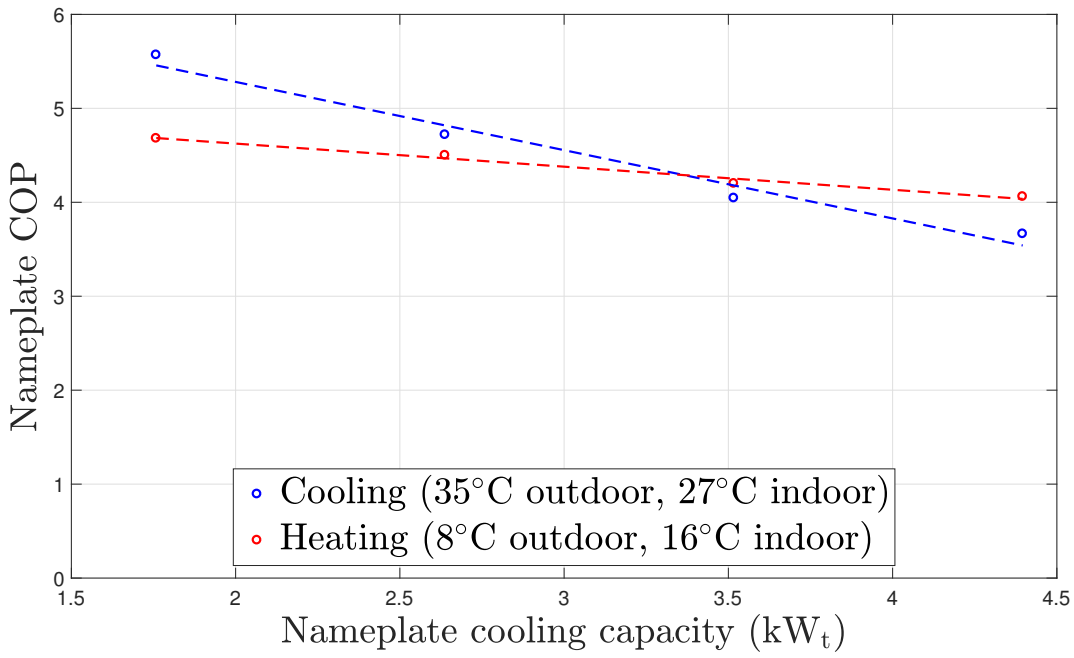

Figure 3.7: Nameplate heating and cooling efficiencies decrease with heat pump size. Data sources: [9, 92]. Heating $R^2 = 0.98$; cooling $R^2 = 0.97$.

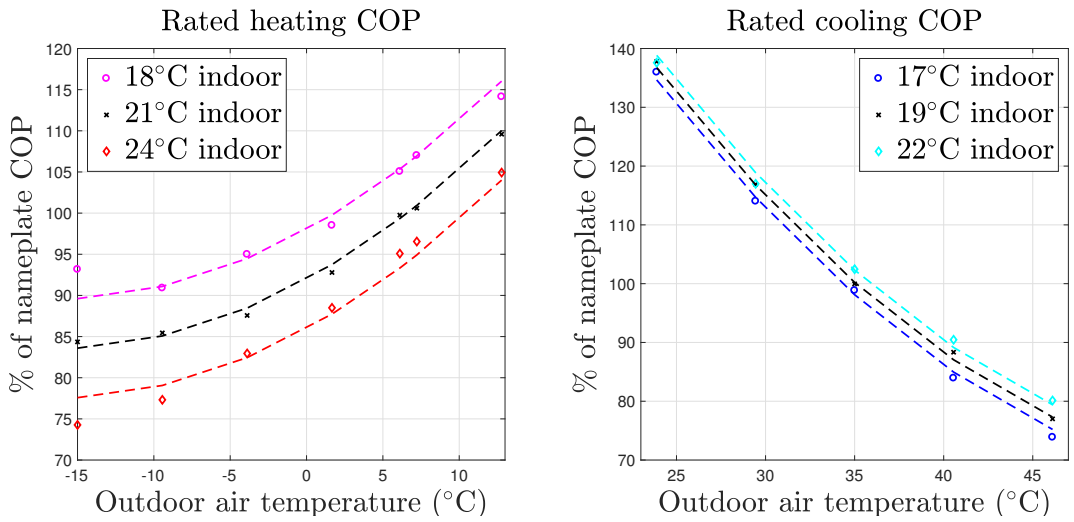

Figure 3.8: Rated efficiencies vary with both indoor and outdoor air temperature. Over the typical operating ranges shown here, efficiencies are linear in indoor air temperatures but curved in outdoor air temperatures. For reference, Figure 3.7 shows each model's nameplate efficiencies. Data sources: [9, 92]. Heating $R^2 = 0.98$; cooling $R^2 = 0.997$.

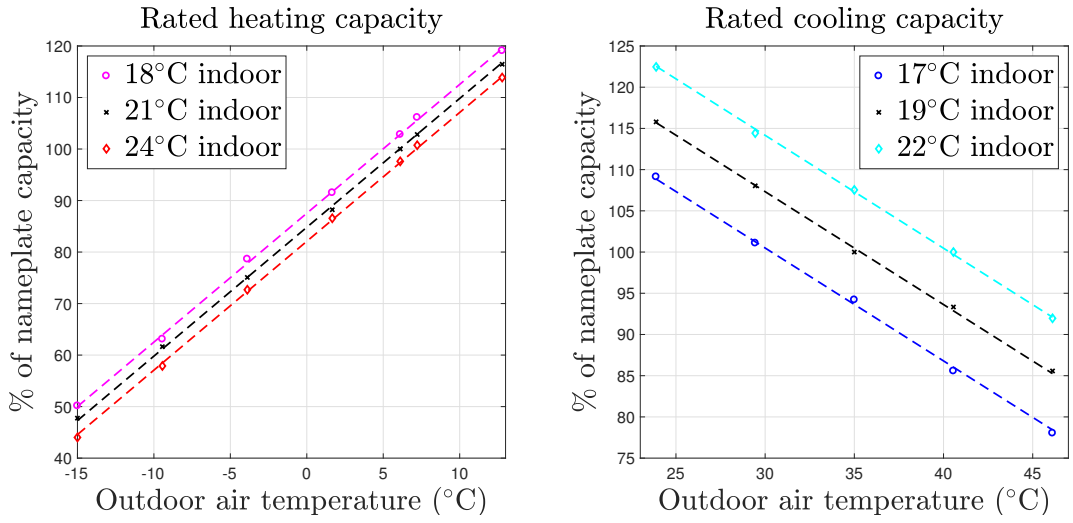

Figure 3.9: Rated capacities vary linearly with both indoor and outdoor air temperatures. Rated capacities are lower in more extreme conditions. Data sources: [9, 92]. Heating $R^2 = 0.999$; cooling $R^2 = 0.999$.

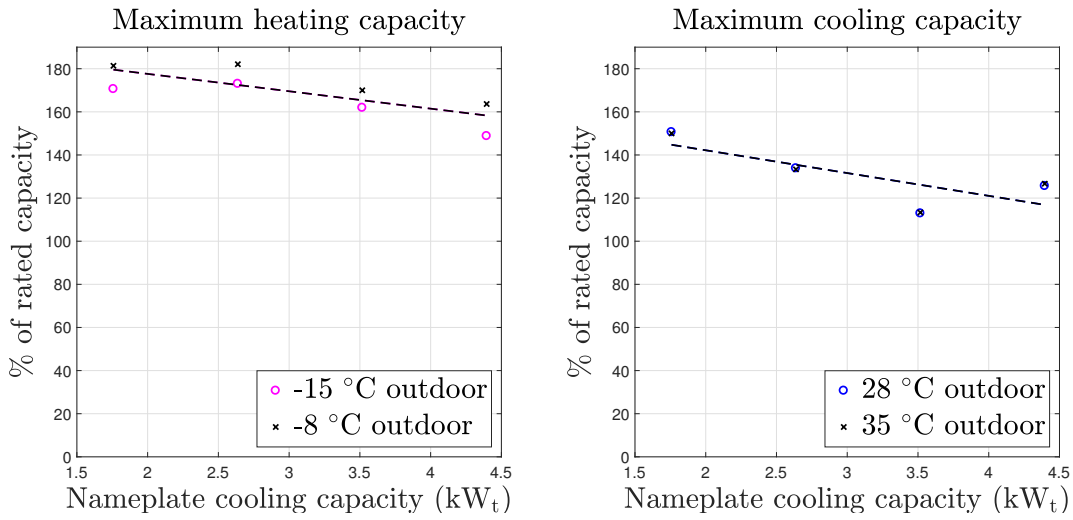

Figure 3.10: Maximum capacities are significantly larger than rated capacities, for both heating and cooling. Percentages (vertical axes) are relatively consistent across to heat pump sizes (horizontal axes), but differ substantially for heating vs. cooling. For heating, maximum capacity is typically 150–185% of rated capacity; for cooling, 110–150%. Data sources: [9, 92]. Heating $R^2 = 0.60$; cooling $R^2 = 0.60$.

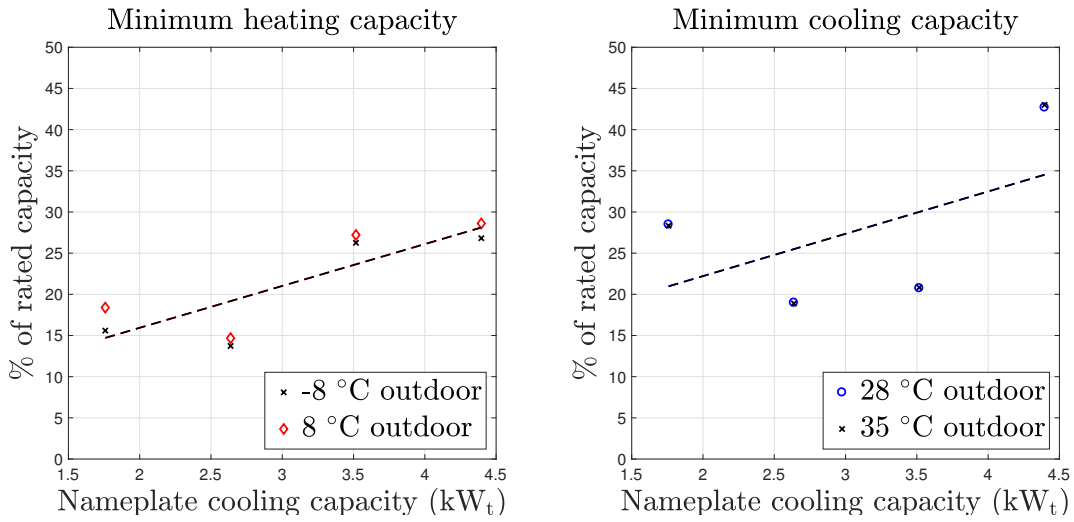

Figure 3.11: Variable-speed heat pumps have minimum capacities, below which they cycle off and on instead of modulating continuously. Minimum capacities vary both with heat pump size and for heating vs. cooling. Typically, minimum capacity is 20–30% of rated capacity. Data sources: [9, 92]. Heating $R^2 = 0.70$; cooling $R^2 = 0.50$.

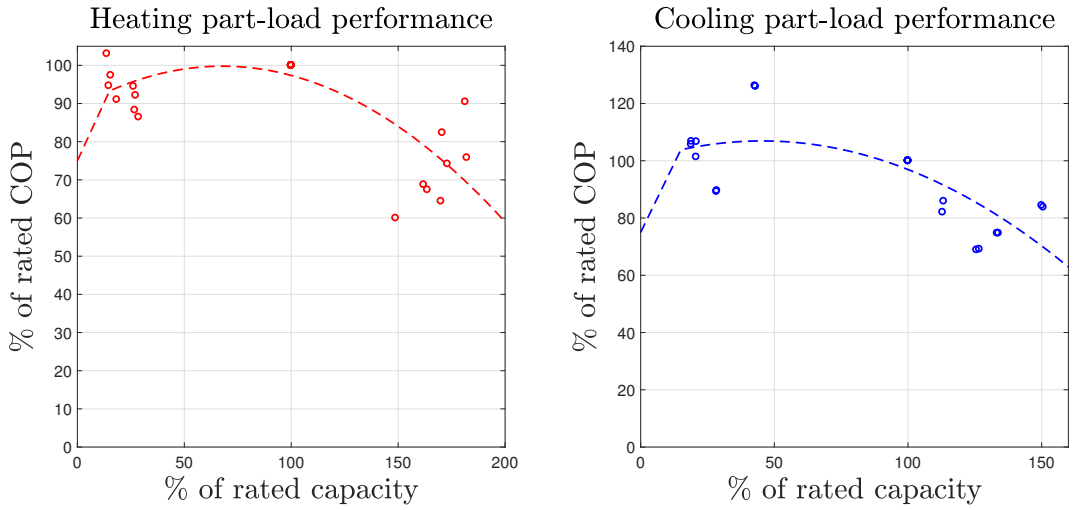

Figure 3.12: Variable-speed heat pump efficiencies depend on how hard the heat pump is working. Efficiencies degrade at very low capacities, when the heat pump cycles on and off rather than modulating continuously, and at very high capacities. The linear portion at the low end of the part-load curves represents COP degradation due to cycling, as opposed to continuous modulation. The intercepts correspond to the 25% worst-case degradation. These curves are somewhat optimistic; in [93], Winkler measured up to 45% COP degradation due to cycling. Data sources: [9, 92, 93]. Heating $R^2 = 0.59$; cooling $R^2 = 0.53$.

3.1.4 Modeling heat pumps for optimization and control

The empirical data in §3.1.3 show that a heat pump's capacity and efficiency can depend nontrivially on the indoor and outdoor air temperatures. Efficiency also varies with how heavily the heat pump is loaded. The variation of efficiency with load is typically referred to as *part-load* performance.

Computer-based optimization and control of heat pumps require mathematical models that can accurately predict the response of a heat pump's electrical power use and thermal power output to the air temperatures and thermal load. It is possible to derive device-specific physical models from first principles, but these models tend to be quite complex. The first-principles compressor model in [95], for example, includes about twenty equations, some highly nonlinear, and sixty input parameters. Specifying some of the input parameters requires manufacturer-level knowledge of hardware details.

Complex first-principles heat pump models are generally not well-suited to optimization and control. The optimization or control engineer may not have access to the proprietary hardware details required to define all of the input parameters. Additionally, high-order nonlinear models often lead to slow or inaccurate computation. For these reasons, it is common to develop low-order models and fit their parameters to empirical data. [44, 96–98] We adopt this approach here.

Literature review

In state-of-the-art research on optimization and control of heat pumps, it is very common to model both thermal capacities and COPs as constant, *i.e.*, as independent of boundary temperatures and part-load ratios. Examples include [11, 12, 37, 38, 65, 67–69, 99–102] and many other highly-cited recent papers in selective, peer-reviewed journals. The ubiquity of the constant capacity/COP heat pump model is likely due to its simplicity and the facts (a)

it can be embedded in otherwise convex numerical optimization problems without breaking convexity, and (b) the data required for more sophisticated heat pump models can be difficult to obtain.

As discussed in the preceding sections, heat pump thermal capacities and COPs are generally not constant. In [96], Verhelst *et al.* show that the constant-COP assumption, when applied to a realistic heat pump with non-constant COP, can degrade controller performance by 7–16% relative to a similar control method with a non-constant-COP model. For more discussion of the limitations of constant-COP/constant-capacity heat pump models, we refer the interested reader to §5.2 of the review paper [97].

There is a small literature on control-oriented heat pump models that capture important effects such as temperature- and part-load-dependence. In [103], Zakula *et al.* develop a data-driven model that captures the dependence of a heat pump's COP on boundary temperatures and its part-load ratio. A key feature of this work is modeling the inverse COP (rather than the COP itself) as a polynomial function of the predictors; Zakula *et al.* find that this leads to more better statistical fits.

In [44], Kim *et al.* develop a data-driven model of a variable-speed heat pump. They view the angular speed of the compressor shaft as the control input. Rather than modeling the COP directly, they model the thermal and electrical power as affine functions of the boundary temperatures and compressor shaft speed. This results in an affine thermal capacity model and a nonlinear COP model. In [98], Lee *et al.* augment this model with a binary variable that indicates its on/off state. The introduction of the binary variable prevents heat pump operation at very low compressor speeds, which can lead to undue equipment wear and tear. [104]

In the remainder of this section, we present the model we use to represent heat pump behavior at relatively slow time scales (*i.e.*, with time steps on the order of 15 minutes or longer). This is the temporal scope of models such as those in [44, 98, 103]. For faster

time scales, we use a different model that includes the closed-loop behavior of the heat pump manufacturer's low-level control system; see §5.2 for more details. The slow-time-scale model presented below is suitable for reversible, variable-speed heat pumps. It captures the dependence of thermal capacities on boundary temperatures, the dependence of COPs on boundary temperatures and part-load ratios, and the fact that variable-speed heat pumps typically cycle off and on, rather than modulating, at very low loads in order to avoid undue compressor wear and tear.

We develop our own heat pump model simply because we are aware of no other model that meets our needs. The models in [44, 98] come close, but treat compressor speed as a control input. This assumption is inappropriate for our purposes because heat pumps on the market today do not allow end-users to manipulate compressor speeds without voiding their warranties, and we do not assume that manufacturer-level hardware access is available.

Capacity and COP functions

For optimization and control purposes, we characterize a reversible variable-speed electric heat pump by four capacity functions and two COP functions:

$$\dot{Q}_h^{\max} : \mathbf{R}^2 \to \mathbf{R}$$

$$\dot{Q}_c^{\max} : \mathbf{R}^2 \to \mathbf{R}$$

$$\dot{Q}_h^{\min} : \mathbf{R}^2 \to \mathbf{R}$$

$$\dot{Q}_c^{\min} : \mathbf{R}^2 \to \mathbf{R}$$

$$\eta_h : \mathbf{R}^3 \to \mathbf{R}$$

$$\eta_c : \mathbf{R}^3 \to \mathbf{R}.$$

We explain these functions through the example of providing thermal power $\dot{Q}$ ($\mathrm{kW_t}$) when the indoor and outdoor air temperatures are T_a (°C) and T_∞ (°C), respectively. We frame

this example in terms of heating, but the discussion also applies to cooling.

In this example, the thermal power output must satisfy

$$\dot{Q} \leq \dot{Q}_h^{\max}(T_a, T_\infty).$$

The heat pump consumes electrical power

$$P = \frac{\dot{Q}}{\eta_h(T_a, T_\infty, \dot{Q})}.$$

We allow the heating coefficient of performance function η_h to depend on $\dot{Q}$ in order to model the part-load performance depicted in Figure 3.12. If $\dot{Q}$ is near the heat pump's rated capacity at (T_a, T_∞), then η_h will be close to the rated COP at (T_a, T_∞). If $\dot{Q}$ is far above or below the rated capacity at these temperatures, then η_h will likely be lower than the rated COP.

If the thermal power is above the heat pump's minimum capacity,

$$\dot{Q} \geq \dot{Q}_h^{\min}(T_a, T_\infty),$$

then the heat pump can modulate continuously. On the other hand, if

$$0 < \dot{Q} < \dot{Q}_h^{\min}(T_a, T_\infty),$$

then the heat pump must cycle on and off periodically in order to deliver $\dot{Q}$ on average over time. For example, the heat pump can provide thermal energy $\dot{Q}\Delta t$ over a duration Δt (h) by providing thermal power $\dot{Q}_h^{\min}(T_a, T_\infty)$ for a fraction

$$\frac{\dot{Q}}{\dot{Q}_h^{\min}(T_{\text{cold}}, T_{\text{hot}})}$$

of the duration Δt, and turning off for the remaining fraction. The 'off' times need not be contiguous; the heat pump could cycle off and on multiple times during the duration Δt. Under typical control schemes, on/off cycles get shorter as $\dot{Q}$ gets further below $\dot{Q}_h^{\min}(T_a, T_\infty)$.

Model fitting

For a given heat pump, statistical models of the capacity and COP functions can be fit to data published by manufacturers. For a comprehensive set of manufacturer data, see [9]. For the line of heat pumps discussed in §3.1.3, we fit the coefficients of polynomial capacity and COP functions using multiple linear regression. For details on fitting polynomial models using multiple linear regression, we refer the interested reader to [105] or any other statistics textbook on linear models.

We use first-order polynomials (*i.e.*, affine functions) for the thermal capacities $\dot{Q}_h^{\max}$ and $\dot{Q}_c^{\max}$ and the minimum modulating capacities $\dot{Q}_h^{\min}$ and $\dot{Q}_c^{\min}$. We use second-order polynomials for the COPs η_h and η_c. We find that only the quadratic term in T_a (in addition to the constant and linear terms) is necessary for accurate COP fits; the coefficients of the other quadratic terms can be set to zero without reducing goodness of fit.

The fits are the dashed lines in Figures 3.6–3.12. In the fits in Figures 3.8–3.9, values of the R^2 statistic are close to unity, indicating good fit. The R^2 values in Figures 3.10–3.12 are lower. This is due primarily to the fact that less manufacturer-reported data are available for these fits, and that the available data are noisier. Fit quality could be improved by obtaining more data by instrumenting a heat pump in a research laboratory, or by adding higher-order polynomial terms to the fits. The latter approach runs the risk of overfitting, however.

3.2 Thermal loads

The primary purpose of a heat pump is to meet thermal load. In this thesis, we assume that all thermal loads represent conditioned space in buildings. We note, however, that heat pumps can serve other thermal loads. The thermal load served by a heat pump water heater, for example, is a tank storing hot water for showers, dish-washing, *etc.*

In this section, we present one method for modeling thermal loads that represent conditioned space in buildings. This method is one option among many; we present it because we feel it strikes a good balance between fidelity, simplicity, and physical interpretability. We note, however, that the methods developed in Chapters 4–5 are agnostic to the thermal load model. They simply require the output of a thermal load model – *i.e.*, a time series of thermal power demand – as input data. Such data can be generated from a wide variety of sources, such as historical measurements from real buildings, pseudorandom number generators, simple quasi-steady-state models, physics-based building simulators, thermal circuit models of arbitrary order, autoregressive processes, artificial neural networks, support vector machines, regression trees, random forests, ensemble models, *etc.* A practitioner interested in implementing a method in Chapter 4 or 5 could use any of the aforementioned thermal load models.

This section is organized as follows. In §3.2.1, we briefly review literature on thermal modeling of buildings. We present our chosen thermal model in §3.2.2 and demonstrate its use for load prediction in §3.2.3. We discuss the interpretations and typical values of the model parameters, states and input signals in §3.2.4. In §3.2.5 and §3.2.6, we provide two methods for instantiating model parameters based on load and weather data. We develop an analogy between our chosen load model and thermal energy storage in §3.2.7.

3.2.1 Literature review

Thermal modeling of buildings is a mature topic. Good textbooks on the subject include [106, 107]. Two recent review papers on control-oriented building modeling are [108] and [109]. The user manuals of EnergyPlus [110] and TRNSYS [111], the current state-of-the-art in building simulation software, also provide a wealth of useful information.

Building thermal modeling techniques can loosely be categorized into those based on first physical principles (termed 'white-box' models in [108, 109]), those that are entirely data-driven ('black-box' models), and semi-physical models based on a mix of data and simplified physics ('grey-box' models). White-box models use laws of physics, such as Fourier's Law, Newton's Law of Cooling and the Stefan-Boltzmann Law, to derive differential equations that govern the evolution of the building's state. EnergyPlus and TRNSYS use a white-box approach. Examples of black-box models are autoregressive processes, artificial neural networks, regression trees and support vector machines. [108, 109] The typical grey-box model structure is a thermal circuit, analogous to an electrical resistor-capacity circuit. [108, 109] In this thesis, we focus on grey-box modeling, specifically using thermal circuits. We choose this approach because it is conceptually simple, is amenable to efficient computation, and has been applied successfully in many recent studies on optimization and control of heating and cooling systems. [112–117]

The fundamental idea that the dominant thermal dynamics of a building can be captured by a low-order thermal circuit model dates back at least to Laret's 1975 thesis. [118] Early publications on this theme include [119–124], where the authors explore the behavior and predictive accuracy of thermal circuit models of various structures and orders. The second-order model we adopt in this thesis is developed in detail by Crabb, Murdoch and Penman in the 1987 paper [125]. The series of papers [126–129] develop techniques for fitting the model parameters to experimental data, and empirically demonstrate the use of a fitted model for

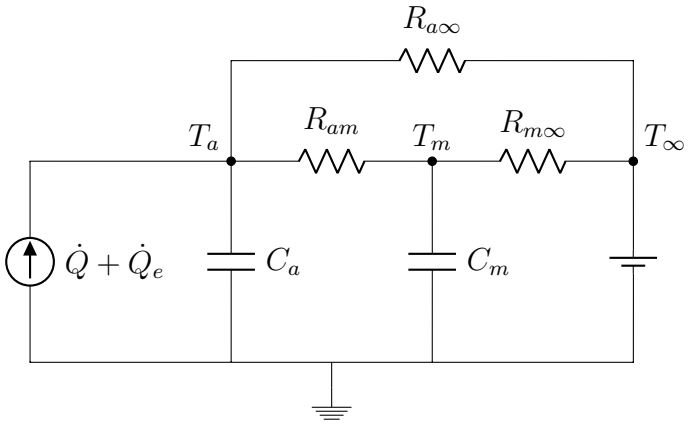

Figure 3.13: A thermal circuit connects the indoor air, thermal mass and surroundings, denoted by subscripts a, m and ∞, respectively.

real-time control in an occupied building. More recent work confirmed the suitability of the second-order model structure in the contexts of houses [130], thermal zones in commercial buildings [113, 131], and individual thermostatically-controlled loads such as refrigerators and window-mounted air conditioners [66, 132]. Other recent developments are reviewed in [133].

3.2.2 Model

Figure 3.13 illustrates our chosen load model. It has the form of a second-order resistor-capacitor thermal circuit. The model includes two energy storage elements: indoor air with thermal capacitance C_a ($\mathrm{kWh_t/°C}$) and temperature T_a (°C), and thermal mass with capacitance C_m ($\mathrm{kWh_t/°C}$) and temperature T_m (°C). The indoor air and thermal mass exchange heat through the effective thermal resistance R_{am} ($\mathrm{°C/kW_t}$), which models combined heat transfer through convection, conduction and (linearized) radiation. The indoor air and thermal mass also exchange heat with the outdoor air through the effective resistances $R_{a\infty}$ and $R_{m\infty}$ ($\mathrm{°C/kW_t}$), respectively. The outdoor air temperature is T_∞ (°C). Mechanical systems inject thermal power $\dot{Q}$ ($\mathrm{kW_t}$) to the indoor air. Similarly, a thermal power $\dot{Q}_e$ ($\mathrm{kW_t}$) is

injected by exogenous sources such as the sun, appliances, lights, occupants' bodies, *etc.*

In this model, the system states T_a and T_m are governed by two coupled linear ordinary differential equations:

$$\begin{aligned} C_a\dot{T}_a(t) &= \frac{T_m(t) - T_a(t)}{R_{am}} + \frac{T_\infty(t) - T_a(t)}{R_{a\infty}} + \dot{Q}(t) + \dot{Q}_e(t) \\ C_m\dot{T}_m(t) &= \frac{T_a(t) - T_m(t)}{R_{am}} + \frac{T_\infty(t) - T_m(t)}{R_{m\infty}}. \end{aligned} \tag{3.3}$$

This model entails several simplifying assumptions:

- The indoor air is well-mixed.
- The thermal mass is lumped, *i.e.*, heat transfers within the thermal mass much faster than across its boundary.
- The indoor air and outdoor air are relatively dry.
- Radiation is well-represented by a linearized model.
- Convection coefficients are independent of temperature and wind speed.

Despite these simplifications, this model has shown good predictive accuracy in many applications. [66, 112–117, 126–132]

3.2.3 Load prediction

Steady-state load prediction

In steady state, the governing equations reduce to

$$\begin{aligned} 0 &= \frac{T_m^{\text{ss}} - T_a^{\text{ss}}}{R_{am}} + \frac{T_\infty^{\text{ss}} - T_a^{\text{ss}}}{R_{a\infty}} + \dot{Q}^{\text{ss}} + \dot{Q}_e^{\text{ss}} \\ 0 &= \frac{T_a^{\text{ss}} - T_m^{\text{ss}}}{R_{am}} + \frac{T_\infty^{\text{ss}} - T_m^{\text{ss}}}{R_{m\infty}}. \end{aligned}$$

Solving the second equation for T_m^{ss} (°C), we see that in steady state, the thermal mass temperature is a weighted average of the indoor air and outdoor air temperatures:

$$T_m^{\text{ss}} = \frac{R_{m\infty} T_a^{\text{ss}} + R_{am} T_\infty^{\text{ss}}}{R_{am} + R_{m\infty}}.$$

Substituting this expression into the first equation gives

$$\dot{Q}^{\text{ss}} + \dot{Q}_e^{\text{ss}} = \frac{T_a^{\text{ss}} - T_\infty^{\text{ss}}}{R},$$

where the effective thermal resistance R (°C/kW$_\text{t}$) satisfies

$$\frac{1}{R} = \frac{1}{R_{a\infty}} + \frac{1}{R_{am} + R_{m\infty}}.$$

Therefore,

$$\dot{Q}^{\text{ss}} = \frac{T_a^{\text{ss}} - T_\infty^{\text{ss}}}{R} - \dot{Q}_e^{\text{ss}}. \tag{3.4}$$

Equation (3.4) predicts thermal load in steady state, where all temperatures and thermal powers are constant. The model can also predict the transient response of load to time-varying T_∞ and $\dot{Q}_e$, as we now discuss.

Dynamic load prediction

Given forecasts of the outdoor temperature T_∞ and exogenous thermal power $\dot{Q}_e$, the load dynamics (3.3) can predict the thermal power $\dot{Q}$ required to maintain the indoor air temperature at a (possibly time-varying) setpoint T_a (°C). The first step is to simultaneously

discretize both equations. The continuous-time equations can be written as

$$\begin{aligned}
\begin{bmatrix} \dot{T}_a(t) \\ \dot{T}_m(t) \end{bmatrix} &= \begin{bmatrix} -\left(1/R_{am} + 1/R_{a\infty}\right)/C_a & 1/(C_a R_{am}) \\ 1/(C_m R_{am}) & -\left(1/R_{am} + 1/R_{m\infty}\right)/C_m \end{bmatrix} \begin{bmatrix} T_a(t) \\ T_m(t) \end{bmatrix} \\
&\quad + \begin{bmatrix} 1/C_a & 1/(R_{a\infty}C_a) & 1/C_a \\ 0 & 1/(R_{m\infty}C_m) & 0 \end{bmatrix} \begin{bmatrix} \dot{Q}(t) \\ T_\infty(t) \\ \dot{Q}_e(t) \end{bmatrix} \\
&= A_c \begin{bmatrix} T_a(t) \\ T_m(t) \end{bmatrix} + B_c \begin{bmatrix} \dot{Q}(t) \\ T_\infty(t) \\ \dot{Q}_e(t) \end{bmatrix}.
\end{aligned}$$

Assuming a zero-order hold on $\dot{Q}$, T_∞ and $\dot{Q}_e$, this continuous-time linear system can be exactly discretized to

$$\begin{bmatrix} T_a(k+1) \\ T_m(k+1) \end{bmatrix} = A \begin{bmatrix} T_a(k) \\ T_m(k) \end{bmatrix} + B \begin{bmatrix} \dot{Q}(k) \\ T_\infty(k) \\ \dot{Q}_e(k) \end{bmatrix},$$

where

$$A = e^{A_c \Delta t}, \quad B = \int_0^{\Delta t} e^{A_c \tau} \mathrm{d}\tau B_c.$$

If A_c is invertible, then the second equation simplifies to

$$B = A_c^{-1}(A - I)B_c.$$

The discrete-time system equations give an exact expression for the load required to drive

the air temperature from $T_a(k)$ to $T_a(k+1)$, given $T_m(k)$, $T_\infty(k)$ and $\dot{Q}_e(k)$:

$$\dot{Q}(k) = \frac{1}{b_{11}} \left(T_a(k+1) - a_{11} T_a(k) - a_{12} T_m(k) - b_{12} T_\infty(k) - b_{13} \dot{Q}_e(k) \right).$$

The next mass temperature is

$$T_m(k+1) = a_{21} T_a(k) + a_{22} T_m(k) + b_{21} \dot{Q}(k) + b_{22} T_\infty(k) + b_{23} \dot{Q}_e(k).$$

3.2.4 Model interpretation

The load model presented in §3.2.2 is defined by five parameters: C_a, C_m, R_{am}, $R_{a\infty}$ and $R_{m\infty}$. Its state is fully characterized by the indoor air and thermal mass temperatures, T_a and T_m. The dynamics are driven by the outdoor air temperature T_∞ and the thermal powers $\dot{Q}$ and $\dot{Q}_e$. Due to the many simplifying assumptions underlying the model, interpreting its parameters, states and disturbances is not straightforward. It is also not straightforward to define the model parameters for a given building, zone or appliance. We now discuss these issues.

States

The state T_a has a relatively clear physical interpretation as the spatial average temperature of the indoor air. The interpretation of the thermal mass temperature depends on the building type. For a building with heavy exterior construction but light interior walls, T_m might represent the spatial average temperature of the exterior walls. For a building with significant interior mass, such as a heavy stone fireplace or dense interior walls, T_m might represent the temperature of the interior mass, or a weighted average temperature of the interior mass and the exterior construction.

Disturbances

For a whole-building model, T_∞ is the outdoor air temperature. For a zone inside a larger building, T_∞ might represent a weighted average of the temperatures of the outdoor air and the surrounding zones. The exogenous thermal power $\dot{Q}_e$ models the combined effects of body heat, appliances, lights, electrical plug loads, and the sun. This term can also be viewed as a catch-all for unmodeled dynamics. This term is generally difficult to define *a priori*, but can be be fit to data.

Capacitances

It is tempting to define the capacitance C_a as the product of the density, specific heat capacity and volume of the indoor air, $\rho_a c_a V$. When fitting C_a to data, however, one typically finds that the best-fit value exceeds $\rho_a c_a V$ by a factor of 10 to 20. [124–130] This can be explained (loosely) by noting that (1) most buildings contain some thermally light material that is strongly coupled to the indoor air, such as ducts, dampers, *etc.*, and (2) the assumption that the indoor air is well-mixed neglects slower physical processes related to mixing. The unexpected additional capacitance in C_a can be attributed to these effects. [126] This gives a rough estimate of the indoor air capacitance:

$$C_a \approx (10 \text{ to } 20)\rho_a c_a V.$$

For reference, $\rho_a c_a = 3.42 \times 10^{-4}$ $\mathrm{kWh_t/(^\circ C{\cdot}m^3)}$.

The interpretation of the thermal mass capacitance C_m varies from load to load. An order-of-magnitude estimate can be obtained by multiplying the volume, density and specific heat capacity of some representative material, such as the wood and concrete in a building. Assuming the mass occupies about ten percent of the volume occupied by the indoor air, for

example,

$$C_m \approx \frac{\rho_m c_m V}{10} \approx \frac{\rho_m c_m}{\rho_a c_a} \frac{C_a}{100 \text{ to } 200}.$$

For materials such as fir, concrete, steel and brick, $\rho_m c_m/(\rho_a c_a)$ ranges between about 1000 and 2000. Therefore, a rough estimate of the mass capacitance is

$$C_m \approx \left(\frac{1000 \text{ to } 2000}{100 \text{ to } 200} \right) C_a = (5 \text{ to } 20) C_a.$$

This rough estimate agrees fairly well with best-fit estimates from real buildings. In [126, 127], for example, C_m/C_a varies between 8 and 16.

Resistances

The interpretations of the resistances R_{am}, $R_{a\infty}$ and $R_{m\infty}$ depend on the interpretation of the thermal mass temperature, and hence on the type of load. Regardless of the load type, however, an estimate of the effective thermal resistance between the indoor and outdoor air, given by

$$\frac{1}{R} = \frac{1}{R_{a\infty}} + \frac{1}{R_{am} + R_{m\infty}},$$

can often be obtained (see §3.2.5).

Under some simplifying assumptions, an estimate of R can provide estimates of R_{am}, $R_{a\infty}$ and $R_{m\infty}$. We now discuss two simple cases.

1. *Exterior mass.* If the mass is interpreted as the exterior walls, then the thermal resistance between the mass and indoor air is similar to the thermal resistance between the mass and outdoor air. Both resistances represent convection in series with conduction through the insulated walls. The indoor and outdoor air, by contrast, are coupled through the faster pathways of conduction through window panes, and infiltration of outdoor air through gaps in the building envelope.

In this case, it is reasonable to assume that

$$R_{am} \approx R_{m\infty} \gg R_{a\infty}.$$

If a fraction $c \in [0, 1]$ of the steady-state heat transfer between the indoor and outdoor air happens via the fast heat transfer pathway, then $R_{a\infty} = R/c$. Given R, this defines $R_{a\infty}$. If the building is drafty with well-insulated walls, then c will be close to one. On the other hand, if the building envelope is tight but the walls are poorly insulated, then c will be close to zero. It remains to resolve R_{am} and $R_{m\infty}$. Assuming $R_{am} = dR_{m\infty}$ for some $d \geq 0$, we have

$$R_{m\infty} = \frac{R}{(1-c)(1+d)}.$$

Because exterior wall surfaces are often subject to forced convection, a faster heat transfer mechanism than natural convection at interior wall surfaces, we would expect d to be somewhat greater than one.

2. *Interior mass.* If the mass is interpreted as the material inside a building (*e.g.*, furniture and interior walls), then the mass is weakly coupled to the outdoor air. In this case, it is reasonable to assume that

$$R_{m\infty} \gg R_{a\infty} \approx R_{am}.$$

Letting $R_{m\infty} = cR_{a\infty} = dR_{am}$ for some choices of $c, d > 1$ gives

$$R_{a\infty} = \left(1 + \frac{d}{c(d+1)}\right) R.$$

Perhaps the best-documented examples in the literature on empirical parameter identification in real buildings are in [126, 127]. In these examples, the average parameter

values over all of the fits satisfy $c = 3.6$, $d = 27.7$.

3.2.5 Estimating effective resistance from data

The methods described in this section are not used elsewhere in this thesis; we present them here simply because we find them interesting and useful.

A thermostat timing experiment

This experiment requires a single-stage central heating system with known capacity, controlled by a thermostat. It should be conducted on a winter night, when the sun is down and the thermal power from exogenous sources is small.

The first step in the experiment is to record the thermostat's 'on' time for several hours. The duty cycle, meaning the ratio of 'on' time to total time, is then computed. The product of the duty cycle and the heating system capacity gives an estimate of the average thermal power output of the heating system during the experiment. If the heat distribution system is in unconditioned space, this value is multiplied by an estimated efficiency of the heat distribution system (*e.g.*, 80–90% for typical forced-air ducts). This gives an estimate of the heat load of the space, $\dot{Q}^{\text{ss}}$. The steady-state temperatures $(T_a^{\text{ss}}, T_\infty^{\text{ss}})$ are then estimated by their respective averages over the experiment runtime. This gives an estimate of the effective resistance:

$$R = \frac{T_a^{\text{ss}} - T_\infty^{\text{ss}}}{\dot{Q}^{\text{ss}} + \dot{Q}_e^{\text{ss}}}.$$

The exogenous thermal power $\dot{Q}_e^{\text{ss}}$ can be estimated by taking an inventory of the lights, appliances and people present during the experiment. An adult body produces about 50 to 100 Watts, depending on activity level. A refrigerator produces about 150 Watts. Lights and electronics typically have rated electrical capacities; most of their power draw ends up as heat. As a sanity check, the total thermal power intensity from internal heat sources is

typically on the order of five Watts per square meter of floor area.

Fitting historical usage data

In this method, based on [134], we suppose a measurement of the total heating fuel usage is available, for example from a natural gas bill. We call this measurement ηQ_h, where η is the heating system efficiency (including the distribution system, if it is in unconditioned space) and Q_h ($\mathrm{kWh_t}$) is the total space heating load over the measurement period. We also assume that measurements of the outdoor air temperature T_∞ are available at each hour of the measurement period. If such measurements are unavailable, heating degree-days may be used instead.

The method requires assuming a heating *balance-point temperature* T^h_{bal} (°C), defined as the outdoor air temperature at which the steady-state conductive heat loss through the building envelope equals the average thermal power from exogenous sources during heating season, $\dot{Q}^h_e$ ($\mathrm{kW_t}$). In other words, T^h_{bal} satisfies

$$\frac{T^h_{\mathrm{set}} - T^h_{\mathrm{bal}}}{R} = \dot{Q}^h_e.$$

Here T^h_{set} (°C) is the indoor air temperature setpoint in heating season. For a typical U.S. home, the heating balance-point temperature is in the range of 15 to 20 °C. [134] Better-insulated buildings with lower heating temperature setpoints, more internal heat sources, and stronger solar forcing have lower balance-point temperatures.

We recall that the steady-state heating load is

$$\dot{Q}^{\mathrm{ss}} = \frac{T^h_{\mathrm{set}} - T^{\mathrm{ss}}_\infty}{R} - \dot{Q}^h_e.$$

This equation suggests a quasi-steady-state approximation of the instantaneous heating load:

$$\begin{aligned}\dot{Q}_h(t) &\approx \left(\frac{T^h_{\text{set}} - T_\infty(t)}{R} - \dot{Q}^h_e\right)_+ \\ &= \left(\frac{T^h_{\text{set}} - T_\infty(t)}{R} - \left[\frac{T^h_{\text{set}} - T^h_{\text{bal}}}{R}\right]\right)_+ \\ &= \left(\frac{T^h_{\text{bal}} - T_\infty(t)}{R}\right)_+ .\end{aligned}$$

Here $(\cdot)_+ = \max\{0, \cdot\}$ is the positive part function. Forward Euler integration of this quasi-steady model gives

$$\begin{aligned}Q_h &= \int_t \dot{Q}_h(t)\mathrm{d}t \\ &\approx \Delta t \sum_t \dot{Q}_h(t) \\ &\approx \frac{\Delta t}{R} \sum_t \left(T^h_{\text{bal}} - T_\infty(t)\right)_+ .\end{aligned}$$

Here Δt (h) is the measurement time step. This gives an estimate of the effective thermal resistance,

$$R \approx \frac{\Delta t}{Q_h} \sum_t \left(T^h_{\text{bal}} - T_\infty(t)\right)_+ .$$

The term

$$\Delta t \sum_t \left(T^h_{\text{bal}} - T_\infty(t)\right)_+$$

is the number of *heating degree-days* at base temperature T^h_{bal} over the measurement period, converted into units of degree-hours. If outdoor air temperature data is unavailable, heating degree-days can be used instead:

$$R \approx \left(\frac{24\text{ h}}{1\text{ d}}\right) \frac{\text{HDD}_{T^h_{\text{bal}}}}{Q_h}.$$

3.2.6 Tuning a model to survey data

We now describe a method for tuning the effective thermal resistance R and a solar susceptibility parameter α to survey data on annual loads. The input parameters are the following.

- The total annual heating and cooling loads, Q_h ($\mathrm{kWh_t}$) and Q_c ($\mathrm{kWh_t}$).
- The ratio of sensible cooling load to total cooling load, σ.
- The sets $\mathcal{H}$ and $\mathcal{C}$ of heating and cooling time indices.
- The floor area A ($\mathrm{m^2}$) and time step Δt (h).

The following input signals are defined at each time step k of a one-year horizon.

- The indoor and outdoor air temperatures, $T_a(k)$ (°C) and $T_\infty(k)$ (°C).
- The global solar irradiance on a horizontal surface, $I(k)$ ($\mathrm{kW/m^2}$).
- The thermal power from internal heat sources, $\dot{Q}_{\mathrm{in}}(k)$ ($\mathrm{kW_t}$). (For typical U.S. homes, the annual average of $\dot{Q}_{\mathrm{in}}(k)$ per unit of floor area is about 4.5 to 6 $\mathrm{W/m^2}$. [135])

The model consists of two equations:

$$Q_h = \Delta t \sum_{k\in\mathcal{H}} \frac{T_a(k) - T_\infty(k)}{R} - \dot{Q}_{\mathrm{in}}(k) - \alpha A I(k)$$
$$\sigma Q_c = \Delta t \sum_{k\in\mathcal{C}} \frac{T_\infty(k) - T_a(k)}{R} + \dot{Q}_{\mathrm{in}}(k) + \alpha A I(k).$$

The term $\alpha A I(k)$ represents the solar heat gain at stage k. The unknowns in these equations are R and α. Solving for α, we have

$$\alpha = \frac{\left(\sum_{k\in\mathcal{H}} T_a(k) - T_\infty(k)\right)\left(\frac{\sigma Q_c}{\Delta t} - \sum_{k\in\mathcal{C}} \dot{Q}_{\mathrm{in}}(k)\right) - \left(\sum_{k\in\mathcal{C}} T_\infty(k) - T_a(k)\right)\left(\frac{Q_h}{\Delta t} + \sum_{k\in\mathcal{H}} \dot{Q}_{\mathrm{in}}(k)\right)}{A\left[\left(\sum_{k\in\mathcal{H}} T_a(k) - T_\infty(k)\right)\left(\sum_{k\in\mathcal{C}} I(k)\right) + \left(\sum_{k\in\mathcal{C}} T_\infty(k) - T_a(k)\right)\left(\sum_{k\in\mathcal{H}} I(k)\right)\right]}.$$

Given α, the effective thermal resistance is

$$R = \frac{\sum_{k \in \mathcal{H}} T_a(k) - T_\infty(k)}{\frac{Q_h}{\Delta t} + \sum_{k \in \mathcal{H}} \dot{Q}_{\text{in}}(k) + \alpha A I(k)}.$$

These values of α and R are obviously not exact, as they are based on a quasi-steady-state assumption and forward Euler integration, but they can provide useful ballpark estimates.

3.2.7 Thermal storage analogy

Thermal loads can be viewed as thermal storage devices, similar to the insulated tanks of hot water or ice that are sometimes used for load shifting in commercial and industrial buildings. We now develop this analogy in part for future use in §5.2.2, and in part because we feel that readers may find it interesting and potentially useful. This analogy is not new; similar developments can be found in [67, 69, 136, 137] and elsewhere in the research literature.

Forecasts and baselines

We suppose that forecasts $\hat{T}_\infty$ (°C) and $\hat{\dot{Q}}_e$ (°C) of the outdoor air temperature and exogenous thermal power trajectories, respectively, are available. We also suppose that a reference indoor air temperature trajectory $\hat{T}_a$ (°C) is available. This reference trajectory could be specified by occupants or obtained from a smart thermostat or building automation system.

We define the mass temperature *baseline* $\hat{T}_m$ (°C) as the trajectory the mass temperature would follow, assuming perfect forecasts and perfect tracking of the indoor air temperature reference trajectory. By definition, the mass temperature baseline solves

$$C_m \hat{\dot{T}}_m(t) = \frac{\hat{T}_a(t) - \hat{T}_m(t)}{R_{am}} + \frac{\hat{T}_\infty(t) - \hat{T}_m(t)}{R_{m\infty}}.$$

The forecasts, air temperature reference, and mass temperature baseline determine the ther-

mal load baseline,

$$\hat{\dot{Q}}(t) = C_a \hat{\dot{T}}_a(t) - \left(\frac{\hat{T}_m(t) - \hat{T}_a(t)}{R_{am}} + \frac{\hat{T}_\infty(t) - \hat{T}_a(t)}{R_{a\infty}} + \hat{\dot{Q}}_e(t) \right).$$

We will work with the following perturbations:

$$\begin{aligned}
\delta_a(t) &= T_a(t) - \hat{T}_a(t) \\
\delta_m(t) &= T_m(t) - \hat{T}_m(t) \\
\delta_\infty(t) &= T_\infty(t) - \hat{T}_\infty(t) \\
\delta(t) &= \dot{Q}(t) - \hat{\dot{Q}}(t) \\
\delta_e(t) &= \dot{Q}_e(t) - \hat{\dot{Q}}_e(t)
\end{aligned}$$

We define the thermal energy stored in the indoor air and mass, respectively, as

$$Q_a(t) = C_a \delta_a(t), \quad Q_m(t) = C_m \delta_m(t).$$

Combining these definitions with the governing equations gives the thermal energy dynamics:

$$\begin{aligned}
\dot{Q}_a(t) &= -\frac{1}{C_a} \left(\frac{1}{R_{am}} + \frac{1}{R_{a\infty}} \right) Q_a(t) + \frac{Q_m(t)}{C_m R_{am}} + \frac{\delta_\infty(t)}{R_{a\infty}} + \delta(t) + \delta_e(t) \\
\dot{Q}_m(t) &= \frac{Q_a(t)}{C_a R_{am}} - \frac{1}{C_m} \left(\frac{1}{R_{am}} + \frac{1}{R_{m\infty}} \right) Q_m(t) + \frac{\delta_\infty(t)}{R_{m\infty}}.
\end{aligned} \tag{3.5}$$

Time scale separation

As the thermal energy dynamics (3.5) show, the indoor air and thermal mass are coupled. In this section, we treat them as approximately decoupled. More specifically, we assume that the indoor air dynamics are much faster than the thermal mass dynamics. Viewed from the fast time scale, the thermal mass temperature is approximately constant. Viewed from the slow time scale, the air dynamics are approximately instantaneous. We make this

assumption in order to clarify the thermal storage analogy.

Time scale separation is a reasonable assumption in many buildings, where air temperature dynamics typically have time constants on the order of minutes, while mass temperature dynamics have time constants on the order of hours or tens of hours; see, *e.g.*, the $\tau = RC$ values for the indoor air and thermal mass states in [124–130]. Because thermal mass time constants are typically much larger than indoor air time constants, the thermal mass temperature responds to changing boundary conditions much slower than the indoor air temperature.

Indoor air

To analyze the indoor air separately from the thermal mass, we assume that the thermal mass temperature approximately equals its baseline:

$$Q_m(t) \approx 0 \text{ for all } t.$$

With this approximation,

$$\dot{Q}_a(t) \approx -\frac{Q_a(t)}{\tau_a} + \delta(t) + w_a(t), \tag{3.6}$$

where

$$\tau_a = \frac{C_a R_{am} R_{a\infty}}{R_{am} + R_{a\infty}}$$
$$w_a(t) = \frac{\delta_\infty(t)}{R_{a\infty}} + \delta_e(t).$$

Equation (3.6) has the form of a thermal storage model, where Q_a is the stored energy, δ is the charging power, and w_a ($\mathrm{kW_t}$) is a disturbance caused by forecast error. The charging efficiency in this model is equal to one. The time constant τ_a (h) determines how quickly stored thermal energy dissipates: Assuming no charging or disturbances, 95% of the energy

stored at $t = 0$ dissipates by $t = 3\tau_a$. The dissipation rate decreases (τ_a increases) as C_a increases, meaning the volume of enclosed air grows, and as R_{am} and $R_{a\infty}$ increase, meaning the indoor air becomes better insulated from the thermal mass and the outdoor air.

We assume that the indoor air temperature perturbations must satisfy the constraints

$$\underline{\delta}_a \leq \delta_a(t) \leq \overline{\delta}_a.$$

These constraints model occupants' thermal comfort requirements. They translate directly into constraints on the thermal energy stored in the air:

$$C_a\underline{\delta}_a \leq Q_a(t) \leq C_a\overline{\delta}_a.$$

In light of these constraints, we define the thermal energy storage capacity of the indoor air as

$$C_a(\overline{\delta}_a - \underline{\delta}_a).$$

Thermal mass

To analyze the thermal mass separately from the indoor air, we consider a quasi-steady-state model of the air thermal energy dynamics:

$$\dot{Q}_a(t) \approx 0 \text{ for all } t.$$

We assume that this holds for all but a countable number of instants, when Q_a undergoes step changes and $\dot{Q}_a$ is undefined. In this limit,

$$Q_a(t) \approx \frac{C_a R_{am} R_{a\infty}}{R_{am} + R_{a\infty}} \left(\delta(t) + \frac{Q_m(t)}{R_{am} C_m} + \frac{\delta_\infty(t)}{R_{a\infty}} + \delta_e(t) \right).$$

Substituting this approximation into the mass dynamics in (3.5) yields

$$\dot{Q}_m(t) \approx -\frac{Q_m(t)}{\tau_m} + \eta_m \delta(t) + w_m(t), \tag{3.7}$$

where

$$\begin{aligned}
\tau_m &= \frac{C_m R_{m\infty}(R_{am} + R_{a\infty})}{R_{m\infty} + R_{am} + R_{a\infty}} \\
\eta_m &= \frac{R_{a\infty}}{R_{am} + R_{a\infty}} \\
w_m(t) &= \frac{C_m \delta_\infty(t)}{\tau_m} + \eta_m \delta_e(t).
\end{aligned}$$

Like the air dynamics in (3.6), Equation (3.7) has the form of a thermal storage model, where Q_m is the stored energy, δ is the charging power, and w_m ($\mathrm{kW_t}$) is a disturbance caused by forecast error. The time constant τ_m (h) determines how quickly stored thermal energy dissipates. The charging efficiency $\eta_m \in [0, 1]$ determines the fraction of charging power that gets stored in the thermal mass; the remaining fraction $1 - \eta_m$ is stored in the indoor air or lost to the surroundings.

The thermal storage approaches ideal performance ($\eta_m \to 1$ and $\tau_m \to \infty$) in the following limits. First, $\eta_m \to 1$ as $R_{am}/R_{a\infty} \to 0$, meaning heat transfer between the indoor air and mass is much faster than heat transfer between the indoor and outdoor air. In this limit,

$$\tau_m \to \frac{C_m}{1/R_{m\infty} + 1/R_{a\infty}}.$$

For fixed resistances, $\tau_m \to \infty$ as $C_m \to \infty$, meaning the mass is large and dense with a high specific heat capacity. For fixed capacitance, $\tau_m \to \infty$ as $R_{a\infty}, R_{m\infty} \to \infty$, meaning the indoor air and mass are very well insulated from the outdoor air.

We define the thermal energy storage capacity of the mass in terms of the energy that can be stored under sustained, extreme perturbations to the indoor air temperature, assuming

perfect forecasts. If $\delta_\infty(t) = 0$ and $\delta_a(t) = \overline{\delta}_a$ for all t, then as $t \to \infty$,

$$\delta_m(t) \to \frac{R_{m\infty}\overline{\delta}_a}{R_{am} + R_{m\infty}}.$$

This gives an upper limit on the energy that can be stored in the thermal mass. Similarly, if $\delta_\infty(t) = 0$ and $\delta_a(t) = \underline{\delta}_a$ for all t, then as $t \to \infty$,

$$\delta_m(t) \to \frac{R_{m\infty}\underline{\delta}_a}{R_{am} + R_{m\infty}}.$$

This gives a lower limit. We define the mass thermal energy storage capacity as the difference between the upper and lower limits,

$$\frac{C_m R_{m\infty}(\overline{\delta}_a - \underline{\delta}_a)}{R_{am} + R_{m\infty}}.$$

Therefore, the combined thermal storage capacity of the air and mass is

$$\left(C_a + \frac{C_m R_{m\infty}}{R_{am} + R_{m\infty}}\right)(\overline{\delta}_a - \underline{\delta}_a).$$

Thermal power limits

We assume that the thermal equipment has capacity constraints of the form

$$g(T_a(t), T_\infty(t)) \leq \dot{Q}(t) \leq h(T_a(t), T_\infty(t)).$$

The temperature dependence in g and h models the variation of heat pump capacities with the condenser and evaporator temperatures. Thermal equipment constraints translate into

constraints on the transient thermal power perturbations:

$$g(T_a(t), T_\infty(t)) - \hat{\dot{Q}}(t) \leq \delta(t) \leq h(T_a(t), T_\infty(t)) - \hat{\dot{Q}}(t).$$

We define the transient thermal power capacity as the difference between the upper and lower limits,

$$h(T_a(t), T_\infty(t)) - g(T_a(t), T_\infty(t)).$$

In addition to the transient limits, the thermal power perturbations that can be sustained for long periods are limited by the indoor air temperature constraints. If $\delta_\infty(t) = 0$ and $\delta_a(t) = \overline{\delta}_a$ for all t, then as $t \to \infty$,

$$\delta(t) \to \frac{\overline{\delta}_a}{R}.$$

This gives an upper limit on the steady-state thermal power. Similarly, if $\delta_\infty(t) = 0$ and $\delta_a(t) = \underline{\delta}_a$ for all t, then as $t \to \infty$,

$$\delta(t) \to \frac{\underline{\delta}_a}{R}.$$

This gives a lower limit. We define the steady-state thermal power capacity as the difference between the upper and lower limits,

$$\frac{\overline{\delta}_a - \underline{\delta}_a}{R}.$$

We note that transient power perturbations may exceed these steady-state limits.

Chapter 4

Data-driven heat pump selection

In this chapter, we consider the problem of selecting an appropriate heat pump for a given application. Solving this problem is fundamental to the analyses of heat pump emissions and economics in Chapter 2. Several parameters in these high-level analyses, such as capital costs and seasonal average coefficients of performance (COPs), vary significantly across heat pump models and sizes. The heat pump selection problem is also of current practical interest, as field studies report that heat pumps are often inappropriately sized, and that this can significantly degrade performance. [94, 138]

4.1 Background

4.1.1 Heat pump usage cases

Heat pumps are typically used either as stand-alone systems or in cooperation with other heating or cooling equipment. A heat pump may be used differently in heating and cooling seasons. For example, a heat pump could be installed in a building with a working furnace but no cooling system. In this case, the heat pump would be a cooperative heating system but a stand-alone cooling system.

Stand-alone operation: 'Replacement'

Stand-alone heat pumps are expected to meet their entire thermal load, unassisted, in all but the most extreme conditions. Stand-alone heat pumps may be installed in new construction – new buildings, or new additions to existing buildings – or in existing construction. In new construction, stand-alone heat pumps are typically installed instead of incumbent systems such as furnaces, boilers, air conditioners, and distribution ducts or pipes. In existing construction, stand-alone heat pumps are typically installed to replace equipment that is aging, inefficient or broken. In industry, stand-alone operation is called *replacement* usage, as stand-alone heat pumps often replace other equipment.

Cooperation: 'Displacement'

Cooperative heat pumps operate with other heating or cooling equipment. In this setting, the heat pump is typically the most efficient system. Its operation is therefore prioritized; the other equipment serve as backups. The heat pump is not expected to meet peak thermal loads, but rather to operate efficiently in typical conditions. In extreme conditions, backup equipment trips on, providing the additional capacity needed to meet peak loads. In industry, cooperation is called *displacement* usage, as cooperative heat pumps often displace some of the fuel used by an existing furnace or boiler, rather than replacing the furnace or boiler entirely.

Cooperation between a heat pump and backup equipment is typically arranged as follows. The heat pump's thermostat is set to whatever temperature the user prefers. The backup thermostat is set several degrees cooler in winter, or several degrees warmer in summer. In typical conditions, the heat pump maintains the desired indoor air temperature and the backup system is off. In extreme conditions, when the heat pump's capacity is insufficient to meet the entire load, the indoor air temperature drifts past the backup thermostat setpoint.

This causes the backup system to trip on and assist the heat pump.

4.1.2 Heat pump selection in current practice

The document [138] describes current industrial best practices for selecting heat pumps in new construction, new additions to existing buildings, and existing construction. It discusses both replacement and displacement usage cases. It was published by the Northeast Energy Efficiency Partnerships, and draws on that group's experience supporting the installation of about 75,000 air-source heat pumps per year in New York and New England. [139] We now briefly summarize its recommendations.

The first recommended step is to estimate thermal loads in design conditions. The recommended load calculation method is detailed in the Air Conditioning Contractors of America's Manual J. [140] Manual J involves steady-state heat transfer calculations. The input data include surface dimensions and thermal properties, outdoor air infiltration rates, and heat gains from the sun and internal sources. The heating design temperature is the highest outdoor air temperature that is exceeded in the location at least 99% of the hours per year. Similarly, the cooling design temperature is the lowest outdoor air temperature that is exceeded in the location at most 1% of the hours per year. As thermal load is highly correlated with outdoor air temperature, designing heating and cooling systems to meet load at the 99% and 1% outdoor air temperature ensures that load will be met in all but the most extreme conditions.

The second step recommended in [138] is to select the heat pump size. For stand-alone heat pumps, the recommended sizing method is detailed in the Air Conditioning Contractors of America's Manual S. [141] The primary sizing consideration in Manual S is the ability to meet design heating and cooling loads. For heating, Manual S selects any heat pump with a maximum heating capacity in design conditions that is 100% to 140% of the design heating

load. For cooling, Manual S selects any heat pump with a maximum cooling capacity – including both sensible and latent heat removal – in design conditions that is 100% to 115% of the design cooling load, and that provides sufficient air flow.

For displacement usage, the ability to meet design loads is not the primary sizing consideration. Rather, [138] notes that "the main tradeoff is between initial cost vs. savings." Therefore, Manual S is not an appropriate selection tool. The sizing recommendation in [138] is the following.

> Heating capacity of system at or near outdoor design temperature is a secondary concern. Undersizing somewhat for heating should improve efficiency and reduce overall heating costs, even though central system may be used slightly more in colder weather. High efficiency at predominant winter outdoor temperatures will reduce operating cost.

While these are useful guidelines for selecting a heat pump for displacement usage, they leave many details ambiguous. For example, what degree of undersizing is 'undersizing somewhat'? How do the guidelines vary between very cold climates, where heating loads dominate cooling loads, and moderate or hot climates? One goal of this chapter is to resolve ambiguities such as these.

4.1.3 Heat pump selection in the research literature

The heat pump selection problem has been approached from several directions in the research literature. [142–148] Most studies consider the context of air-to-water heat pumps providing joint space and water heating. [142–146] In this context, the heat pump charges a hot water storage tank. Water from the tank is circulated through emitters to heat space, or withdrawn for showers and other domestic uses. Due to this broader context, the studies [142–146] consider the heat pump selection problem alongside the coupled problems of sizing

the storage tank and scheduling heat pump operation. The sizing of solar photovoltaic systems is also considered in [144–146]. In [142–146], the selection problem is formulated as a linear program or mixed-integer linear program and solved via numerical optimization.

Fewer studies consider the heat pump selection problem in the context of reversible heat pumps that provide space heating and cooling. [147, 148] In [147], Dongellini *et al.* analyze the influence of an air-to-air heat pump's size on how efficiently it serves a given building. They consider single-stage and variable-speed heat pumps in a variety of European climates. While they do not develop an explicit selection method, Dongellini *et al.* find that efficiency is sensitive to the heat pump's size relative to the load it serves. They conclude that different sizing methods are likely needed for different climates and heat pump types.

In [148], Zhang *et al.* compare a reversible air-to-air heat pump to incumbent heating and cooling technologies. They develop an explicit method for selecting the best option from a finite set of candidate heating and cooling systems. Their method involves simulating each system's operation over a typical year. The systems are then ranked according to their simple payback periods, *i.e.*, their ratios of capital cost to annual operating cost. The system with the shortest simple payback period is selected.

4.1.4 Our contributions to heat pump selection

The methods developed in this chapter are conceptually similar to those in [148]. Following Zhang *et al.*, we formulate the heat pump selection problem as one of *ranking and selection*. [149] In other words, rather than treating heat pump capacity as a continuous decision variable as in [142–146], we suppose that the designer has a finite set of options from which to choose. We develop methods for ranking those options and choosing between them.

We prefer the ranking and selection formulation because in practice, the number of available heat pump models that may be appropriate for a given application is always finite,

and rarely exceeds a few tens. Treating thermal capacity as a continuous variable is generally not a good approximation; with the possible exception of heat pump manufacturers, heating and cooling practitioners cannot procure a heat pump with arbitrary thermal capacity. This problem is compounded when multiple heat pump parameters, such as heating and cooling capacities and COPs, are treated as decision variables. In this case, the odds that a practitioner can find a heat pump on the market with the parameters generated by solving a continuous optimization problem are vanishingly small. The ranking and selection formulation, by contrast, naturally includes in the selection process all such parameters of all candidate heat pumps.

The key difference between this chapter and [148] lies in the treatment of uncertainty. In [148], candidate systems are ranked according to their performance in a single nominal scenario. This deterministic approach does not account for the uncertainty introduced by weather, occupant behavior, imperfect thermal models, *etc.* Our approach, by contrast, explicitly handles uncertainty through the use of a large number of scenarios obtained from historical data, pseudorandom number generation, or both. Using the theory developed in [150], we derive probabilistic guarantees on the selected heat pump's performance in unseen scenarios that may arise in the future. This scenario approach is substantially more robust than the deterministic approach, and therefore reduces the risk of selecting an inappropriate heat pump.

In addition to providing a new, more robust method for heat pump selection, we conduct several numerical investigations. These investigations suggest that over-sizing variable-speed heat pumps can significantly increase emissions and costs. This is because over-sized heat pumps spend more time cycling, which degrades COPs.

4.1.5 Constrained ranking and selection in the research literature

The field of ranking and selection deals with the general problem of choosing between a finite number of candidate systems under uncertainty. Study of this problem dates back at least to the contributions of Bechhofer in 1954 [151] and Gupta in 1956 [152]. Until recently, the field dealt primarily with systems whose performance was evaluated through the expected value of a single objective function, typically representing a cost or profit, with no constraints. [153–158] In the last decade, however, researchers have begun to investigate *constrained* ranking and selection problems. [159–162] The general heat pump selection problem considered in this chapter involves constraints on unmet thermal loads, so we focus this literature review on constrained ranking and selection.

In [159], Andradottir and Kim consider the problem of selecting the system with the best expected objective function value while restricting the expected value of a constraint function. This paper is among the first contributions to the constrained ranking and selection literature. The solution procedure in [159] involves a feasibility screening stage followed by a selection stage. As is typical in the ranking and selection literature, Andradottir and Kim assume that the objective and constraint functions are observed through stochastic simulation. They further assume that the simulation outputs are normally distributed and independent across systems.

In [160], Healey *et al.* relax the independence assumption in [159] to allow for the use of common random numbers across systems, a variance reduction technique that can significantly improve computational efficiency. [163] Healey *et al.* also broaden the setting of [159] to include multiple constraint functions. The normality assumption of [159] remains in [160], however.

In [161], Hong *et al.* consider a somewhat narrower problem than [159, 160]. By contrast to [159, 160], which consider expectation constraints, [161] consider *chance constraints*, *i.e.*,

constraints on the probability of constraint satisfaction. (A probability can always be viewed as the expectation of an indicator function, so the setting in [161] specializes that in [159, 160].) Restricting attention to this structured special case, Hong *et al.* develop a solution procedure with rigorous guarantees of statistical validity. Hong *et al.* also partially relax the normality assumption of [159, 160]: the constraint observations may be arbitrarily distributed, but the objective observations are assumed to be normal. As in [160], the setting of [161] accommodates multiple constraint functions.

To our knowledge, the only existing method for constrained ranking and selection with arbitrary objective and constraint distributions is in [162]. In [162], Monks and Currie develop a heuristic two-stage method based on bootstrapping. By contrast to [159–161], the problem in [162] is to identify a subset of feasible systems (with respect to expectation constraints) whose expected objective values are within a user-specified percentage of the optimal expected objective value. While the heuristic procedure in [162] has no guarantees of statistical validity, it applies to a very general class of constrained ranking and selection problems, and performs well in a real-world problem involving the design of a hospital's elder-care ward.

A key assumption underlying the guarantees of statistical validity in [159–161] is that the expected objective value of the best system is better than that of all other systems by at least a given threshold. This *indifference zone* assumption on the problem data dates back to Beckhhofer's original 1954 paper. [151]. It facilitates validity proofs. In practice, however, the expected objective values of the candidate systems are not known *a priori*, so the requisite threshold is difficult to specify. As the validity guarantees are contingent upon this assumption, an incorrect threshold invalidates the guarantees in [159–161]. For more discussion of the indifference zone assumption, we refer the interested reader to §2.2.1 of [164].

4.1.6 Our contributions to constrained ranking and selection

For the purposes of heat pump selection, we seek a ranking and selection procedure that

1. accommodates multiple chance constraints,
2. makes no distributional assumptions, and
3. provides a rigorous performance guarantee.

The first condition reflects the facts that the heat pump selection problem may include constraints on both unmet heating and cooling loads, and that chance constraints are sufficiently expressive for our purposes. The second condition reflects the fact that the distributions in our problem are not normal. For example, building codes often specify that heating and cooling equipment be sized such that the temporal frequencies of unmet heating and cooling load are below certain thresholds. [165, 166] The temporal frequencies are random variables supported on $[0, 1]$, so are not well-modeled by normal distributions. The third condition reflects our preference for proven methods over heuristics.

The existing methods that most nearly meet our specifications are those in [161] and [162]. As discussed in §4.1.5, the heuristic procedure in [162] accommodates multiple constraints and admits arbitrary distributions, but comes with no performance guarantees. The procedure in [161] very nearly meets our requirements, except that (a) it assumes normality in the objective and (b) its performance guarantee is contingent on the indifference zone assumption[1], which we find unsatisfactory.

As we are aware of no existing methods that meet our specifications, in this chapter we develop a new constrained ranking and selection procedure. Appendix A expands on

[1] Corrollary 1 of [161] attempts to remove the indifference-zone assumption, but the proof is incorrect; it does not "properly account for the possibility that a good system can eliminate the best system early on and then be eliminated by a bad system" during the selection stage. See [164], §2.3.4 for more discussion.

this procedure and proves an associated performance guarantee. The procedure probabilistically guarantees that the selection is feasible and approximately optimal. The selection and suboptimality threshold are computed by solving an optimization problem with constraints enforced sample-wise. The robustness level of the probabilistic guarantee is computed after solving this problem, and depends on the observed structure of the feasible region. Most of the computation involved can parallelized over systems or scenarios. The use of common random numbers is accommodated. The proof of the probabilistic guarantee is a straightforward application of the recent theory in [150]. The guarantee holds for arbitrary distributions and does not require the indifference-zone assumption.

It is worth noting that our approach entails two conceptual departures from established conventions in the ranking and selection literature. First, we adopt a risk-averse approach that emphasizes performance under unfavorable scenarios. Second, rather than viewing the input data as something to be generated internally in order to guarantee good selection at a user-specified robustness level, we use what data is available and derive a posterior performance guarantee. While unconventional, this approach may be appealing to risk-averse decision-makers, or in settings where input data or computational resources are limited.

4.2 Deterministic problem statement

In this section, we formulate the heat pump selection problem in a deterministic setting. We assume that all input data, such as future weather and loads, are known exactly. We begin in the deterministic setting in order to introduce the physics, objectives and constraints in a relatively simple context. In §4.3, we will adapt the deterministic problem statement to a more general context where uncertainty is explicitly considered.

Throughout this chapter, we assume that the selected heat pump is evaluated relative to an incumbent system. In replacement applications, the heat pump must be large enough

to meet load in all but the worst conditions. In displacement applications, the amount of load displaced, and therefore the energy cost savings, depend on the heat pump's thermal capacity. We also assume that the following data are available: coincident air temperatures, loads and prices; estimates of each heat pump's installed cost, annual maintenance cost, and lifetime; and mathematical models of each heat pump's thermal capacity and coefficient of performance under varying temperatures and loads.

The problem we consider is to select one of a finite set of candidate heat pumps in order to maximize the net present value of installing the heat pump and operating it over its lifetime, possibly subject to constraints on the frequencies of unmet heating or cooling load. This problem arises under two distinct ownership models. In the first model, a user owns the heat pump and pays for its maintenance and input electricity over its lifetime. In the second model, an HPA aggregator owns the heat pump, pays for its maintenance and electricity, sells its thermal output to the user, and earns revenue from providing ancillary services.

In the HPA ownership model, we assume that the aggregator and user negotiate the HPA using the process discussed in §2.3.4–2.3.5. In this process, the total value of a heat pump HPA (see Equation (2.5)) is determined by comparing the heat pump to an incumbent system. The aggregator and user negotiate the user's share $\phi \in [0, 1]$ of the total value. The net present value of the aggregator's heat pump investment is $1 - \phi$ times the total value. Therefore, maximizing the aggregator's net present value is equivalent to maximizing the total value. The total HPA value in Equation (2.5) is structurally identical to the user's net present value under traditional ownership, as shown in Equation (2.2). For this reason, it suffices to consider only net present value expressions of the form of Equations (2.2) and (2.5).

4.2.1 Physics

We consider a one-year discrete time span indexed by $k = 1, \ldots, K$ with time step Δt (h). We also consider a finite set of heat pumps indexed by $j = 1, \ldots, J$. At each stage k, the thermal power output of heat pump j is $\dot{Q}_j(k)$ ($\mathrm{kW_t}$). If $\dot{Q}_j(k)$ is positive, then heat pump j provides heating at stage k. If $\dot{Q}_j(k)$ is negative, then it provides cooling.

Capacity, modulation and cycling

The thermal power output of heat pump j must satisfy

$$\dot{Q}_{cj}^{\mathrm{cap}}(T_a(k), T_\infty(k)) \leq \dot{Q}_j(k) \leq \dot{Q}_{hj}^{\mathrm{cap}}(T_a(k), T_\infty(k)). \tag{4.1}$$

Here $T_a(k)$ (°C) and $T_\infty(k)$ (°C) are the indoor and outdoor air temperature, respectively, at stage k. The function $\dot{Q}_{hj}^{\mathrm{cap}} : \mathbf{R}^2 \to \mathbf{R}$ gives the heating capacity of heat pump j under varying indoor and outdoor air temperatures. Similarly, $\dot{Q}_{cj}^{\mathrm{cap}} : \mathbf{R}^2 \to \mathbf{R}$ gives the cooling capacity of heat pump j.

We assume that heat pump j modulates continuously throughout stage k if

$$\dot{Q}_{hj}^{\mathrm{mod}}(T_a(k), T_\infty(k)) \leq \dot{Q}_j(k) \leq \dot{Q}_{hj}^{\mathrm{cap}}(T_a(k), T_\infty(k))$$

or

$$\dot{Q}_{cj}^{\mathrm{cap}}(T_a(k), T_\infty(k)) \leq \dot{Q}_j(k) \leq \dot{Q}_{cj}^{\mathrm{mod}}(T_a(k), T_\infty(k)).$$

On the other hand, if

$$\dot{Q}_{cj}^{\mathrm{mod}}(T_a(k), T_\infty(k)) < \dot{Q}_j(k) < \dot{Q}_{hj}^{\mathrm{mod}}(T_a(k), T_\infty(k)),$$

then heat pump j cycles off and on during stage k. Here the functions $\dot{Q}_{hj}^{\mathrm{mod}} : \mathbf{R}^2 \to \mathbf{R}$

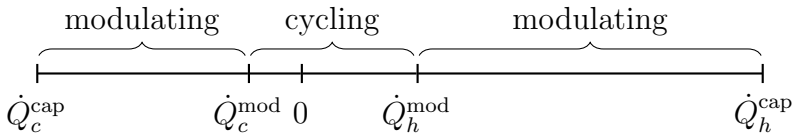

Figure 4.1: A variable-speed heat pump cycles off and on if the load is smaller than its modulating threshold $\dot{Q}_h^{\text{mod}}$ (in heating mode) or $\dot{Q}_c^{\text{mod}}$ (in cooling mode). Otherwise, it modulates continuously. A single-speed heat pump, by contrast, never modulates; its modulating thresholds equal its capacities $\dot{Q}_h^{\text{cap}}$ and $\dot{Q}_c^{\text{cap}}$.

and $\dot{Q}_{cj}^{\text{mod}} : \mathbf{R}^2 \to \mathbf{R}$ give the minimum modulating capacity when heating and cooling, respectively. If heat pump j has a single-speed motor, then $\dot{Q}_{hj}^{\text{mod}} = \dot{Q}_{hj}^{\text{cap}}$, $\dot{Q}_{cj}^{\text{mod}} = \dot{Q}_{cj}^{\text{cap}}$, and the modulating ranges reduce to singletons. In this case, heat pump j either cycles or saturates at every stage. Figure 4.1 illustrates the modulation behavior.

Load and thermal power

We denote the load at stage k by $L(k)$ (kW_t). If $L(k)$ is positive, then heating is required at stage k. If $L(k)$ is negative, then cooling is required. We assume that each heat pump j is controlled such that if it has sufficient capacity to meet load, then it meets load exactly; otherwise, its thermal power output saturates at its capacity. Mathematically,

$$\dot{Q}_j(k) = \max\left\{\dot{Q}_{cj}^{\text{cap}}(T_a(k), T_\infty(k)), \min\left\{L(k), \dot{Q}_{hj}^{\text{cap}}(T_a(k), T_\infty(k))\right\}\right\}. \tag{4.2}$$

Figure 4.2 shows a plot of thermal power output vs. load for fixed indoor and outdoor air temperatures.

By construction, the thermal power output (4.2) respects the equipment constraints (4.1). Load is not necessarily met, however. The unmet heating load by heat pump j at stage k is

$$U_j^h(k) := (L(k) - \dot{Q}_j(k))_+,$$

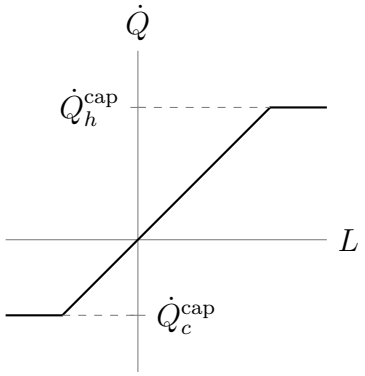

Figure 4.2: The thermal power output $\dot{Q}$ is equal to the thermal load L whenever $L \in [\dot{Q}_c^{\text{cap}}, \dot{Q}_h^{\text{cap}}]$. Otherwise, the thermal power output saturates at the heating capacity $\dot{Q}_h^{\text{cap}}$ or cooling capacity $\dot{Q}_c^{\text{cap}}$. The heating and cooling capacities vary across heat pumps and with the indoor and outdoor air temperatures.

where $(\cdot)_+ = \max\{0, \cdot\}$ is the positive part function. Similarly, the unmet cooling load is

$$U_j^c(k) := (\dot{Q}_j(k) - L(k))_+.$$

Electrical power

We denote the electrical power consumed by heat pump j at stage k by

$$P_j(k) := \frac{|\dot{Q}_j(k)|}{\eta_j(T_a(k), T_\infty(k), \dot{Q}_j(k))}.$$

The function $\eta_j : \mathbf{R}^3 \to \mathbf{R}$ gives the COP of heat pump j under various operating conditions. The dependence of η_j on $\dot{Q}_j$ accounts for the heat pump's part-load performance. It also allows η_j to distinguish between heating and cooling COPs based on the sign of $\dot{Q}_j$.

We define the electrical power capacity of heat pump j at stage k as the power it would

consume if operated at its current thermal capacity:

$$P_j^{\text{cap}}(k) := \begin{cases} \dot{Q}_{hj}^{\text{cap}}(T_a(k), T_\infty(k))/\eta_j(T_a(k), T_\infty(k), \dot{Q}_{hj}^{\text{cap}}(T_a(k), T_\infty(k))) & \dot{Q}_j(k) \geq 0 \\ -\dot{Q}_{cj}^{\text{cap}}(T_a(k), T_\infty(k))/\eta_j(T_a(k), T_\infty(k), \dot{Q}_{cj}^{\text{cap}}(T_a(k), T_\infty(k))) & \dot{Q}_j(k) < 0. \end{cases}$$

We also define the electrical power modulation threshold

$$P_j^{\text{mod}}(k) := \begin{cases} \dot{Q}_{hj}^{\text{mod}}(T_a(k), T_\infty(k))/\eta_j(T_a(k), T_\infty(k), \dot{Q}_{hj}^{\text{mod}}(T_a(k), T_\infty(k))) & \dot{Q}_j(k) \geq 0 \\ -\dot{Q}_{cj}^{\text{mod}}(T_a(k), T_\infty(k))/\eta_j(T_a(k), T_\infty(k), \dot{Q}_{cj}^{\text{mod}}(T_a(k), T_\infty(k))) & \dot{Q}_j(k) < 0. \end{cases}$$

If $P_j(k) < P_j^{\text{mod}}(k)$, then heat pump j cycles off and on at stage k.

4.2.2 Constraints

When sizing for equipment stand-alone operation, building codes and industry standards such as [140, 141, 165, 166] typically require that the frequencies of unmet heating and cooling load, f_j^h and f_j^c, satisfy

$$\begin{aligned} f_j^h &:= \frac{1}{K}\sum_{k=1}^{K} \mathcal{I}_+(U_j^h(k)) \leq \varepsilon_h \\ f_j^c &:= \frac{1}{K}\sum_{k=1}^{K} \mathcal{I}_+(U_j^c(k)) \leq \varepsilon_c. \end{aligned} \tag{4.3}$$

Here $\mathcal{I}_+ : \mathbf{R} \to \mathbf{R}$ is the indicator function of the positive real numbers; it returns one if its argument is strictly positive and zero otherwise. The unmet load frequencies f_j^h and f_j^c always lie between zero and one.

The parameters $\varepsilon_h, \varepsilon_c \in [0, 1]$ could be specified by the designer, the building owner or occupants, an industry standard or a building code. As discussed in §4.1.2, the typical value of ε_h and ε_c for stand-alone operation is 0.01. In cooperative heating usage, however, the

backup system meets any unmet heating load. In this case, the frequency of unmet load is unconstrained (or, equivalently, $\varepsilon_h = 1$). The same applies for cooperative cooling usage.

4.2.3 Objectives

Energy

The electrical energy cost of heat pump j at stage k is

$$\Delta t \pi(k) P_j(k),$$

where $\pi(k)$ (\$/kWh) is the electricity price at stage k. We also consider the avoided energy cost of heating or cooling with an incumbent system. In heating mode ($\dot{Q}_j(k) \geq 0$), the avoided energy cost is

$$\frac{\Delta t \tilde{\pi}_h(k) \dot{Q}_j(k)}{\tilde{\eta}_h(T_a(k), T_\infty(k), \dot{Q}_j(k))},$$

where $\tilde{\pi}_h(k)$ (\$/kWh) is the incumbent heating fuel price at stage k and $\tilde{\eta}_h : \mathbf{R}^3 \to \mathbf{R}$ gives the incumbent heating COP or efficiency. In cooling mode ($\dot{Q}_j(k) < 0$), the avoided energy cost is

$$\frac{-\Delta t \pi(k) \dot{Q}_j(k)}{\tilde{\eta}_c(T_a(k), T_\infty(k), \dot{Q}_j(k))},$$

where $\tilde{\eta}_c : \mathbf{R}^3 \to \mathbf{R}$ gives the incumbent cooling COP. For brevity, we consolidate the incumbent heating and cooling energy costs into one term:

$$\tilde{\pi}(k) \tilde{E}_j(k).$$

Here

$$\tilde{\pi}(k) = \begin{cases} \tilde{\pi}_h(k) & \dot{Q}_j(k) \geq 0 \\ \pi(k) & \dot{Q}_j(k) < 0 \end{cases}$$

and

$$\tilde{E}_j(k) = \begin{cases} \Delta t \dot{Q}_j(k)/\tilde{\eta}_h(T_a(k), T_\infty(k), \dot{Q}_j(k)) & \dot{Q}_j(k) \geq 0 \\ -\Delta t \dot{Q}_j(k)/\tilde{\eta}_c(T_a(k), T_\infty(k), \dot{Q}_j(k)) & \dot{Q}_j(k) < 0. \end{cases}$$

We note that the avoided energy costs vary from heat pump to heat pump. This is because the avoided load equals the load met by the heat pump, which depends in general on the heat pump capacity.

Ancillary services

We consider the joint provision of two ancillary services: reserve and regulation. Reserve is the capacity to curtail load at the power system operator's request. We restrict our attention to so-called *spinning* or *synchronous* reserve, which requires the fastest responses (typically within ten minutes of receiving the request) and has the highest prices of the various reserve products. Reserve is infrequently dispatched (typically once or twice per month), and dispatch durations are rarely more than ten minutes.

Regulation involves continuously perturbing electrical power in order to track a reference signal sent by the power system operator. Some power system operators define two regulation products, distinguished by the direction of the power perturbation. Other power system operators define regulation as the ability to perturb power symmetrically in either direction. To keep notation relatively light, we restrict our attention to symmetric regulation markets, but asymmetric regulation can easily be accommodated.

Regulation prices are significantly higher than reserve prices, so we assume that regulation is prioritized. If heat pump j provides regulation at stage k, then it earns revenue

$$\Delta t \pi^{\text{reg}}(k) P_j^{\text{reg}}(k),$$

where $\pi^{\text{reg}}(k)$ (\$/kWh) is the regulation price at stage k. We define the regulation capacity

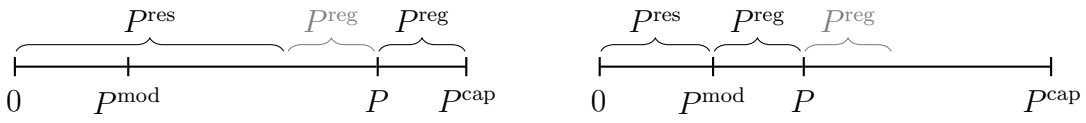

(a) High power case (b) Low power case

Figure 4.3: Regulation and reserve capacities in the cases where the heat pump's nominal power consumption P is near its (a) maximum capacity P^{cap}, and (b) minimum modulating capacity P^{mod}. In case (a), the regulation capacity is determined by the upward flexibility. In case (b), the regulation capacity is determined by the downward flexibility. In both cases, the reserve capacity is the downward flexibility that remains when the heat pump modulates to $P - P^{\text{reg}}$.

as

$$P_j^{\text{reg}}(k) := \begin{cases} \min\left\{P_j^{\text{cap}}(k) - P_j(k), P_j(k) - P_j^{\text{mod}}(k)\right\} & P_j(k) \geq P_j^{\text{mod}}(k) \\ 0 & P_j(k) < P_j^{\text{mod}}(k). \end{cases}$$

With this definition, a variable-speed heat pump can provide no regulation while cycling.

Reserve capacity depends on regulation capacity:

$$P_j^{\text{res}}(k) := \begin{cases} P_j(k) - P_j^{\text{reg}}(k) & P_j(k) \geq P_j^{\text{mod}}(k) \\ 0 & P_j(k) < P_j^{\text{mod}}(k). \end{cases}$$

(No reserve capacity can be offered when $P_j(k) < P_j^{\text{mod}}(k)$, because a heat pump cannot curtail load during 'off' periods while cycling.) If heat pump j provides reserve at stage k, then it earns revenue

$$\Delta t \pi^{\text{res}}(k) P_j^{\text{res}}(k),$$

where $\pi^{\text{res}}(k)$ (\$/kWh) is the reserve price at stage k. Figure 4.3 illustrates the regulation and reserve capacity definitions.

Power system operators typically require a minimum capacity on the order of 100 kW to 1 MW to enter ancillary service markets. Individual heat pumps typically have electrical

capacities on the order of 1 kW. To earn ancillary service revenue, therefore, heat pumps need to be aggregated by the hundreds or thousands. Aggregation can significantly increase the capacity that can be offered for ancillary services, as well as the associated revenues. We discuss this further in §5.3. In this chapter, however, we assume for simplicity that the heat pump provides ancillary services independently.

Installed and maintenance costs

Each heat pump has an installed cost c_j (\$) that includes rebates or tax credits, hardware and labor costs, the installer's overhead and profit, and all other related expenses and incentives. Each heat pump also has an annual maintenance cost m_j, again including hardware, labor, overhead and profit. We denote the lifetime of heat pump j by Y_j. Similarly, the incumbent system has capital cost $\tilde{c}$ (\$) and annual maintenance cost $\tilde{m}$ (\$).

Emissions

As discussed in §2.2.5, the cost of greenhouse gas emissions caused by consuming electricity can be internalized by redefining the electricity price to

$$\pi(k) \leftarrow \pi(k) + \pi_{\mathrm{g}}\mu(k),$$

where $\mu(k)$ (kg/kWh) is the greenhouse gas intensity of electricity at stage k and π_{g} (\$/kg) is the price of greenhouse gas emissions. Similarly, the cost of the incumbent heating system's greenhouse gas emissions can be internalized by redefining

$$\tilde{\pi}_h(k) \leftarrow \tilde{\pi}_h(k) + \pi_{\mathrm{g}}\tilde{\mu}(k),$$

where $\tilde{\mu}(k)$ (kg/kWh) is the greenhouse gas intensity of the incumbent heating fuel at stage k.

To internalize the cost of greenhouse gas emissions due to manufacturing and shipping, c_j can be redefined to

$$c_j \leftarrow c_j + \pi_{\mathrm{g}} M_j,$$

where M_j (kg) is the mass of CO_2-equivalent embodied in heat pump j. Similarly, the incumbent system's capital cost can be redefined to

$$\tilde{c} \leftarrow \tilde{c} + \pi_{\mathrm{g}} \tilde{M},$$

where $\tilde{M}$ (kg) is the mass of CO_2-equivalent embodied in the incumbent system.

Net present value

The net present value of heat pump j includes its installed cost, its avoided installed cost (for stand-alone usage), and the discounted annual maintenance and operating costs over its lifetime:

$$\begin{aligned}\mathrm{NPV}_j &:= \tilde{c} - c_j \\ &+ \gamma_j \left[\tilde{m} - m_j + \sum_{k=1}^{K} \tilde{\pi}(k) E_j(k) + \Delta t \left(\pi^{\mathrm{reg}}(k) P_j^{\mathrm{reg}}(k) + \pi^{\mathrm{res}}(k) P_j^{\mathrm{res}}(k) - \pi(k) P_j(k) \right) \right].\end{aligned}$$

Here the parameter

$$\gamma_j := \sum_{y=1}^{Y_j} \frac{1}{(1+\rho)^y}$$

governs the trade-off between installed cost and operating costs over the the lifetime of heat pump j, with future cash flows discounted at rate $\rho \geq 0$. As discussed in §2.5, this expression for the net present value assumes that the loads, temperatures and prices will be similar from

year to year over the heat pumps' lifetimes. This assumption can be relaxed; we make it mainly for notational convenience.

4.2.4 Summary

In summary, the deterministic formulation of our heat pump sizing problem is to

$$\begin{aligned} \underset{j\in\{1,\ldots,J\}}{\text{maximize}} \quad & \text{NPV}_j \\ \text{subject to} \quad & f_j^h \leq \varepsilon_h \\ & f_j^c \leq \varepsilon_c. \end{aligned} \tag{4.4}$$

This optimization problem has one discrete scalar decision variable and two constraints. If the heat pump is installed for heating displacement, then $\varepsilon_h = 1$ and the first constraint can be deleted. The same applies for ε_c and the second constraint if the heat pump is installed for cooling displacement. Problem (4.4) can be solved by simulating all candidate systems and computing their net present values and unmet load frequencies. A feasible heat pump with maximal net present value is optimal.

4.3 Scenario framework

In §4.2, we assumed that all of the input data – loads, temperatures, prices, *etc.* – were known exactly. We now relax this assumption. We first discuss the input data, then formulate a scenario-based version of the deterministic heat pump sizing problem (4.4). Solving this problem and implementing a post-processing step yields a heat pump selection with probabilistic feasibility and optimality guarantees. As this selection method is original and potentially of interest in broader applications, we discuss it in more detail and a more general setting in Appendix A. The appendix also includes a proof of the probabilistic guarantee.

4.3.1 Input data

The input parameters to the method discussed in §4.2 are J, Δt, K, ρ, ε_h, ε_c, $c_1, \ldots, c_J$, $\tilde{c}_1, \ldots, \tilde{c}_J$, $m_1, \ldots, m_J$, $\tilde{m}_1, \ldots, \tilde{m}_J$, and $Y_1, \ldots, Y_j$. We assume that J, Δt, K, ρ, ε_h, ε_c are known at decision time, as they are specified by the designer or occupants. The remaining parameters could be random. The installed costs c_j, for example, could depend on fluctuating hardware prices and unforeseen installation complications.

The input signals, each defined for $k = 1, \ldots, K$, are $L(k)$, $T_a(k)$, $T_\infty(k)$, $\pi^{\text{reg}}(k)$, $\pi^{\text{res}}(k)$ and $\pi(k)$. All of these signals could be random. The load $L(k)$, for example, depends on the weather and occupant behavior. The indoor air temperature $T_a(k)$ depends on occupant preferences. The electricity price $\pi(k)$ could be tied to a market clearing price.

In this section, we denote the stacked vector of all of the uncertain input data by $\delta \in \Delta$, where Δ is a probability space equipped with a σ-algebra and probability measure. The dimension of δ could be very large, as δ contains all uncertain input parameters and all uncertain input signals at all time steps. We emphasize, however, that the results in this section do not depend on the dimension of δ.

4.3.2 Stochastic problem statement

In the stochastic framework, the net present values and the frequencies of unmet heating and cooling load are random due to their dependence on δ. (Going forward, we emphasize this dependence by writing $\text{NPV}_j(\delta)$, $f_j^h(\delta)$ and $f_j^c(\delta)$.) The goals of minimizing $\text{NPC}_j(\delta)$ and constraining $f_j^h(\delta)$ and $f_j^c(\delta)$ are therefore ambiguous.

To resolve this ambiguity, we specify the following optimization problem:

$$\begin{aligned} &\text{minimize} \quad \tau \\ &\text{subject to} \quad \mathbf{Prob}\left\{ \begin{array}{l} \mathrm{NPV}^\star(\delta) - \mathrm{NPV}_j(\delta) \leq \tau \\ f_j^h(\delta) \leq \varepsilon_h, \;\; f_j^c(\delta) \leq \varepsilon_c \end{array} \right\} \geq 1 - \alpha, \end{aligned} \tag{4.5}$$

where $\mathrm{NPV}^\star : \Delta \to \mathbf{R}$ gives the optimal value under uncertainty δ,

$$\mathrm{NPV}^\star(\delta) = \max_{j=1,\ldots,J} \left\{ \mathrm{NPV}_j(\delta) \;\middle|\; f_j^h(\delta) \leq \varepsilon_h, \;\; f_j^c(\delta) \leq \varepsilon_c \right\}.$$

The probability in Problem (4.5) refers to the joint distribution of δ.

The decision variable in Problem (4.5) is $(j, \tau) \in \{1, \ldots, J\} \times \mathbf{R}$. A solution $(j^\star, \tau^\star)$ provides a probabilistic guarantee that the selection $j^\star$ will be feasible and that its net present value will be within $\tau^\star$ of the maximum achievable under whatever value of δ is realized. The smaller the robustness level $\alpha \in (0, 1)$ and suboptimality threshold $\tau^\star$, the stronger the guarantee. In the extreme case of $\tau^\star = 0$, we obtain a probabilistic guarantee that $j^\star$ will be optimal.

4.3.3 Approximate solution by scenario optimization

As the distribution of δ may not be known, Problem (4.5) is intractable in general. We therefore resort to approximate solution by scenario optimization. In this approach, we suppose that an independent, identically distributed sample $(\delta^1, \ldots, \delta^N)$ from the distribution of δ is available. We refer to the δ^i as *scenarios*.

Given $\delta^1, \ldots, \delta^N$, we form a scenario version of Problem (4.5):

$$\begin{array}{ll} \text{minimize} & \tau \\ \text{subject to} & \text{NPV}^\star(\delta^i) - \text{NPV}_j(\delta^i) \leq \tau, \ i = 1, \ldots, N \\ & f_j^h(\delta^i) \leq \varepsilon_h, \ f_j^c(\delta^i) \leq \varepsilon_c, \ i = 1, \ldots, N. \end{array} \tag{4.6}$$

As in Problem (4.5), the decision variable in Problem (4.6) is $(j, \tau) \in \{1, \ldots, J\} \times \mathbf{R}$. A solution $(j_N^\star, \tau_N^\star)$ to Problem (4.6) can be computed by exhaustive search as follows.

1. Feasibility screening:
   (a) Compute $f_j^h(\delta^i)$ and $f_j^c(\delta^i)$ for each $j = 1, \ldots, J$ and $i = 1, \ldots, N$.
   (b) Set $\mathcal{J} = \left\{ j \in \{1, \ldots, J\} \mid f_j^h(\delta^i) \leq \varepsilon_h, \ f_j^c(\delta^i) \leq \varepsilon_c, \ i = 1, \ldots, N \right\}$.
2. Minimization:
   (a) Compute $\text{NPV}_j(\delta^i)$ for each $j \in \mathcal{J}$ and $i = 1, \ldots, N$.
   (b) Compute $\text{NPV}^\star(\delta^i) = \max_j \{\text{NPV}_j(\delta^i) \mid j \in \mathcal{J}\}$ for each $i = 1, \ldots, N$.
   (c) Compute $\tau_j = \max_i \{\text{NPV}^\star(\delta^i) - \text{NPV}_j(\delta^i) \mid i = 1, \ldots, N\}$ for each $j \in \mathcal{J}$.
   (d) Compute $\tau_N^\star = \min_j \{\tau_j \mid j \in \mathcal{J}\}$ and set $j_N^\star$ to a corresponding minimizer, using a tie-break rule if there are multiple minimizers.

This procedure is a function that takes a sample $(\delta^i, \ldots, \delta^N)$ as its input and outputs a selection $j_N^\star$ and suboptimality threshold $\tau_N^\star$. We denote this function by $\mathcal{A}_N : \Delta^N \to \{1, \ldots, J\} \times \mathbf{R}$ and write

$$(j_N^\star, \tau_N^\star) = \mathcal{A}_N(\delta^1, \ldots, \delta^N).$$

We also define functions $\mathcal{A}_m : \Delta^m \to \{1, \ldots, J\} \times \mathbf{R}$ for $m = 1, \ldots, N$. Each $\mathcal{A}_m$ implements the above procedure on a sample of cardinality m.

4.3.4 Robustness guarantee

The recent theory in [150] allows a solution $(j_N^\star, \tau_N^\star)$ to the scenario problem (4.6) to be evaluated with respect to the chance constraint in Problem (4.5). Given a confidence parameter $\beta \in (0,1)$, this theory guarantees with $100(1-\beta)\%$ confidence that

$$\textbf{Prob}\left\{\begin{array}{l} \mathrm{NPV}^\star(\delta) - \mathrm{NPV}_{j_N^\star}(\delta) \le \tau_N^\star \\ f_{j_N^\star}^h(\delta) \le \varepsilon_h,\ \ f_{j_N^\star}^c(\delta) \le \varepsilon_c \end{array}\right\} \ge 1 - \alpha_N^\star. \tag{4.7}$$

To compute the robustness level $\alpha_N^\star$, we must find a *support subsample*. A support subsample is a sequence of scenarios $(\delta^{i_1}, \ldots, \delta^{i_k})$ with $i_1 < \cdots < i_k$ such that $\{i_1, \ldots, i_k\} \subseteq \{1, \ldots, N\}$ and

$$\mathcal{A}_k(\delta^{i_1}, \ldots, \delta^{i_k}) = \mathcal{A}_N(\delta^1, \ldots, \delta^N).$$

In other words, optimizing over a support subsample yields the same selection and suboptimality threshold as optimizing over the full sample. Given a support subsample of cardinality $s_N^\star$, a robustness level $\alpha_N^\star$ for which the guarantee (4.7) holds is given by

$$\alpha_N^\star = \begin{cases} 1 & \text{if } s_N^\star = N \\ 1 - \left[\beta \Big/ N\binom{N}{s_N^\star}\right]^{1/(N-s_N^\star)} & \text{otherwise.} \end{cases} \tag{4.8}$$

The right-hand side of (4.8) is an increasing function of $s_N^\star$. To strengthen the guarantee (4.7), therefore, we would like to find a small support subsample. The following procedure, adapted from [150], can be shown to yield an irreducible subsample (though not necessarily one of minimal cardinality).

1. Initialize $S \leftarrow (\delta^1, \ldots, \delta^N)$.

2. For $i = 1, \ldots, N$,

(a) Set $S_i = S \setminus \delta^i$.

(b) If $\mathcal{A}_{|S_i|}(S_i) = A_N(\delta^1, \ldots, \delta^N)$, set $S \leftarrow S_i$.

When this procedure terminates, the final sample S is an irreducible support subsample. Its cardinality $s_N^\star$ can be used in (4.8) to compute a robustness level $\alpha_N^\star$ valid in the probabilistic guarantee (4.7).

4.4 Numerical example

In this section, we numerically investigate various aspects of the heat pump selection problem through Monte Carlo simulation. We focus on heating displacement and cooling replacement in a typical United States building and location. In all simulations, we use a time step of $\Delta t = 1$ h, horizon $K = 8760$, and sample size of $N = 1000$ scenarios.

The simulation input data include $\rho, \varepsilon_h, \varepsilon_c \in \mathbf{R}$, $Y, c, \tilde{c}, m, \tilde{m} \in \mathbf{R}^J$, and L, T_a, T_∞, $\pi^{\text{reg}}, \pi^{\text{res}}, \pi \in \mathbf{R}^K$. The annual cash flow discount rate ρ ranges from 5% and 15%, while the heat pump lifetimes Y_j range from 10 to 20 years. The parameters ρ and Y_j are sampled independently from uniform distributions over these ranges. The maximum allowable frequency of unmet cooling load is set at $\varepsilon_c = 0.01$, in keeping with international building energy codes. [165, 166] The heat pumps are used for heating displacement, so $\varepsilon_h = 1$.

The electrical energy price π, ancillary service prices $\pi^{\text{reg}}, \pi^{\text{res}}$, and the outdoor air temperature T_∞ are discussed in the relevant subsections of §4.4.1. The thermal load L and indoor air temperature T_a are discussed in §4.4.2. The installed and maintenance costs $c, \tilde{c}, m, \tilde{m}$ are discussed in §4.4.3.

4.4.1 Setting

We locate simulations in Philadelphia. We consider this city to be representative, in the sense that its weather, electricity price and greenhouse gas intensity, and natural gas price are close to the United States averages. See §2.1.1–2.1.2 and §2.2.1–2.2.2 for more discussion of these parameter values and their variation across the United States. Simulations include hourly historical weather and price data for the last six years (January 1, 2013 through December 31, 2018). This is the longest recent period for which all data, notably including ancillary service prices, are available.

Weather

Philadelphia is located at sea level and 40° north latitude. The 99% heating design temperature and 1% cooling design temperatures are −9.4 °C and 31.7 °C, respectively. [140] Between 2013 and 2018, the average annual heating and cooling degree-days at base 18 °C were 2410 °C-days and 910 °C-days, respectively. Figure 4.4 shows the hourly average outdoor air (dry bulb) temperature and global horizontal solar irradiance between 2013 and 2018. The weather data source is [167], a compendium of historical weather data in Pennsylvania maintained by meteorology researchers at Pennsylvania State University.

Electrical energy

We simulate heat pump operation under a residential rate plan of the largest utility company in Philadelphia. [168] This rate plan includes both a monthly fixed charge and a variable charge based on electrical energy consumption. The electrical energy price π is 0.1335 \$/kWh from June through September and 0.1167 \$/kWh from October through May. The discounted winter energy price reflects the fact that this rate plan is designed for customers with electrical heating. The source [168] details the utility's electricity rate plan for residen-

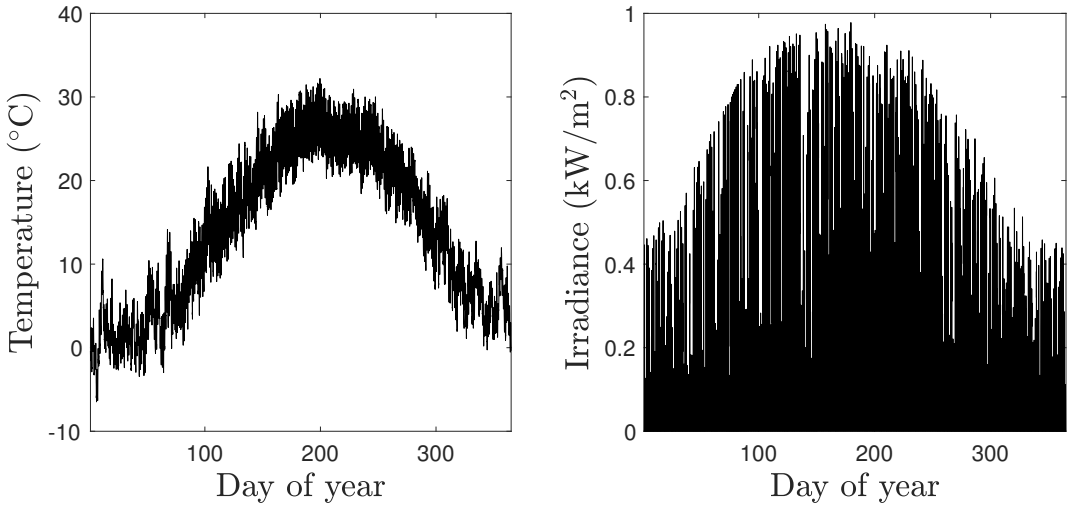

Figure 4.4: Hourly average outdoor air temperature (left) and global horizontal solar irradiance (right) in Philadelphia from 2013–2018.

tial customers with electric heating systems. The electricity prices are deterministic.

Ancillary services

Philadelphia lies in the service territory of the PJM Interconnection, the largest power system in the United States. PJM operates wholesale markets for both energy and ancillary services. [169] We restrict our attention to the regulation and synchronized reserve ancillary service markets. Figure 4.5 shows histograms of the 2013–2018 regulation and synchronized reserve market clearing prices. The synchronized reserve capacity price is typically about one order of magnitude less than regulation capacity price, which in turn is about one order of magnitude lower than the Philadelphia retail electricity price. The data source is [170], an online database of historical data from PJM's ancillary service markets. We use all available regulation and synchronous reserve price data, and note that this data is geographically and temporally coincident with the historical weather data used in simulations.

PJM's regulation market requires symmetric capacity. In other words, resources providing regulation must be capable of upward and downward power perturbations of the same

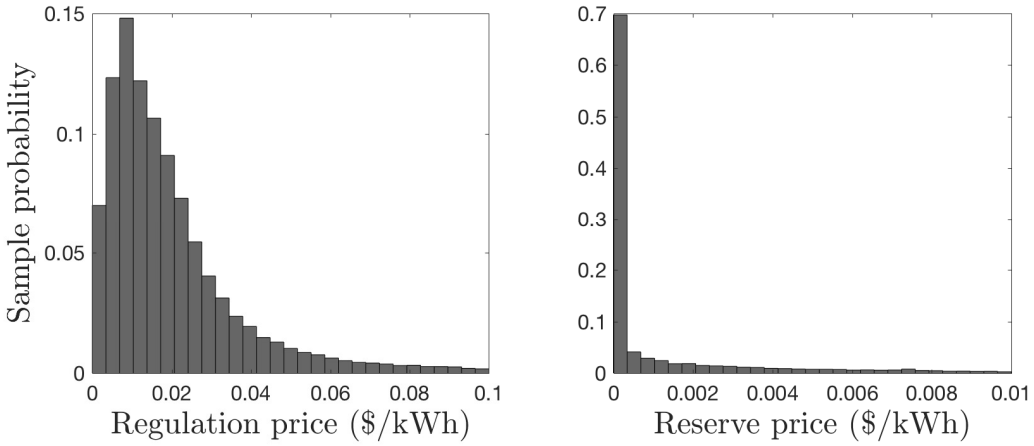

Figure 4.5: Histograms of the PJM market clearing prices of regulation (left) and reserve (right) from 2013–2018. The mean regulation and reserve prices are 0.0265 $/kWh and 0.0029 $/kWh, respectively.

magnitude. The PJM regulation signal is filtered into two components: RegA and RegD. RegA is a lower frequency, nonzero-mean signal. RegD is a higher frequency signal that is designed to be approximately zero-mean over any 15-minute period. We focus on RegD, as experiments have shown that variable-speed heat pumps can track the RegD signal without causing noticeable perturbations to indoor air temperatures. [45, 46] We discuss this further in §5.2.

Regulation payments include both capacity and performance components. The former is based on commitments cleared in advance, while the latter is based on the actual tracking of power perturbations requested by PJM during operations. We consider both components. The left plot in Figure 4.5 shows a histogram of the 2013–2018 total (capacity plus performance) regulation prices, π^{reg}. In simulations, we treat the regulation prices as deterministic.

Synchronized reserve is the fastest and highest-priced of PJM's reserve ancillary services. Synchronized reserve involves the ability to curtail load (or increase generation) within ten minutes of PJM's request. Synchronized reserve is primarily a capacity service. As shown in Figure 4.6, synchronized reserve resources are typically deployed about one to four times

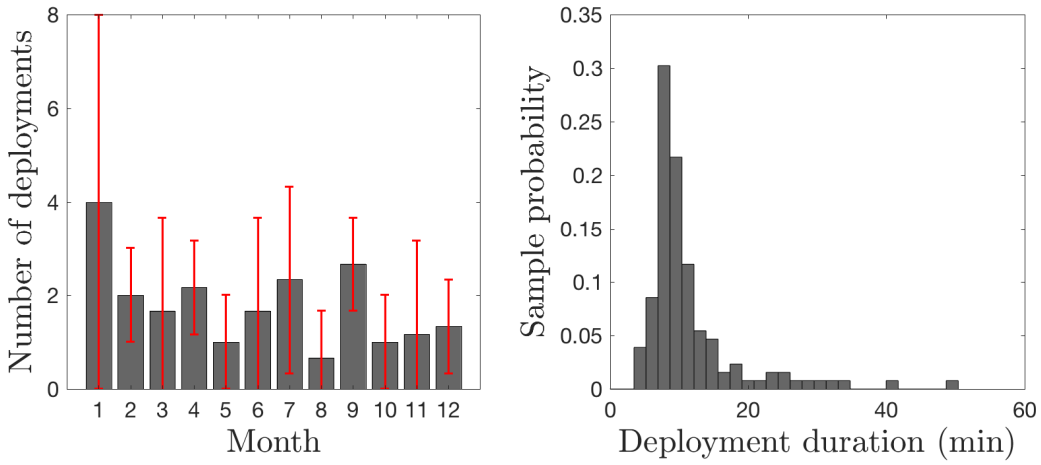

Figure 4.6: PJM synchronous reserve deployment data for 2013–2018. Left plot: monthly average deployment counts, with error bars indicating ± one standard deviation. Right plot: deployment duration histogram. On average, reserves were deployed 22 times per year for 12 minutes per deployment.

per month. Deployments typically last eight to twelve minutes. This suggests that heat pumps can provide synchronized reserve with only infrequent, brief interruptions of service. We discuss this further in §5.1.

Like regulation payments, PJM synchronized reserve payments include both capacity and performance components. The former is based on commitments cleared in advance, while the latter is based on actual load curtailment during deployment events. We restrict our attention to the capacity component, which is the bulk of the total synchronous reserve payment. The right plot in Figure 4.5 shows a histogram of the 2013–2018 synchronized reserve capacity prices, π^{res}. In simulations, we treat the reserve prices as deterministic.

4.4.2 Thermal load

In this section, we discuss the thermal load $L \in \mathbf{R}^K$ used in the simulations reported in the sequel. We discuss one method for producing L. We stress, however, that L could be

produced from *any* source. The methods in this chapter are completely agnostic to the thermal load model; only scenarios of L are needed. For example, L could be produced from measurements in a real building, a first-principles building simulator such as EnergyPlus or TRNSYS, a thermal circuit model of arbitrary order and structure, an autoregressive process, an artificial neural network, a support vector machine, a decision tree, a random forest, an ensemble model, *etc.*

In the subsequent simulations, we consider one story of a stand-alone single-family home of typical size and envelope efficiency. We model the temperature dynamics of this space using a 3R2C thermal circuit model. For more discussion of this model, including its widespread use in state-of-the-art research on heating and cooling systems, see §3.2.2.

We do not assume that the thermal properties of the space are known exactly. Rather, we suppose that the annual heating and cooling loads are known to lie within $\pm 10\%$ of assumed nominal values. In each simulated scenario, we randomly generate annual heating and cooling loads from the corresponding uncertainty sets, then fit the model parameters using the methods discussed in §3.2.4, *Capacitances* and *Resistances – Exterior mass*, and §3.2.5, *Tuning a model to survey data*. The model parameters depend on the random annual loads, so they are also random.

We base the nominal heating and cooling loads on the survey data in [85] for detached single-family homes in Philadelphia's climate zone. The nominal heating and cooling load intensities used in simulations are 58.6 $\text{kWh}_\text{t}/\text{m}^2$ and 18.8 $\text{kWh}_\text{t}/\text{m}^2$, respectively. For more discussion of the data source [85], see §2.4.2.

Once the model parameters are tuned to survey data using the methods discussed above, thermal load is calculated using the method discussed in the *Dynamic load prediction* subsection of §3.2.3. These thermal load calculations also require trajectories of the outdoor air temperature, indoor air temperature, and exogenous thermal power from the sun and internal sources. As discussed above, we use historical outdoor air temperature and so-

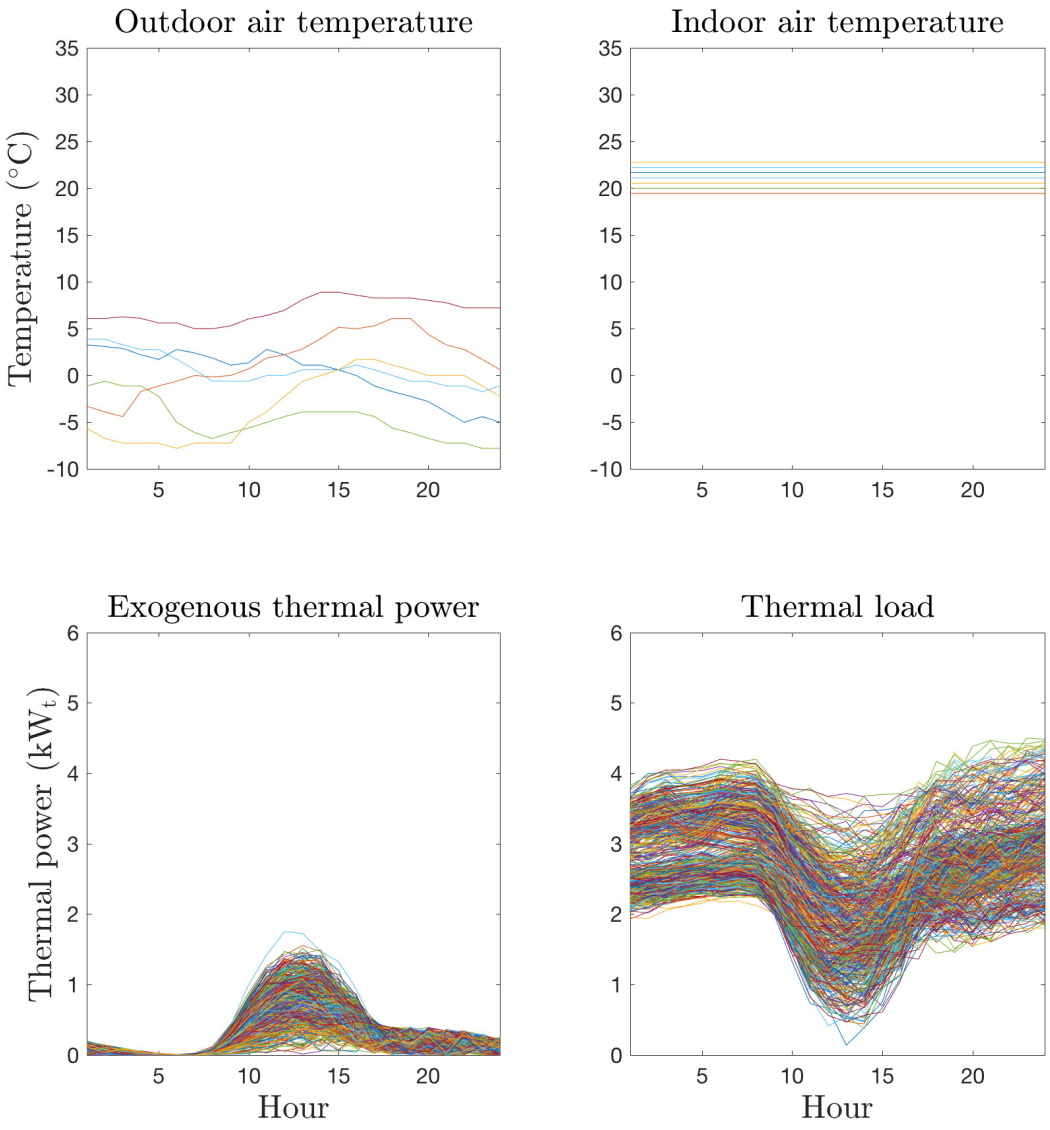

Figure 4.7: Input signals on January 18 in $N = 1000$ scenarios. The historical outdoor air temperature data (top left) are resampled with replacement. The indoor air temperature setpoints (top right) follow a discrete uniform distribution with increments of 1 °F. The exogenous thermal power (bottom left) from the sun and internal heat sources is also random. The thermal load (bottom right) depends on these random inputs, as well as uncertain model parameters.

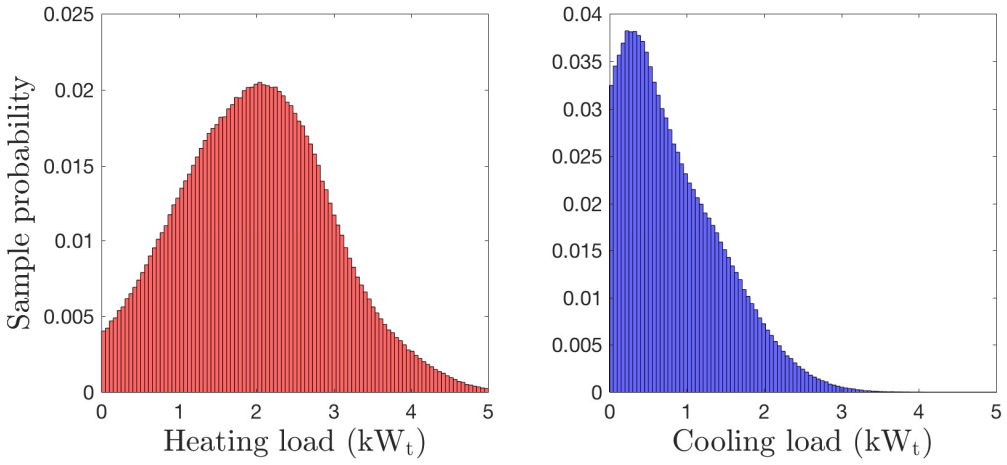

Figure 4.8: Histograms of hourly thermal load during heating (left) and cooling (right) seasons.

lar irradiance data from [167]. We randomly generate thermal power gained from internal sources based on the parameters recommended in [135] for residential building prototypes. We randomly generate indoor air temperature trajectories, $T_a \in \mathbf{R}^K$, based on the thermostat setpoint survey data in [85]. These data include thermostat setpoints during different operating modes: day vs. night, occupied vs. unoccupied, and heating vs. cooling. The data include both constant setpoints and setpoint adjustments during off-peak hours. In the simulations presented here, we use the constant setpoint data from [85].

Figure 4.7 shows the input signal scenarios (outdoor air temperature, indoor air temperature setpoint, exogenous thermal power from the sun and internal sources, and thermal load) for a typical winter day. Figure 4.8 shows histograms of the heating and cooling loads over all time steps and all scenarios.

4.4.3 Heat pumps and incumbent system

We focus on ductless variable-speed air-to-air heat pumps with one indoor unit and one outdoor unit. We consider one manufacturer's line of these products, with $J = 5$ nameplate

cooling capacities ranging from 1.8 to 5.3 kW_t (6000–18000 BTU/h, in evenly-spaced increments of 3000 BTU/h). These are highly efficient units with wide modulating ranges and useful heating capacity even in very cold conditions. We fit capacity and COP curves for these units to manufacturer data, as discussed in §3.1.3 and the *Model fitting* subsection of §3.1.4. We recall the following key features of this line of heat pumps.

- Heating and cooling capacities vary strongly with outdoor air temperature.
- Maximum capacities are significantly higher than rated capacities.
- COPs degrades at low load, due to cycling, and at high load.
- Bigger models have lower rated COPs.

We randomly generate installed costs and annual maintenance costs for these units based on data available from Internet retailers such as hvacdirect.com, as well as conversations with industry practitioners. Heat pump installed costs c are modeled as linear in nameplate heat pump capacity with a slope of 275 \$/kW_t and a (random) intercept of \$3100–4100. Mean installed heat pump costs range from \$4000 for the smallest unit to \$5000 for the largest unit. These installed costs are typical of a traditional heat pump contractor; for an HPA aggregator, installed costs would likely be somewhat lower. The incumbent system installed cost $\tilde{c}$ range from \$2000–3000; this range is intended to represent either the cost of a number of high-efficiency window air conditioners or the floor-area-weighted cost of a central air conditioning system. For more discussion of heat pump costs, see §2.4.2. The annual maintenance costs m and $\tilde{m}$ vary from \$50–100 and \$25–50, respectively. We do not claim that this range exactly reflects reality, only that it is plausible based on our conversations with industry practitioners. In simulations, the random parameters in this paragraph are drawn independently from uniform distributions over the aforementioned ranges.

4.4.4 Input data quality and limitations

The key input data underlying the simulations reported in this section are the weather, energy and ancillary service prices, thermal load, heat pump performance curves, and equipment costs. In our qualitative assessment, we rate the weather and price data fidelity as *excellent*, as they are drawn from historical databases maintained by trustworthy sources. These sources are the meteorology and atmospheric science department of Pennsylvania State University for weather, the official rate plan documentation of the major electric utility in Philadelphia for energy prices, and PJM's online database for ancillary service prices. We note that the weather and price datasets are both geographically and temporally coincident, so they accurately capture the statistical dependence between weather and prices.

The thermal load data is generated from a physics-based model that has seen widespread use in state-of-the-art research on heating and cooling systems; see §3.2.2 for more discussion. The model parameters are tuned to data from the United States Energy Information Agency's Residential Energy Consumption Survey, which collects real heating and cooling data from a representative sample of residential buildings; see §2.4.2 for more discussion. We therefore rate the thermal load data fidelity as *fair*. We acknowledge that the thermal load data is not as high-fidelity as the weather and price data, which are direct measurements by reliable sources. We emphasize, however, that the selection method developed in this chapter is agnostic to the source of the thermal load data. The basic requirement of the method is that *some* thermal load time series data are available. These data could come from historical measurements, from a thermal circuit model such as the one we use here, from a building simulator such as EnergyPlus [110] or TRNSYS [111], or from a data-driven predictive model such as an autoregressive process, artificial neural network, regression tree, support vector machine, *etc.*

The heat pump performance curves are fit to empirical data reported by a heat pump

manufacturer, as discussed in §3.1.3. The overall accuracy of the fits is decent, although accuracy could be improved if more high-quality data were available. The accuracy of most of the statistical fits is high, with values of the R^2 statistic of 0.97 or above. A few fits have lower accuracy, however, with R^2 in the range of 0.5–0.7. In terms of reliability, we view manufacturer-reported empirical data as second only to empirical data reported by an independent third party. Independent, third-party data is unfortunately difficult to obtain. However, the technical report [93] compares the empirical data reported by the heat pump manufacturer considered in this chapter to empirical data obtained from third-party laboratory experiments and finds good agreement between the two. (For more discussion, see §3.1.3.) We therefore rate the fidelity of the heat pump performance curves as *fair*. In our opinion, the most important area for improvement in the heat pump model is COP degradation while cycling; see the *COP and cycling* subsection of §3.1.3.

The lowest-fidelity input data are the equipment costs. While retail equipment costs are readily available, total installed equipment costs also include the installer's labor, overhead and profit. The latter are generally not reported by installers, so must be estimated. For more discussion, see §2.4.2, *Incumbent system costs* and *Heat pump costs*, and the cost estimates in [11]. While the equipment costs in the simulations that follow include our best estimates based on homeowner and installer testimony on the Internet, and our own conversations with practitioners, we acknowledge that the fidelity of the equipment cost data is *poor*. To account for this uncertainty, the distributions we assume on the equipment costs cover wide ranges. The spread of the net present value estimates that follow are due in large part to this. We note, however, that the selection method developed in this chapter is agnostic to the distribution of the input parameters. Furthermore, in practice the method would likely be employed by an equipment installer with clear knowledge of their own labor costs, overhead and profit margins.

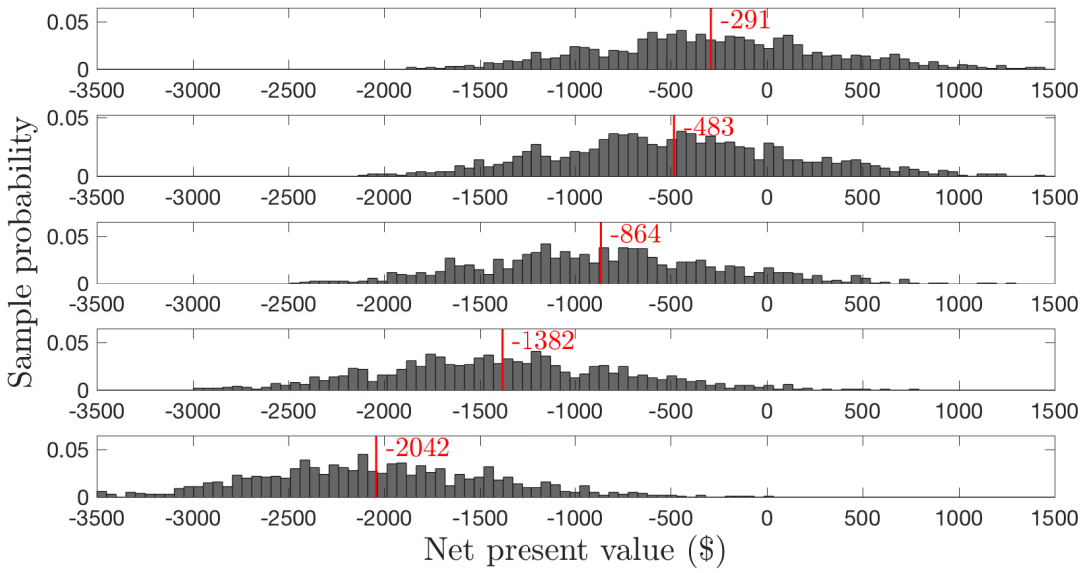

Figure 4.9: Histograms of the net present value of the smallest (top) to largest (bottom) heat pumps. Red lines indicate sample means.

4.4.5 Results

In this section, we present the results of Monte Carlo simulation of each heat pump under $N = 1000$ scenarios. We present these results as histograms in Figures 4.9–4.13. The plots in these figures are ordered vertically by heat pump size, with the smallest heat pump at the top and the largest at the bottom. We emphasize that these results are the outputs of computer simulations, not real-world experiments, and their validity is therefore limited by the fidelity of the input data, as discussed in §4.4.4.

Net present values, unmet loads and selection

Figure 4.9 shows histograms of the candidate heat pumps' net present values. Two messages can be taken from this figure. First, net present values decrease with heat pump size. This is because the smaller heat pumps have lower capital costs and higher COPs. While larger

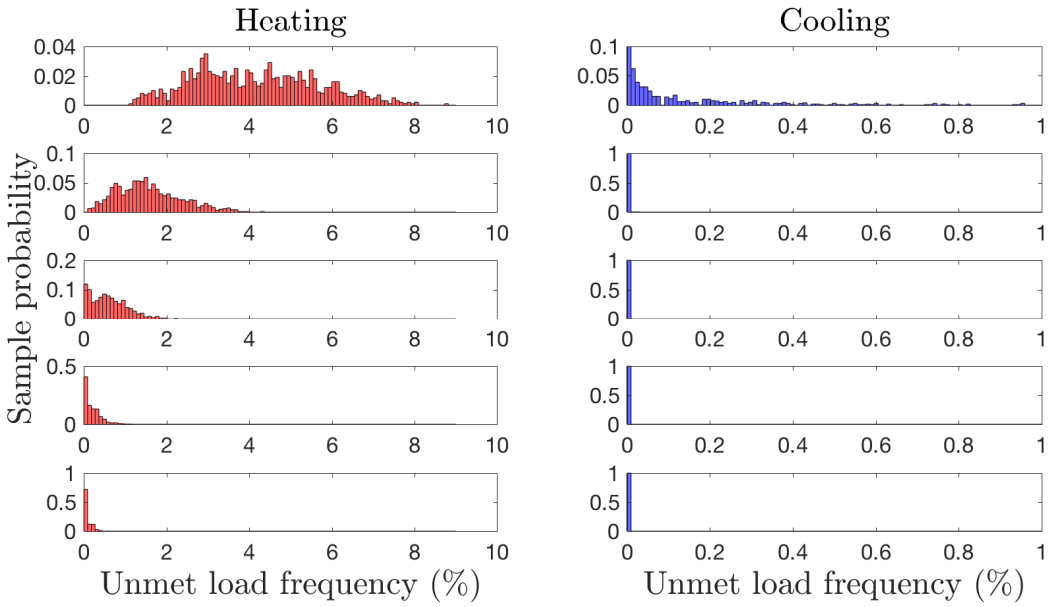

Figure 4.10: Unmet load frequency histograms for heating (left), cooling (right), and the smallest (top) through largest (bottom) heat pumps.

heat pumps displace more heating load, they do so less efficiently. Second, all of the sample-average net present values are negative. While the smaller heat pumps' net present values are positive in some Monte Carlo runs, on average they are all negative. This implies that none of the heat pumps considered here are economically attractive, at least in the simulated scenario of displacing natural gas heating and replacing an efficient air conditioner.

Figure 4.10 shows histograms of the temporal frequencies of unmet heating and cooling load. As expected, larger heat pumps meet load more frequently. Surprisingly, even the smallest heat pump meets most of the heating load; its sample-average temporal frequency of unmet heating load is under 5%. For cooling, the four largest heat pumps meet load even in the most extreme conditions. The smallest heat pump, however, does not meet the requirement of maintaining the temporal frequency of unmet cooling load under 1% in all scenarios. Therefore, the selection algorithm deems the first heat pump infeasible. The algorithm selects the second-smallest heat pump, which has nameplate cooling capacity of

2.6 $\mathrm{kW_t}$ (9000 BTU/h).

In this simulation, the cardinality of the support subsample is two. With $N = 1000$ and $\beta = 10^{-4}$, the selection algorithm returns the following guarantee:

> With 99.99% confidence, the probability that the second heat pump is feasible and no more than \$336-suboptimal is at least 97.1%.

We view this robustness level as satisfactory: the chance that the selection is infeasible is less than 3%. We interpret the returned value of $\tau_N^\star = \$336$ as the 97th percentile of the distribution of the second heat pump's optimality gap. The gap reflects the fact that in almost all scenarios, the smallest heat pump is feasible and attains a higher net present value than the second-smallest heat pump. The second-smallest heat pump is selected because it meets load in all scenarios; this robustness comes at a cost of several hundred dollars.

Although the application simulated here is heating displacement, it is worth noting that only the largest heat pump meets heating load with a frequency above 99%. If the user required heating replacement, rather than displacement, only the largest heat pump would be feasible. This would increase the expected net present cost by about \$1560.

Emission reductions

Figure 4.11 shows histograms of the annual greenhouse gas emission reductions. The reductions are relative to the incumbent natural gas furnace and efficient air conditioner. Four messages can be taken from this figure.

1. The emission reductions come almost entirely from displacing natural gas use for heating. Emission reductions from cooling are small (~10%) by comparison.

2. The total emission reductions are larger for smaller heat pumps. This is because the smaller heat pumps are more efficient (see Figure 4.12). While the larger heat pumps

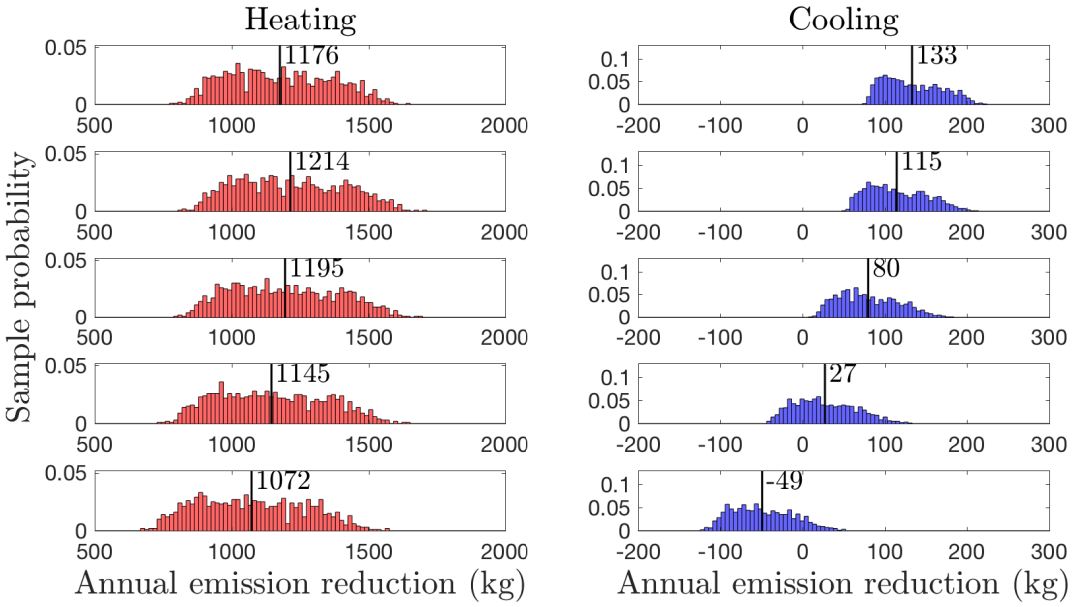

Figure 4.11: Emission reduction histograms for heating (left), cooling (right), and the smallest (top) through largest (bottom) heat pumps. Black lines indicate sample means.

displace more natural gas usage, they do so less efficiently, resulting in a net increase in emissions. The largest heat pump *increases* emissions from cooling.

3. The selected heat pump (the second-smallest) maximizes the emission reduction. This is coincidental; the selection algorithm in these simulations does not explicitly value reducing emissions. The value of reducing emissions could be internalized through a greenhouse gas price, as discussed in §4.2.3.

Seasonal performance and cycling

Figure 4.12 shows histograms of the heating and cooling seasonal COPs. The key message of this figure is that over-sizing hurts efficiency. The heating seasonal COPs decrease relatively mildly with heat pump size, but for cooling the trend is stark. This is because the simulations are set in Philadelphia, where winters are significantly more severe than summers. While

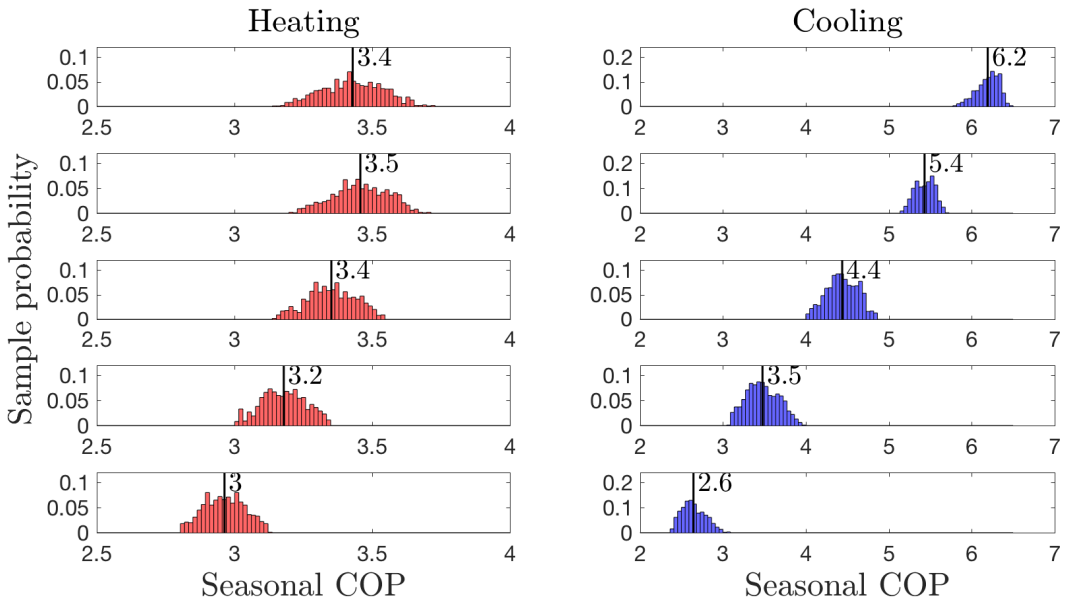

Figure 4.12: Seasonal COPs histograms for heating (left), cooling (right), and the smallest (top) through largest (bottom) heat pumps. Black lines indicate sample means.

the heat pumps are mostly within a reasonable size range for heating in this climate, they are all oversized for cooling. The larger units are oversized for heating and severely oversized for cooling.

Why does oversizing hurt efficiency? Because oversized units spend most of their time cycling off and on, rather than modulating. (We refer the reader to Figure 3.12 and the nearby discussion of cycling and efficiency.) This can be seen in Figure 4.13, which shows histograms of the cycling frequencies over the hours during which the heat pumps provide heating and cooling. The two larger units spend significant portions of the heating season cycling; all but the smallest unit cycle for most cooling hours.

We note that the cycling results in this numerical example are based on the part-load curve depicted in Figure 3.12. As discussed in §3.1.3, the low end of this part-load curve is subject to significant uncertainty. Empirical data on COP degradation while cycling are scarce. The only such data we are aware of are reported in [93]. Unfortunately, the number of

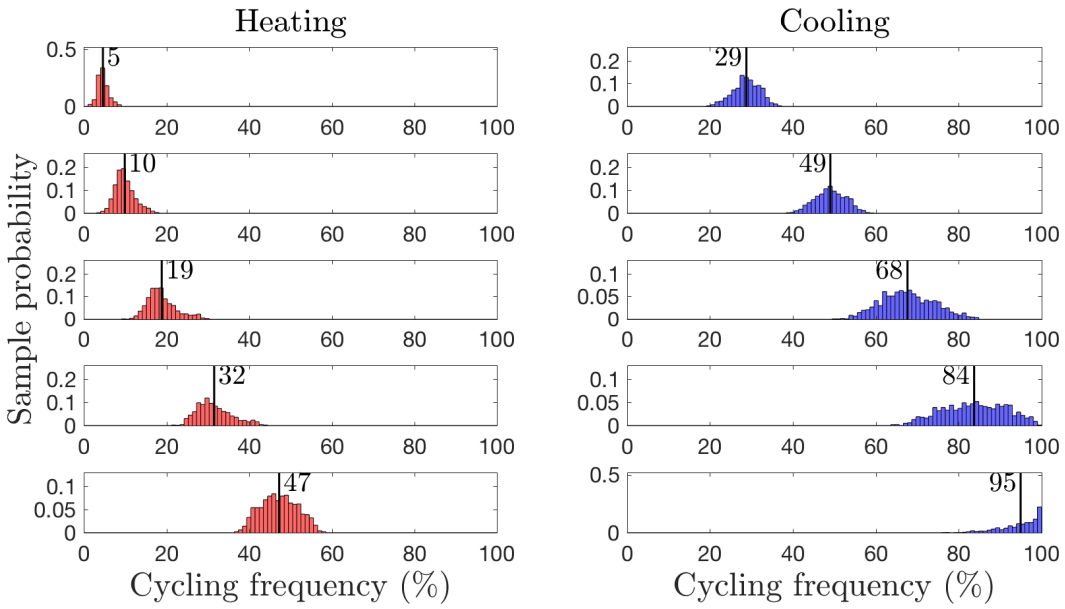

Figure 4.13: Cycling frequency histograms for heating (left), cooling (right), and the smallest (top) through largest (bottom) heat pumps. Black lines indicate sample means.

cycling data points in [93] is small and the variability in measured COP degradation is high. Relative to the measured degradation in [93], our model of COP degradation is optimistic in the heat pump's favor: our worst-case degradation is 25%, while the worst-case degradation measured in [93] is 45%.

4.4.6 Potential impact and extensions

The practical value of this chapter is an algorithm for selecting an appropriate heat pump for a given application. This algorithm applies to both stand-alone operation and cooperative usage. It is relatively straightforward to implement and comes with probabilistic performance guarantees. Using it could reduce the rates of heat pump under- and over-sizing, and thereby improve actual operating efficiencies. [94, 138, 147, 171] This, in turn, could reduce heat pumps' greenhouse gas emissions and lifetime costs, improve their value proposition to users, and accelerate heat pump adoption.

A drawback of the heat pump selection method developed in this chapter is that it requires heat pump performance curves. These can be fit to manufacturer data in submittal sheets, but the process is time consuming and requires some statistical expertise. A useful extension of this work would be an open compendium of heat pump performance curves fit to empirical data for various manufacturers and models. A good starting point would be the manufacturer data compiled by the Northeast Energy Efficiency Partnerships in [9]. These data include manufacturer-reported capacity and COP measurements for heating and cooling at several boundary temperatures for hundreds of heat pump models.

Chapter 5

Ancillary services

In this chapter, we consider the provision of ancillary services from an aggregation of variable-speed heat pumps. We begin by investigating the technical feasibility of providing spinning reserve and regulation. We then estimate the ancillary service capacities that aggregated heat pumps could provide and the revenues that they could earn.

5.1 Spinning reserve feasibility

In this section, we consider the feasibility of providing spinning reserve from aggregated heat pumps. The technical requirements for providing spinning reserve are low: heat pumps only need the ability to turn off within ~10 minutes of a dispatch signal. We therefore focus on the impact of heat pump curtailment on the thermal comfort of building occupants. Specifically, we estimate how far indoor air temperatures drift away from setpoints in response to heat pump curtailment during spinning reserve events. We note that the methods in this section can apply to other heating and cooling equipment and to other curtailment services, such as price-based demand response.

5.1.1 Literature review

The technical feasibility of curtailing heat pumps and air conditioners in response to a spinning reserve dispatch signal was demonstrated in hardware in [172]. In this paper, Kirby *et al.* describe experimental provision of spinning reserve from air conditioners and heat pumps in a 162-room hotel in Tennessee. All rooms' thermal devices were equipped with networked on/off controllers capable of responding to commands issued remotely, *e.g.*, from the hotel's front desk or over the Internet. Four spinning reserve dispatch experiments were conducted over two days in September, 2008. The average outdoor air temperature during the experiments was 32 °C. In all four experiments, load was curtailed to prescribed levels within 12–60 seconds, much faster than the 10-minute response required by most power system operators. Curtailments were sustained for 15 minutes, during which time room temperatures rose by at most 0.9 °C. After the curtailment window, equipment was gradually ramped back up; room temperatures returned to their setpoints within another 15 minutes. Kirby *et al.* conclude that temperature perturbations during "short curtailments normally associated with spinning reserve events should not be a significant concern". [172]

The experiments in [172] demonstrate that, at least for hotel air conditioners on hot days, brief curtailments for spinning reserve are non-disruptive to building occupants. These results are somewhat specific, however, as they were conducted only for 15-minute dispatch durations, hotel rooms, and ~32 °C outdoor air temperatures. In the remainder of this section, we augment the experimental results of Kirby *et al.* by simulating all available historical dispatch durations in PJM (the 2013–2018 data from [170]), a fairly wide variety of space heating and cooling loads, and outdoor air temperatures from -20 to 35 °C. These simulations build confidence that the results in [172] extend to more conditions than those under which the experiments were conducted.

We note that other authors have simulated the provision of spinning reserve from heat

pumps; see, *e.g.*, [173–175] and §3.1 of the review paper [8]. However, indoor air temperature perturbations are not investigated in these studies. This is likely due to their different hardware scope, which includes thermal storage that acts as a buffer between the heat pump and the conditioned space.

5.1.2 Model

We consider the thermal load model discussed in §3.2. As in §3.2.7, we define the state of the system as the perturbations of the indoor air and mass temperatures about their respective baselines. The perturbation dynamics are

$$\begin{aligned} C_a \dot{\delta}_a(t) &= -\left(\frac{1}{R_{am}} + \frac{1}{R_{a\infty}}\right)\delta_a(t) + \frac{\delta_m(t)}{R_{am}} + \frac{\delta_\infty(t)}{R_{a\infty}} + \delta(t) + \delta_e(t) \\ C_m \dot{\delta}_m(t) &= \frac{\delta_a(t)}{R_{am}} - \left(\frac{1}{R_{am}} + \frac{1}{R_{m\infty}}\right)\delta_m(t) + \frac{\delta_\infty(t)}{R_{m\infty}}. \end{aligned}$$

For $t < 0$, we assume that the heat pump and thermal load are in baseline operation; the heat pump regulates the indoor air temperature at its setpoint. At $t = 0$, the heat pump is turned off and the indoor air temperature begins to drift away from its setpoint. Therefore,

$$\delta(t) = \begin{cases} 0 & t < 0 \\ -\hat{\dot{Q}}(t) & t \geq 0, \end{cases}$$

where $\hat{\dot{Q}}$ is the baseline thermal power output of the heat pump. The other perturbations are identically zero for $t \leq 0$. We are interested in the response of the indoor air temperature perturbation δ_a to the thermal power perturbation δ.

Exact solution

Defining the state $x = (\delta_a, \delta_m)$ and input $u = (\delta, \delta_\infty, \delta_e)$, the perturbation dynamics can be written as

$$\dot{x}(t) = Ax(t) + Bu(t),$$

where the matrices A and B are defined as in §3.2.3. The solution to this system of linear differential equations is

$$x(t) = e^{At}x_0 + \int_0^t e^{A(t-\tau)}Bu(\tau)\mathrm{d}\tau. \tag{5.1}$$

Given an initial state x_0 and input signal u, Equation (5.1) gives an exact expression for the indoor air perturbation after a curtailment duration t. As this expression involves matrix exponentials and an integral, however, it does not give a clear interpretation in terms of the basic model parameters. We therefore make a simplifying assumption that allows for a more informative solution without compromising much accuracy.

Simplification

The basic simplifying assumption we make is that of time scale separation, as discussed in §3.2.7. More specifically, we assume that

$$\delta_m(t) \approx 0 \text{ for all } t.$$

In words, we assume that the thermal mass temperature is approximately constant throughout the curtailment event. This is a reasonable assumption in most buildings, where thermal mass time constants are typically on the order of ten hours, while most curtailment events last on the order of ten minutes. In simulations of curtailments lasting up to several hours, we find that this assumption yields indoor air temperature approximation errors on the order of 10^{-6} °C. We also assume that the outdoor air temperature and exogenous thermal power

are known and constant over the curtailment event.

Under these assumptions, it is straightforward to show that the heat pump thermal power baseline is approximately constant:

$$\delta(t) \approx -\hat{\dot{Q}}(0) \text{ for all } t \geq 0.$$

For $t \geq 0$, therefore, the air temperature perturbation dynamics simplify to

$$C_a \dot{\delta}_a(t) \approx -\left(\frac{\delta_a(t)}{\tilde{R}} + \hat{\dot{Q}}(0) \right),$$

where

$$\tilde{R} = \frac{R_{am} R_{a\infty}}{R_{am} + R_{a\infty}}.$$

Solving this differential equation, we have

$$\delta_a(t) \approx -\tilde{R} \hat{\dot{Q}}(0) \left[1 - \exp\left(\frac{-t}{C_a \tilde{R}} \right) \right] \text{ for all } t \geq 0. \tag{5.2}$$

Equation (5.2) gives an approximate expression for the indoor air temperature perturbation after any curtailment duration $t \geq 0$.

5.1.3 Simulation

In this section, we numerically investigate the relationship between curtailment durations and indoor air temperature perturbations via Monte Carlo simulation. In each simulation run, we randomly generate thermal model parameters representative of up to 100 m^2 of conditioned floor area[1] in a typical United States home. Parameters are generated using the

[1] According to the field studies reported in [79], 100 m^2 is approximately the largest floor area that can effectively be conditioned by point-source heating and cooling systems such as the ductless mini-split heat pumps modeled here. For larger spaces, air distribution becomes a limitation and multiple point-source units (or a central unit with a distribution system) are needed.

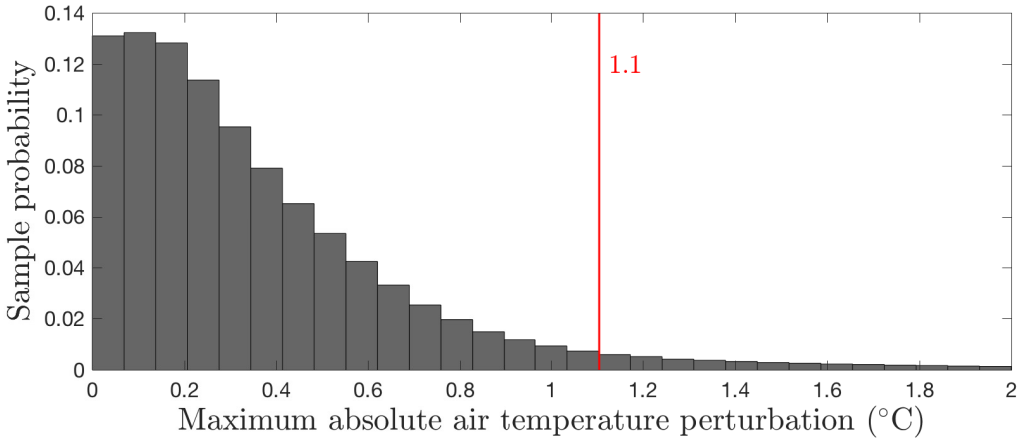

Figure 5.1: Histogram of the maximum absolute indoor air temperature perturbations over the durations of the 10^6 simulated curtailment events. The red line is the 95th sample percentile.

procedure described in §3.2.4–3.2.5 with input data from the survey in [85]; see §2.4.2 and §4.4.4 for discussion of this data source. This yields C_a and $\tilde{R}$. We then randomly generate an indoor air temperature setpoint between 18 and 24 °C, an outdoor air temperature between −20 and 35 °C, and an exogenous thermal power (from the sun and internal sources) between 0 and 1.5 $\mathrm{kW_t}$. We use the steady-state thermal load under those conditions as the initial (pre-curtailment) load. We then draw a random curtailment duration t_c (h) from PJM's spinning reserve[2] event durations from 2013–2018 [170], and compute $\delta_a(t_c)$ using Equation (5.2). This is all publicly available historical data on PJM spinning reserve deployment durations. We use uniform distributions throughout, and run 10^6 simulations. We choose uniform distributions because we are interested in the system behavior over the full specified ranges of boundary conditions.

Figure 5.1 shows a histogram of $|\delta_a(t_c)|$, where t_c is the curtailment event duration. Because the right-hand side of Equation (5.2) is a monotone function of t, $|\delta_a(t_c)|$ gives

[2]PJM uses the term *synchronous reserve* to refer to an ancillary service that most system operators call spinning reserve. While we adopt the more widely-used term, spinning reserve, the spinning reserve data in this thesis are from PJM's synchronous reserve market.

the maximum absolute indoor air temperature perturbation over the curtailment time span $t \in [0, t_c]$. The key message of Figure 5.1 is that space heating and cooling loads can provide PJM spinning reserve without causing thermal discomfort to building occupants. This can be seen from the red line in Figure 5.1, which shows the 95th sample percentile at 1.1 °C. We therefore conclude that with 95% probability, the indoor air temperature will drift no more than 1.1 °C away from its setpoint during a PJM reserve curtailment event. As a typical thermostat regulates indoor air temperature within a deadband of several °C, we view a 1.1 °C perturbation as essentially unnoticeable.

It is worth noting that the histogram in Figure 5.1 has a fairly heavy tail. Its 99th percentile is 2.1 °C, and its support extends to 4 °C. This heavy tail is due to two outlier deployment events that occurred during the Polar Vortex cold snap of 2014. During the Polar Vortex, record-low temperatures caused extreme heating demand, leading to shortages of both natural gas and electricity. We suspect that these shortages stressed the PJM power system and led to the outlier spinning reserve deployment durations. While the mean deployment duration over the 130 events that occurred between 2013 and 2018 was 12 minutes, the two outlier events lasted 41 and 56 minutes. To construct the histogram in Figure 5.1, we uniformly resampled from the historical event durations with replacement. The two outlier events were therefore drawn with about 2/130 probability, resulting in a low but nonzero sample frequency of long events and relatively large indoor air temperature perturbations. For this reason, the results reported here likely over-estimate the risk of occupant discomfort during reserve deployments.

5.2 Regulation feasibility

In this section, we consider the feasibility of providing regulation from aggregated variable-speed heat pumps. We begin by reviewing two related research threads. The first thread

involves aggregated thermostatically-controlled loads. The second thread involves individual variable-speed heating and cooling equipment. We then develop a regulation controller for aggregated variable-speed heat pumps, quantify its tracking performance, and evaluate the impact on building occupants' thermal comfort.

5.2.1 Literature review

Aggregated thermostatically-controlled loads

A thermostat is a controller that regulates the temperature of thermal loads such as refrigerators, water heaters and air-conditioned spaces. Thermostatically-controlled loads are typically found in residential and small commercial buildings. A thermostat maintains its load temperature within an acceptable range called a deadband. When regulating the temperature of a heating load, a thermostat switches the heater on when the load temperature drops below the lower deadband limit and switches it off when the temperature rises above the upper deadband limit. The load temperature then drifts back down and the cycle repeats. Thermostats control cooling equipment similarly.

Aggregated thermostatically-controlled loads can provide regulation by coordinating their switching behavior. Aggregate-level controllers are typically designed to maintain individual load temperatures within their thermostat deadbands, so can be considered non-disruptive to building occupants.

In the last ten years, many researchers have worked on the problem of providing regulation from thermostatically-controlled loads. A few highly-cited papers in this area include [37, 65–67, 70], but there are many more. Simulation results in this area are extensive. Good tracking performance has been demonstrated under a number of control schemes. [37, 65–67, 70] Sensing requirements and estimation algorithms were explored in depth in [37, 67]. Problems related to control over networks, including communication delays and bandwidth

constraints, were considered in [176].

Experimental results on power system services from thermostatically-controlled loads are more limited than simulation results. In [177], 26 refrigerators and two electric resistance space heaters were controlled on an island in the Baltic Sea. Experiment durations varied from days to months. The devices showed good performance in responding to frequency deviations; response times varied from seconds to a few minutes. In [178], 25 refrigerators were controlled in an isolated Danish test system with 12 kW of peak load and a diesel generator. The refrigerators were used for reserve, rather than regulation, but showed good performance in returning the system to nominal frequency within about three minutes of a step change in system load.

While this thesis focuses on variable-speed heat pumps that are not thermostatically-controlled, the extensive research on thermostatically-controlled, fixed-speed loads builds confidence in the ability of aggregated variable-speed heat pumps to provide regulation. Intuitively, a variable-speed machine is more flexible than a fixed-speed machine. If aggregated fixed-speed machines can provide regulation, then aggregated variable-speed machines probably can, too. In this section, we will provide evidence that supports this intuition.

Individual variable-speed devices

Research on aggregated thermostatically-controlled loads focuses on the collective behavior of many fixed-speed devices. A second thread of relevant research involves the individual behavior of variable-speed devices. Many contributions in this area study the provision of power system services from large equipment, such as supply air fans and chiller compressors, in industrial and large commercial buildings. [38–43, 71–74] The experimental results in this area are fairly extensive, relative to experiments with aggregated thermostatically-controlled loads. This is most likely a matter of scale; it is easier to instrument a single, large device than many small, thermostatically-controlled loads.

In the context of this thesis, the most relevant research on individual, variable-speed devices is in [44–46]. In [46], Cai *et al.* retrofit a fixed-speed air-source heat pump with after-market variable-speed compressor and fan drives. Cai *et al.* develop a regulation controller that manipulates compressor and fan speeds as control inputs. In laboratory experiments under steady-state boundary conditions, the controller earned a composite score of 97% in tracking PJM's RegD test signal. The resulting indoor air temperature perturbations were on the order of 0.1 °C.

In practice, compressor and fan speeds may not be available as control inputs without manufacturer-level hardware access. In [44, 45], Kim *et al.* also develop a regulation controller for variable-speed air-source heat pumps. The simulations in [44] use compressor speed as a control input, but the laboratory experiments in [45] use supply temperature instead. More precisely, the control input in [45] is the supply temperature reference sent to the manufacturer's low-level control system.

Whether the control input is compressor speed or supply temperature, the closed-loop system behaves like a stable first-order linear system that drives the reference power perturbation tracking error to zero. (See Figure 10 of [45].) However, Kim *et al.* show that manipulating the supply temperature reference, rather than the compressor speed, increases the closed-loop time constant from less than one second to about ten seconds. This introduces tracking delays and, at times, relatively large tracking errors. In a range of laboratory experiments, the composite scores in tracking PJM's RegD test signal varied between 77 and 81%. While these scores are significantly lower than those reported in [46] for compressor and fan speed control, they are high enough to earn entrance into PJM's regulation market. [179]

Contributions of this section

As discussed above, there is a large body of high-quality work on controlling heating and cooling equipment for regulation. This body of work spans a variety of devices, control schemes, information patterns and aggregation levels. Many simulations and a growing number experiments show promising results. In our view, these results suggest with high confidence that heating and cooling loads in general, and variable-speed heat pumps in particular, can reliably provide regulation without disrupting building occupants.

In light of this view, we keep the scope of this section narrow. As in [44–46], we consider variable-speed air-source heat pumps. Following [45], we do not assume that manufacturer-level access to hardware is available. For this reason, we choose a temperature reference, rather than compressor or fan speeds, as our control input. We choose this control input because it is accessible today on many heat pumps by way of smart thermostats and the Internet.

In this section, we extend the work in [45], which considers a single variable-speed heat pump, by considering an aggregation of many variable-speed heat pumps. We assume that each heat pump is equipped with its own control system that can imperfectly track an individual power perturbation reference signal. Based on the experimental results in [45], we model the low-level control system's closed-loop behavior as a first-order linear system with a time constant on the order of ten seconds. This approach to modeling the fast dynamics of a heat pump is conceptually similar to the approach employed in [101], although the details differ.

We develop an aggregate controller that intelligently splits the aggregate reference signal received from the power system operator into individual reference signals that are sent to each heat pump. The aggregate controller achieves accurate tracking despite the use of supply temperature, rather than compressor or fan speeds, as the control input at each

heat pump. Accurate tracking is achieved mainly by including a predictive model of the aggregate reference signal in the controller design process. In simulations, the aggregate controller earns a composite score of 97% when tracking PJM's RegD test signal. This is on par with the score reported in [46] for compressor and fan speed control inputs.

5.2.2 Dynamics

Temperature and power

We consider an aggregation of J heat pumps serving loads modeled as in §3.2. We work with perturbations about nominal temperature and power trajectories as in §3.2.7. We denote the indoor air temperature perturbations by $\theta \in \mathbf{R}^J$ (°C) and the electrical power perturbations by $p \in \mathbf{R}^J$ (kW). Under normal, unperturbed operation, $\theta = p = 0$.

We assume that, viewed from the time scale of the indoor air temperature dynamics, the thermal mass temperatures and the heat pump coefficients of performance $\eta \in \mathbf{R}^J$ are approximately constant. The control input $u \in \mathbf{R}^J$ (kW) consists of the individual power perturbation references sent to the heat pumps. We assume that the heat pumps' individual control systems behave in closed-loop as decoupled first-order linear systems that drive the heat pumps' actual power perturbation p toward u with time constants $\tau \in \mathbf{R}^J$ (h).

With these assumptions, the continuous-time temperature and power dynamics are

$$\begin{bmatrix} \dot{p} \\ \dot{\theta} \end{bmatrix} = \begin{bmatrix} A_p^c & \\ A_{\theta p}^c & A_\theta^c \end{bmatrix} \begin{bmatrix} p \\ \theta \end{bmatrix} + \begin{bmatrix} B_p^c \\ \end{bmatrix} u, \tag{5.3}$$

where the continuous-time system matrices are

$$A_p^c = \begin{bmatrix} -1/\tau_1 & & \\ & \ddots & \\ & & -1/\tau_J \end{bmatrix}, \quad B_p^c = -A_p^c$$

$$A_\theta^c = \begin{bmatrix} -1/\tau_{a1} & & \\ & \ddots & \\ & & -1/\tau_{aJ} \end{bmatrix}, \quad A_{\theta p}^c = \begin{bmatrix} \eta_1/C_{a1} & & \\ & \ddots & \\ & & \eta_J/C_{aJ} \end{bmatrix}.$$

Here $C_a \in \mathbf{R}^J$ ($\mathrm{kWh_t}/^\circ\mathrm{C}$) contains the indoor air thermal capacitances and $\tau_a \in \mathbf{R}^J$ (h) contains the indoor air temperature time constants as defined in Equation (3.6). The discrete-time temperature and power dynamics are

$$\begin{bmatrix} p_{t+1} \\ \theta_{t+1} \end{bmatrix} = \begin{bmatrix} A_p & \\ A_{\theta p} & A_\theta \end{bmatrix} \begin{bmatrix} p_t \\ \theta_t \end{bmatrix} + \begin{bmatrix} B_p \\ B_\theta \end{bmatrix} u_t, \tag{5.4}$$

where $t = 0, \ldots, T$ indexes discrete time. The matrices A_p, $A_{\theta p}$, A_θ, B_p and B_θ are defined by discretizing the continuous-time dynamics (5.3) with time step Δt.

Equation (5.4) describes the *nominal* power perturbation dynamics. While the nominal dynamics are linear, the true dynamics have saturation nonlinearities at the upper and lower capacity limits:

$$p_{t+1} = \min\left\{P^{\mathrm{mod}}, \max\left\{P^{\mathrm{cap}}, A_p p_t + B_p u_t\right\}\right\}.$$

Here $P^{\mathrm{cap}}, P^{\mathrm{mod}} \in \mathbf{R}^J$ are the maximum capacities and minimum modulating capacities of the heat pumps, and the minima and maxima are interpreted component-wise. We use the linear dynamics for controller synthesis, but the nonlinear, saturated dynamics in simulating closed-loop performance. This is a form of plant-model mismatch.

Aggregate power perturbation reference

The PJM reference power perturbation signal $r \in \mathbf{R}$ (kW) is highly autocorrelated. Past reference signal realizations therefore carry significant information about future realizations. To make use of this information, we fit an autoregressive model to the reference signal. This model takes the form

$$r_{t+1} = a_1 r_t + \cdots + a_m r_{t-m+1} + n_t,$$

where m is the number of stages of memory and the n_t (kW) form a Gaussian white noise sequence with variance σ^2 (kW^2). We fit the parameters

$$\hat{a} = \begin{bmatrix} 0.8033 \\ 0.3741 \\ 0.1209 \\ -0.0289 \\ -0.1063 \\ -0.1699 \end{bmatrix}, \quad \hat{\sigma}^2 = 1.752 \times 10^{-3}$$

to 2018 signal data using linear regression and cross-validation. We found that $m = 6$ gave an acceptable bias-variance trade-off in the validation data. The reference model adds a new system state $\xi_t = (r_t, \ldots, r_{t-m+1}) \in \mathbf{R}^m$ with dynamics

$$\xi_{t+1} = A_\xi \xi_t + e_1 n_t,$$

where

$$A_\xi = \begin{bmatrix} \hat{a}_1 & \dots & \hat{a}_{m-1} & \hat{a}_m \\ 1 & & & \\ & \ddots & & \\ & & 1 & \end{bmatrix}, \quad e_1 = \begin{bmatrix} 1 \\ \\ \\ \end{bmatrix}.$$

Integrators

In order to track the aggregate power perturbation reference signal, we need to penalize the integral tracking error. To do this, we keep track of the forward-Euler integrals of the individual power perturbation integrals,

$$s_t^p = \Delta t \sum_{k=0}^{t} \lambda^{t-k} p_k \text{ (kWh)},$$

where $\lambda \in [0, 1]$ is a forgetting factor. The integrator dynamics are

$$s_{t+1}^p = \lambda s_t^p + \Delta t p_t.$$

We also keep track of the forward-Euler integral of the aggregate power perturbation reference,

$$s_t^r = \Delta t \sum_{k=0}^{t} \lambda^{t-k} r_k \text{ (kWh)}.$$

As r_t can be recovered from ξ_t via

$$r_t = (\xi_t)_1 = e_1^\top \xi_t,$$

the dynamics of the integral state s_t^r can be written as

$$s_{t+1}^r = \lambda s_t^r + \Delta t e_1^\top \xi_t.$$

Full system

We define the full system state as

$$x_t = (p_t, \theta_t, \xi_t, s_t^p, s_t^r) \in \mathbf{R}^{3J+m+1}.$$

The full dynamics are

$$x_{t+1} = Ax_t + Bu_t + w_t,$$

where

$$A = \begin{bmatrix} A_p & & & & \\ A_{\theta p} & A_\theta & & & \\ & & A_\xi & & \\ \Delta t I & & & \lambda I & \\ & & \Delta t e_1^\top & & \lambda \end{bmatrix}, \quad B = \begin{bmatrix} B_p \\ B_\theta \\ \\ \\ \end{bmatrix}, \quad w_t = \begin{bmatrix} \\ \\ e_1 \\ \\ \end{bmatrix} n_t.$$

5.2.3 Cost

The control objectives are the following.

- The load temperatures should remain near their baseline values.
- The sum of the measured individual power perturbations should track the aggregate power perturbation reference signal.
- The power perturbations should remain within the heat pumps' capacity limits.

To achieve these control objectives, we seek to minimize a sum of stage costs of the form

$$x_t^\top Q x_t + u_t^\top R u_t.$$

We define the weighting matrices Q and R so that the stage costs include four terms. The terms include tunable weights $\alpha_1, \alpha_2, \alpha_3 \geq 0$.

1. The first term penalizes indoor air temperature perturbation magnitudes:

$$\alpha_1 \theta_t^\top \theta_t.$$

2. The second term penalizes instantaneous tracking error:

$$\alpha_2(\mathbf{1}^\top p_t - r_t)^2 = \alpha_2(\mathbf{1}^\top p_t - e_1^\top \xi_t)^2.$$

3. The third term penalizes integral tracking error:

$$\alpha_3(\mathbf{1}^\top s_t^p - s_t^r)^2.$$

4. The final term,

$$u_t^\top R u_t + p_t^\top R p_t,$$

penalizes the magnitudes of the individual power perturbations (reference and actual). To penalize perturbation magnitudes in proportion to the tightness of the heat pumps' upper and lower capacity limits, we define

$$R = \begin{bmatrix} 1/(P_1^{\text{cap}} - P_1^{\text{mod}})^2 & & \\ & \ddots & \\ & & 1/(P_1^{\text{cap}} - P_1^{\text{mod}})^2 \end{bmatrix}.$$

To incorporate the above terms into the stage cost, we define

$$Q = \begin{bmatrix} R + \alpha_2 \mathbf{1}\mathbf{1}^\top & & -\alpha_2 \mathbf{1} e_1^\top & & \\ & \alpha_1 I & & & \\ -\alpha_2 e_1 \mathbf{1}^\top & & \alpha_2 e_1 e_1^\top & & \\ & & & \alpha_3 \mathbf{1}\mathbf{1}^\top & -\alpha_3 \mathbf{1} \\ & & & -\alpha_3 \mathbf{1}^\top & \alpha_3 \end{bmatrix},$$

where $\mathbf{1}$ denotes a column vector of ones of appropriate dimension.

5.2.4 Controller synthesis

We are interested in designing a state-feedback policy, *i.e.*, functions $\phi_0, \ldots, \phi_{T-1} : \mathbf{R}^{3J+m+1} \to \mathbf{R}^J$ that map states into control inputs. Our goal is to

$$\begin{array}{ll} \underset{\phi_0,\ldots,\phi_{T-1}}{\text{minimize}} & \frac{1}{T}\,\mathbf{E}\left[\sum_{t=0}^{T-1} x_t^\top Q x_t + u_t^\top R u_t\right] \\ \text{subject to} & x_{t+1} = Ax_t + Bu_t + w_t,\ t = 0, \ldots, T-1 \\ & u_t = \phi_t(x_t),\ t = 0, \ldots, T-1. \end{array}$$

This is a finite-horizon linear-quadratic optimal control problem that can be solved via dynamic programming. As the number of stages T is large, however, we instead search for a stationary policy $\phi : \mathbf{R}^{3J+m+1} \to \mathbf{R}^J$ to

$$\begin{array}{ll} \underset{\phi}{\text{minimize}} & \lim_{T\to\infty} \frac{1}{T}\,\mathbf{E}\left[\sum_{t=0}^{T-1} x_t^\top Q x_t + u_t^\top R u_t\right] \\ \text{subject to} & x_{t+1} = Ax_t + Bu_t + w_t,\ t = 1, \ldots, T \\ & u_t = \phi(x_t),\ t = 0, \ldots, T-1. \end{array}$$

This infinite-horizon problem can be solved by standard software such as Matlab's `lqr` function. The resulting policy is linear state feedback:

$$\phi^{\mathrm{lq}}(x_t) = Kx_t.$$

Here $K \in \mathbf{R}^{J \times 3J+m+1}$ is computed by solving an algebraic Riccati equation. We note that the stationary state-feedback law ϕ^{lq} is not optimal for our problem, as our true dynamics are nonlinear due to state saturation. Nevertheless, ϕ^{lq} provides closed-loop performance that achieves our objectives. We demonstrate this through simulation in the next section.

Heuristic policy

We compare ϕ^{lq} to a heuristic policy of allocating the aggregate reference signal among heat pumps in proportion to constraint slack:

$$\phi^{\mathrm{h}}(x_t) = \begin{cases} (P^{\mathrm{cap}} - p_t)r_t/\mathbf{1}^\top(P^{\mathrm{cap}} - p_t), & r_t \geq 0 \\ (p_t - P^{\mathrm{mod}})r_t/\mathbf{1}^\top(p_t - P^{\mathrm{mod}}), & r_t < 0. \end{cases}$$

(We recall that p_t and r_t are components of the state x_t, so ϕ^{h} is a [nonlinear] state-feedback policy.) Under this policy, heat pumps further from their constraints receive larger shares of the aggregate perturbation. We simulate this policy because it is intuitive, computationally efficient to implement, and relies only on the tracking capabilities of the low-level heat pump controllers. Essentially no computation happens at the aggregate scale; the aggregate controller simply splits the aggregate reference signal proportionally and passes it on to the individual controllers.

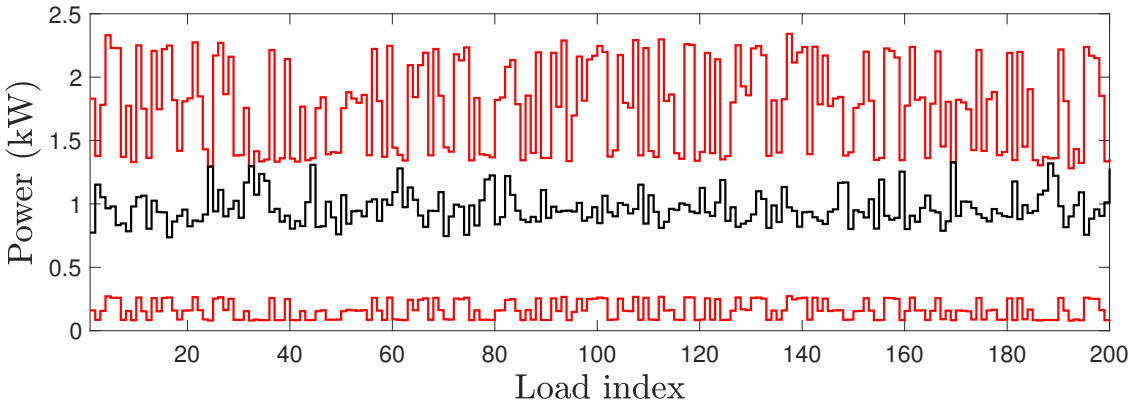

Figure 5.2: Nominal electrical power (black), maximum capacities (upper red trace) and minimum modulating capacities (lower red trace) of the $J = 200$ simulated heat pumps.

5.2.5 Simulation

To evaluate the performance of the state-feedback control law ϕ^{lq}, we simulate the closed-loop system under PJM's RegD self-test signal. [179] This is the signal data under which PJM recommends that prospective regulation market entrants test their hardware. We simulate $J = 200$ heat pumps over a 40-minute horizon with time step $\Delta t = 2$ s.

The simulation input data are $\tau, \tau_a, C_a, \eta, P, P^{\text{cap}}, P^{\text{mod}} \in \mathbf{R}^J$. The low-level heat pump control system reference tracking time constants τ are independent and identically distributed from a uniform distribution supported on [18 s, 22 s]. This support range is tuned to the empirical data reported in the laboratory experiments in [45]; see Figure 10 of [45] and the surrounding discussion.

The indoor air temperature time constants τ_a and thermal capacitances C_a are extracted from the 3R2C thermal circuit model discussed in §3.2. The model parameters are tuned to the annual thermal load survey data as discussed in §4.4.2. After this process, the minimum, mean and maximum of τ_a are 6.1, 9 and 13.4 h, respectively. The minimum, mean and maximum of C_a are 0.72, 0.77 and 0.82 kWh/°C, respectively.

The heat pump COPs η, the nominal power P, maximum capacities P^{cap} and the mini-

mum modulating capacities P^{mod} are defined by propagating the weather data discussed in §4.4.1 through the 3R2C thermal circuit model to generate thermal load, then propagating the thermal load through the heat pump models discussed in §4.4.3. This process results in time-varying η, P, P^{cap} and P^{mod}, defined for each hour in the weather data. In the simulations reported below, the minimum, mean and maximum of η are 2.5, 3.2 and 3.6, respectively.

Figure 5.2 shows the heat pumps' maximum capacity, nominal power, and minimum modulating capacity. In this figure, the horizontal axis is the index of the loads, $j = 1, \ldots, J$. The black trace is the nominal electrical power consumption over the current regulation market time step; this is the power that each heat pump would consume if not providing regulation. The upper red trace is the maximum electrical power consumption. The lower red trace is the electrical power consumption at minimum modulating speed (below its minimum modulating capacity, a heat pump must cycle off and on rather than modulating continuously). In this figure, the resulting aggregate symmetric regulation capacity from 200 heat pumps is 160 kW.

The simulations reported below use values $\alpha_1 = 10^{-2}$, $\alpha_2 = J \times 10^{-3}$ and $\alpha_3 = J \times 10^4$ of the tunable parameters embedded in the state cost weighting matrix Q defined in §5.2.3 and a value of $\lambda = 0.99$ for the forgetting factor in the integrator dynamics. These values are the product of manual tuning.

Heuristic policy performance

Figure 5.3 shows the tracking performance of the heuristic policy ϕ^{h}. The top plot shows the reference (red) and measured (black) aggregate power perturbations. With perfect tracking, these curves would be identical. Due to the ~20-second time constants of the low-level heat pump controllers, however, the measured perturbation lags the reference perturbation. The bottom plot in Figure 5.3 shows the instantaneous tracking error, *i.e.*, the difference between

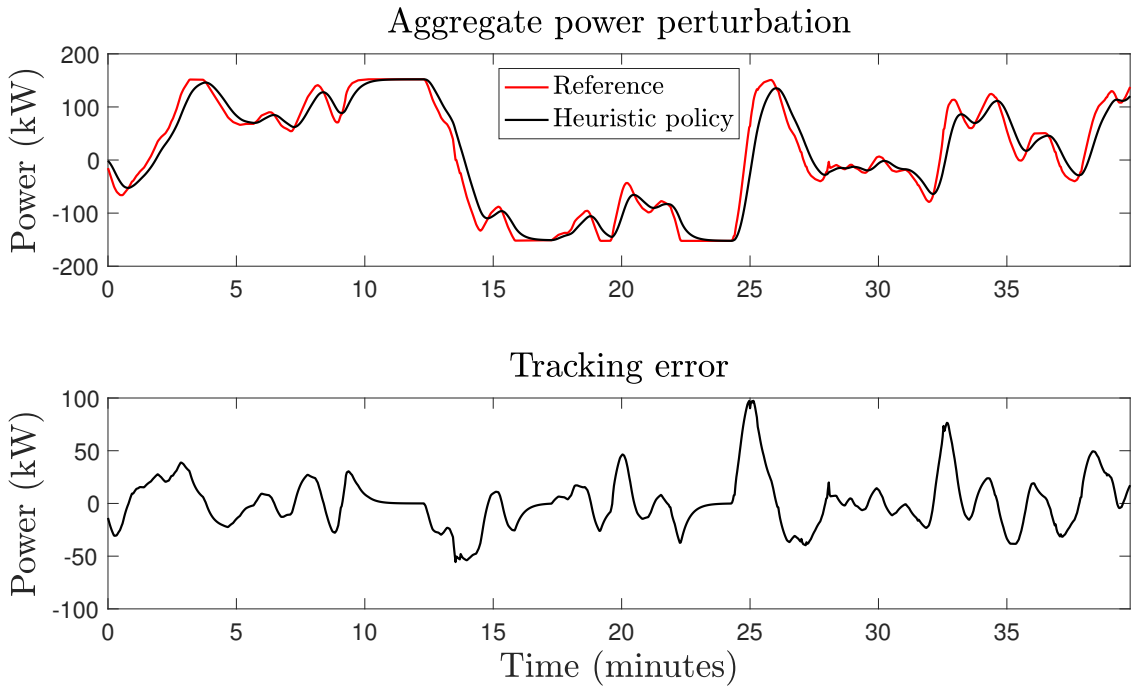

Figure 5.3: Tracking performance of the heuristic policy ϕ^{h}.

the red and black curves in the top plot. In this simulation, the maximum absolute tracking error is 97 kW (61% of the committed regulation capacity). The root mean square tracking error is 25 kW (16%).

Linear-quadratic policy performance

Figure 5.4 shows the tracking performance of the linear-quadratic policy ϕ^{lq}. Comparing Figure 5.4 to Figure 5.3, we see that the linear-quadratic policy eliminates the tracking lag. This greatly reduces the tracking error. In this simulation, the maximum absolute tracking error is 19 kW (12% of the committed regulation capacity) and the root mean square tracking error is 1 kW (0.6%). The PJM composite score is 97%. We attribute this improvement in tracking performance primarily to the fact that the linear-quadratic policy includes a predictive model of the aggregate reference power perturbation signal. In other words, the

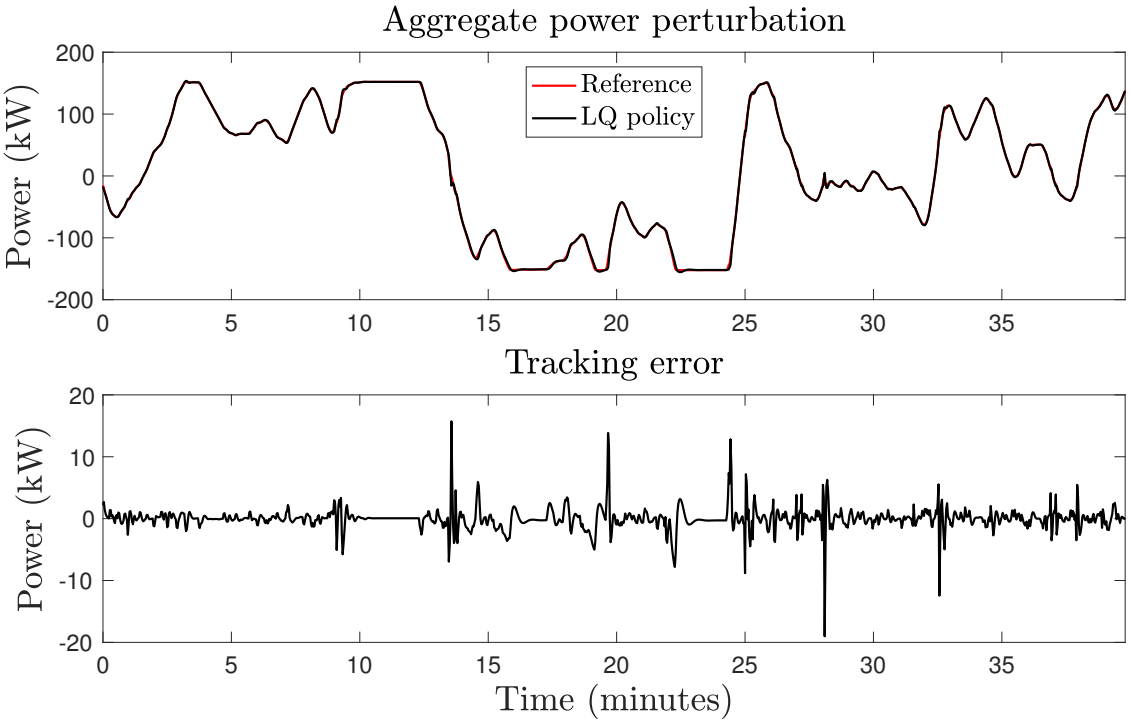

Figure 5.4: Tracking performance of the linear-quadratic policy ϕ^{lq}. This policy eliminates the tracking lag in Figure 5.3, reducing the root mean square tracking error from 25 kW to 1 kW.

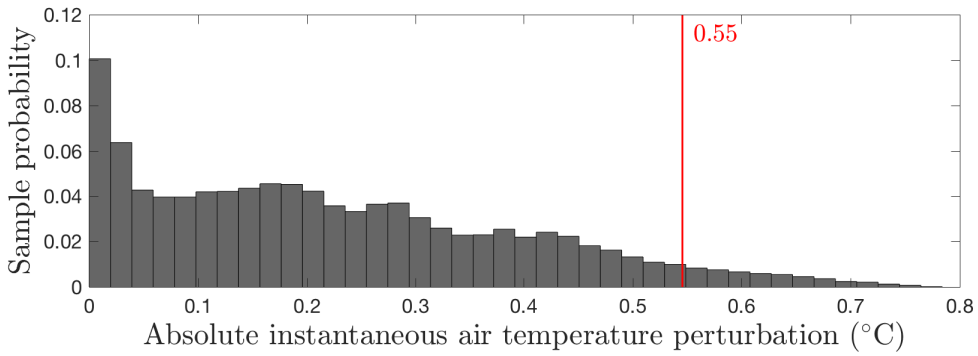

Figure 5.5: Histogram of the absolute instantaneous indoor air temperature perturbations of all loads at all time steps under the linear state feedback policy ϕ^{lq}. The red line is the 95th percentile.

linear-quadratic policy uses feed-forward control action.

We simulated the linear-quadratic policy under varying weather conditions and with varying low-level controller time constants. We found that the tracking performance is robust on both fronts. In fact, the root mean square tracking error remains below 3 kW (2%) even with time constants up to 360 s. This suggests that good aggregate tracking can be achieved even with low-level heat pump controllers that take ~10 minutes to deliver requested step changes in indoor air temperature setpoints.

Indoor air temperature perturbations

Figure 5.5 shows a histogram of the absolute instantaneous indoor air temperature perturbations of all loads at all time steps under the linear state feedback policy ϕ^{lq}. The key message of this figure is that the indoor air temperature perturbations caused by providing regulation are small. The red line in this figure shows the 95th percentile at 0.55 °C. In this simulation, the maximum absolute perturbation was 0.78 °C and the root mean square perturbation was 0.28 °C. These temperature perturbations are significantly smaller than thermostat deadband widths, which are typically 2 to 5 °C. We can therefore conclude that aggregated heat

pumps can provide regulation without causing thermal discomfort to building occupants

This conclusion is robust to variations in the size of the heat pump aggregation. In simulations of larger and smaller aggregations, the worst-case temperature perturbations are similarly small. We attribute this to the facts that (a) the RegD signal is zero-mean, and (b) the LQR cost function penalizes the power perturbation at each heat pump, both instantaneously and through their time-integrals. The latter effectively drives all individual power perturbation signals toward zero, instantaneously and integrated over time, regardless of the aggregation size. This, in turn, keeps air temperature perturbations small.

5.3 Capacity and revenue estimation

In this section, we investigate how much regulation and spinning reserve capacity a heat pump aggregator can offer and how much revenue they can earn. Our ultimate goal is to understand the net present value of providing these services. This involves comparing the initial cost of developing the necessary sensing, communication and control capabilities to the discounted lifetime revenue. If the net present value is positive, then a heat pump aggregator has an economic incentive to provide these services. We focus on estimating the total annual revenue, which requires modeling loads, heat pumps, and the aggregator's process of deciding day-ahead capacity offers.

We begin by reviewing related research. We then develop a method for co-optimizing day-ahead regulation and spinning reserve capacity offers under uncertainty. We implement this method in Monte Carlo simulation of a fleet of 1000 heat pumps in the PJM Interconnection. The Monte Carlo simulations provide estimates of the annual average capacities and annual revenues from regulation and spinning reserve.

Table 5.1: Per-device capacity and revenue estimates from [68].

	Annual average capacity (W)	Annual revenue ($)
Regulation	440	28–52
Spinning reserve	57	1.2–3.2

5.3.1 Literature review

Fixed-speed device capacities and revenues in California

The research literature on joint provision of regulation and spinning reserve from aggregated heat pumps is sparse. The main contributions in this area are [68, 99].

In [68], Mathieu *et al.* estimate the capacity and revenue potential in California of aggregations of thermostatically-controlled refrigerators, electric water heaters, central air conditioners, and central heat pumps. Regulation, spinning reserve and non-spinning reserve are considered. The modeled air conditioners and heat pumps are fixed-speed machines. The heat pumps provide heating but not cooling. Each device's thermal capacity, electrical capacity and COP is modeled as constant. Across devices, electrical capacities vary from 4–7.2 kW; COPs vary from 2–3 for air conditioners and 3–4 for heat pumps. Thermal capacities therefore vary from 8–21.6 kW_t for air conditioners and 12–28.8 kW_t for heat pumps.

Table 5.1 summarizes a subset of the capacity and revenue estimates from [68]. While the estimates in [68] vary by climate zone, we report estimates only for climate zone 3, which is fairly populous and representative of statewide averages. To allow a fair comparison to the reversible heat pumps studied in this thesis, we combine the air conditioning and heat pump estimates from [68]. The estimated revenue ranges are the means plus or minus one standard deviation.

In [99], Hao *et al.* also estimate the capacity and revenue potential in California of aggregated fixed-speed refrigerators, electric water heaters, central air conditioners, and central heat pumps that provide heating only. By contrast to [68], however, [99] does not

Table 5.2: Per-device regulation capacity and revenue estimates from [99].

Annual average capacity (W)	Annual revenue ($)
460	18–75

consider spinning or non-spinning reserve; attention is restricted to regulation. Like Mathieu *et al.*, Hao *et al.* model each device's thermal capacity, electrical capacity and COP as constant. Heat pump and air conditioner electrical capacities vary from 4–7.2 kW; COPs are 2.5 for air conditioners and 3.5 for heat pumps. Thermal capacities therefore vary from 10–18 kW_t for air conditioners and 14–25.2 kW_t for heat pumps.

Table 5.2 summarizes the regulation capacity and revenue estimates from [99]. As in Table 5.1, in Table 5.2 we combine the (cooling-only) air conditioner estimates with the (heating-only) heat pump estimates to allow fair comparison to reversible heat pumps that provide both heating and cooling. Like Mathieu *et al.*, Hao *et al.* report capacity and revenue estimates for different regions of California. The capacity estimate in Table 5.2 is the average of the regional capacities. The revenue estimate range is the regional-average revenue estimate from [99] plus or minus one standard deviation.

Variable-speed air conditioner capacities and revenues in PJM

While the California capacity and revenue estimates in [68] provide a useful data point, the numerical examples in this thesis use prices and market rules from PJM. Prices and market rules vary between system operators, so we expect our results to differ somewhat from those in [68]. The simulations in [47] provide a PJM-specific data point. In [47], Cai and Braun simulate PJM regulation from an individual rooftop air-conditioning unit on a typical July day in Miami. They simulate this day under energy and regulation prices from 2014–2018. On the simulated day, the rooftop unit consumes 63 kWh of electrical energy and provides 14.8 kW-h of integrated regulation capacity (a daily average of 617 W).

Absolute regulation revenue is not reported in [47], but relative regulation revenue is reported at 12–26% of the energy cost under wholesale energy prices. To estimate absolute regulation revenue, we assume that the daily average wholesale energy price is between 30 and 50 $/MWh (3 to 5 ¢/kWh), a plausible range for PJM. At these prices, the 63 kWh of electricity used over the simulation day would cost $1.9–3.2. The 12–26% relative revenue therefore translates to $0.23–0.83 for the day. Alternatively, assuming a daily average regulation price of 20-50 $/MW-h (another plausible range for PJM), the 14.8 kW-h of integrated regulation capacity would earn $0.3–0.74 on the simulated day. Extrapolating the daily revenue ranges over the course of a year yields an order-of-magnitude estimate of $10–100 annual regulation revenue. This estimate is very rough, but provides at least one data point suggesting that regulation revenue in PJM could be comparable to that in California.

Our contributions to capacity and revenue estimation

The work in this section is most similar to that in [68]. Following [68], we consider aggregated heat pumps providing regulation and reserve. We estimate annual average capacities and annual revenues using Monte Carlo simulation. The main distinctions of the work in this section are the following.

- We simulate operation in PJM, rather than California.
- We consider reversible variable-speed heat pumps, rather than fixed-speed air conditioners and fixed-speed heating-only heat pumps.
- Our heat pump capacities and COPs vary with boundary temperatures and (for COPs) part-load ratios.
- We develop a method for co-optimizing day-ahead regulation and reserve capacity offers

under uncertainty, and include this method in simulations.

Other approaches to deciding day-ahead capacity offers

To the best of our knowledge, this section contains the first analysis of ancillary service capacities and revenues that explicitly models the aggregator's process of deciding day-ahead capacity offers under uncertainty. This is an important process to model, as an aggregator must reliably meet any capacity offers that the power system operator accepts, regardless of the realizations of uncertain influences related to weather and occupant behavior. This reliability requirement encourages risk-aversion in the aggregator's decision process. As the existing literature assumes perfect information [47, 68, 99], it does not capture the aggregator's risk-aversion, and so could over-estimate the aggregator's capacity offers and the associated revenues.

We are not the first to consider the problem of deciding ancillary service capacity offers for aggregated heating and cooling systems under uncertainty, only (we believe) the first to embed a solution to this problem in long-term capacity and revenue estimation. Other research on deciding day-ahead capacity offers includes [72, 100–102, 180, 181]. This body of work centers on providing frequency regulation from large equipment in commercial buildings, such as fans and chillers. The papers [72, 180, 181] consider individual buildings, while [100–102] consider building aggregations. As we are interested in deciding ancillary service capacity offers from building aggregations, we focus this portion of the literature review on the most relevant papers, [100–102].

In [100, 101], Vrettos *et al.* develop a three-level control hierarchy for providing regulation from aggregations of commercial buildings. The highest level (termed Level 1 in [100, 101]) decides day-ahead aggregate regulation capacity offers. The lower levels involve model predictive control of individual buildings (Level 2) with a time step of 15–60 minutes, and regulation tracking from individual devices (Level 3) with a time step of ~1 second. Build-

ings are modeled as linear resistor-capacitor circuits. Thermal equipment capacities and COPs are assumed to be constant. Prices, weather, setpoints and occupancy are assumed to be predicted perfectly. The power system operator's regulation signal is allowed to be nonzero-mean, as is common in European and some North American power systems.

The paper [100] introduces the control hierarchy and develops methods for deciding capacity offers when the power and energy content of the regulation signal are uncertain but lie within known, bounded intervals. The Level 1 problem in [100] is formulated in a robust framework, while in [101] it is extended to include chance constraints on indoor air temperatures. In both papers, the Level 1 problem is framed as a large-scale optimization problem and solved by a single, central computer. In addition to capacity offers, the Level 1 decision variables in [100, 101] include nominal thermal power trajectories for all buildings' heating and cooling systems. The Level 1 problem dimensions scale approximately linearly with the number of buildings, making it computationally challenging for large aggregations. The Level 1 controller requires models of all buildings and all heating and cooling systems.

In [102], Rey *et al.* propose deciding day-ahead capacity offers via distributed optimization using the alternating directions method of multipliers [182]. The method shifts much of the Level 1 computational burden from the central controller to controllers at the individual buildings, improving scalability to large aggregations. As in [100, 101], in [102] Rey *et al.* model buildings as linear resistor-capacitor circuits, assume thermal equipment capacities and COPs are constant, and assume perfect predictions of prices, weather, and occupant-driven disturbances.

Our contributions to deciding day-ahead capacity offers

The control architecture we study in this chapter is similar to the control architecture in [100, 101], except that at Level 2 we require each heat pump to accurately track its user-specified indoor air temperature setpoint. This requirement ensures occupant comfort and simplifies

Level 1 substantially. We also assume that the power system operator's regulation reference signal is approximately zero-mean over any Level 1 time step. This is the case in our current scope of PJM ancillary services; PJM's RegD regulation signal is designed to be zero-mean over any 15-minute interval. [169]

The distinguishing characteristics of the methods in this section, relative to those in [100–102], are the following.

- We co-optimize regulation and spinning reserve capacity offers, rather than considering regulation only.
- We accommodate realistic models of heating and cooling equipment, rather than modeling thermal capacities and COPs as constant. (In simulations, we use nonlinear, temperature-dependent heat pump models fit to empirical data, as described in §3.1.3.)
- Our method combines the robustness of [100, 101] with the scalability of [102]. Our method explicitly accounts for uncertainty from weather, occupant behavior, and imperfect building models. The dimensions of our offer decision problem are independent of the size of the aggregation.

5.3.2 Co-optimizing regulation and spinning reserve

In this section, we consider the problem of deciding how much aggregate regulation and spinning reserve capacity to offer into the day-ahead market. We suppose that each heat pump $j = 1, \ldots, J$ simulates its operation under N independent, identically distributed scenarios of its uncertain influences. Example uncertain influences include outdoor air temperatures and indoor air temperature setpoints. We assume that each heat pump's local control system can obtain scenarios of these influences, *e.g.*, by downloading forecasts from an Internet weather service, by communicating with a learning thermostat capable of predicting indoor air temperature setpoints, or by running its own on-board prediction algorithms.

After simulating its operation under each scenario $i = 1, \ldots, N$, heat pump j reports its power consumption scenarios $P_{ij} \in \mathbf{R}^K$. Here K is the number of time steps of length Δt (h) in the day-ahead planning horizon; most North American power system operators use $\Delta t = 1$ h and $K = 24$. Heat pump j also reports planned trajectories $P_{ij}^{\text{cap}} \in \mathbf{R}^K$ and $P_{ij}^{\text{mod}} \in \mathbf{R}^K$ of its maximum capacity and minimum modulating capacity, respectively, under each scenario $i = 1, \ldots, N$.

The day-ahead planning decision variables are the capacity trajectories $P^{\text{reg}} \in \mathbf{R}^K$ and $P^{\text{res}} \in \mathbf{R}^K$ to be offered into the day-ahead regulation and reserve markets, respectively. We decide them by solving the following scenario optimization problem:

$$\begin{array}{ll} \text{maximize} & \Delta t\, \mathbf{E}\left[(\pi^{\text{reg}})^\top P^{\text{reg}} + (\pi^{\text{res}})^\top P^{\text{res}}\right] \\ \text{subject to} & P^{\text{reg}} \preceq \min\left\{\sum_{j=1}^J P_{ij} - P_{ij}^{\text{mod}}, \sum_{j=1}^J P_{ij}^{\text{cap}} - P_{ij}\right\},\ i = 1, \ldots, N \\ & P^{\text{reg}} + P^{\text{res}} \preceq \sum_{j=1}^J P_{ij},\ i = 1, \ldots, N \\ & P^{\text{reg}} \succeq 0,\ P_{\text{res}} \succeq 0, \end{array} \tag{5.5}$$

where the minimum in the first constraint is taken component-wise.

Problem (5.5) is a randomized linear program with $2K$ decision variables and $2K(N+1)$ inequality constraints. The problem dimension is independent of J, the number of heat pumps, so this problem can be solved efficiently even for very large heat pump aggregations. The number of decision variables is independent of N and the number of constraints is affine in N, so the problem scales fairly well with the number of scenarios.

The objective in Problem (5.5) is to maximize the expected revenue from providing regulation and reserve over the planning horizon. The expectation is taken with respect to the conditional distribution of the regulation and reserve prices π^{reg} (\$/kW-h) and π^{res} (\$/kW-h), conditioned on the information available at decision time. Assuming the conditional means $\bar{\pi}^{\text{reg}}$ (\$/kW-h) and $\bar{\pi}^{\text{res}}$ (\$/kW-h) of π^{reg} and π^{res} are known, the objective simplifies

to

$$\Delta t \left[(\bar{\pi}^{\text{reg}})^\top P^{\text{reg}} + (\bar{\pi}^{\text{res}})^\top P^{\text{reg}} \right].$$

As Problem (5.5) is convex, probabilistic guarantees on a solution's generalization properties can be obtained from the convex scenario theory in [183–185]. In simulations, we found that a sample size of $N = 200$ yielded out-of-sample violation frequencies below 1%.

An important feature of the PJM day-ahead regulation and reserve markets is that regulation prices are almost always higher than reserve prices. This was the case in 98% of the hours between 2013 and 2018. [170] In this case, Problem (5.5) can be solved analytically. Regulation prices are always nonnegative, so if $\bar{\pi}^{\text{reg}} \succeq \bar{\pi}^{\text{res}}$, it is optimal to offer as much regulation as possible at each time step under each scenario. This can be accomplished by setting

$$P^{\text{reg}} = \min_{i=1,\ldots,N} \left\{ \min \left\{ \sum_{j=1}^{J} P_{ij} - P_{ij}^{\text{mod}}, \sum_{j=1}^{J} P_{ij}^{\text{cap}} - P_{ij} \right\} \right\}.$$

Reserve prices are also nonnegative, so revenue is maximized by offering any remaining capacity for reserve:

$$P^{\text{res}} = \min_{i=1,\ldots,N} \left\{ \sum_{j=1}^{J} P_{ij} - P^{\text{reg}} \right\}.$$

These analytical expressions provide good approximations to the true solutions to Problem (5.5). They can be useful when computational resources are limited.

5.3.3 Simulation setup

We now illustrate the day-ahead capacity planning method through Monte Carlo simulation. In each Monte Carlo run, we simulate the operation of $J = 1000$ heat pumps for one day with a time step of one hour. Each run consists of two stages: first, optimization of day-ahead offers under N scenarios, and second, simulation under a different scenario representing the 'true' system evolution. We use a sample size of $N = 200$ and run $M = 2190$ simulations (6

years in total).

The input data to each daily simulation are $\pi^{\text{reg}}, \pi^{\text{res}} \in \mathbf{R}^K$ and $P_{ij}, P_{ij}^{\text{cap}}, P_{ij}^{\text{mod}} \in \mathbf{R}^K$, $i = 1, \ldots, N$, $j = 1, \ldots, J$. The ancillary service prices $\pi^{\text{reg}}, \pi^{\text{res}}$ are from PJM's public-access historical price database. [167] The nominal powers P_{ij}, maximum capacities P_{ij}^{cap} and minimum modulating capacities P_{ij}^{mod} are defined by propagating weather data through thermal load models, then propagating the resulting thermal loads through heat pump capacity and COP models. The simulations in this section use essentially the same weather data, load and heat pump models, and propagation processes as the simulations in Chapter 4. We therefore refer the reader to §4.4.1–4.4.3 for detailed discussion of the relevant data, models and processes. We briefly summarize those details here for the sake of readability.

Thermal loads are modeled as 3R2C thermal circuits with parameters tuned to the annual heating and cooling load data from a survey of United States residential buildings. [85] Each load represents approximately 100 m^2 of conditioned residential floor area. Heat pumps are modeled via functions describing their maximum thermal capacities, minimum modulating thermal capacities, and COPs. These functions are low-order polynomials whose parameters are fit to manufacturer-reported empirical data. The heat pumps are ductless mini-split units sized for stand-alone cooling and for heating displacement. The median nameplate cooling capacity of the heat pump fleet is 2.6 kW_t (9000 BTU/h). In simulations, we use coincident hourly 2013–2018 Philadelphia weather and PJM ancillary service price data from [167] and [170], respectively. The full data set consists of 52560 hours of outdoor air temperatures, global horizontal solar irradiances, regulation prices and spinning reserve prices.

We refer the interested reader to §4.4.4 for a discussion of the data quality and limitations. To summarize that discussion, in our qualitative assessment, we rank the weather and ancillary service price data fidelity as *excellent*, the thermal load data fidelity as *fair* and the heat pump model fidelity as *fair*. In §4.4.4, we also ranked the fidelity of the equipment installed cost data as *poor*, but those data are not relevant to the simulations in this section.

5.3.4 Decision methods

We simulate three methods of deciding day-ahead capacity offers.

1. *Local scenario optimization.* In this method, each heat pump decides its individual regulation and reserve offers using only local information. The aggregate offers are simply the sum of the individual offers.

2. *Central scenario optimization.* In this method, by contrast to the first, we gather the individual power and capacity scenarios for each load and optimize centrally over the full set of data by solving Problem (5.5). Central scenario optimization generally performs better than local scenario optimization; we refer to the revenue gap as the *value of aggregation*.

3. *Central prescient optimization.* This method assumes perfect foreknowledge at decision time of all uncertain influences on all heat pumps over the entire planning horizon. This method is not implementable in practice, as we cannot see the future, but it gives an upper bound on the achievable revenue. We refer to the revenue gap between central prescient optimization and central scenario optimization as the *cost of uncertainty*.

In all methods, we assume that perfect forecasts of ancillary service prices are available. All electrical power trajectories (*i.e.*, nominal power, maximum capacity, and minimum modulating capacity), however, are random.

5.3.5 Results

In this section, we present numerical results on ancillary service capacities and revenues. We emphasize that these are *simulation* results, and so their validity is limited by the fidelity of the input data. We discuss these limitations further in §4.4.4 and in Appendix B.

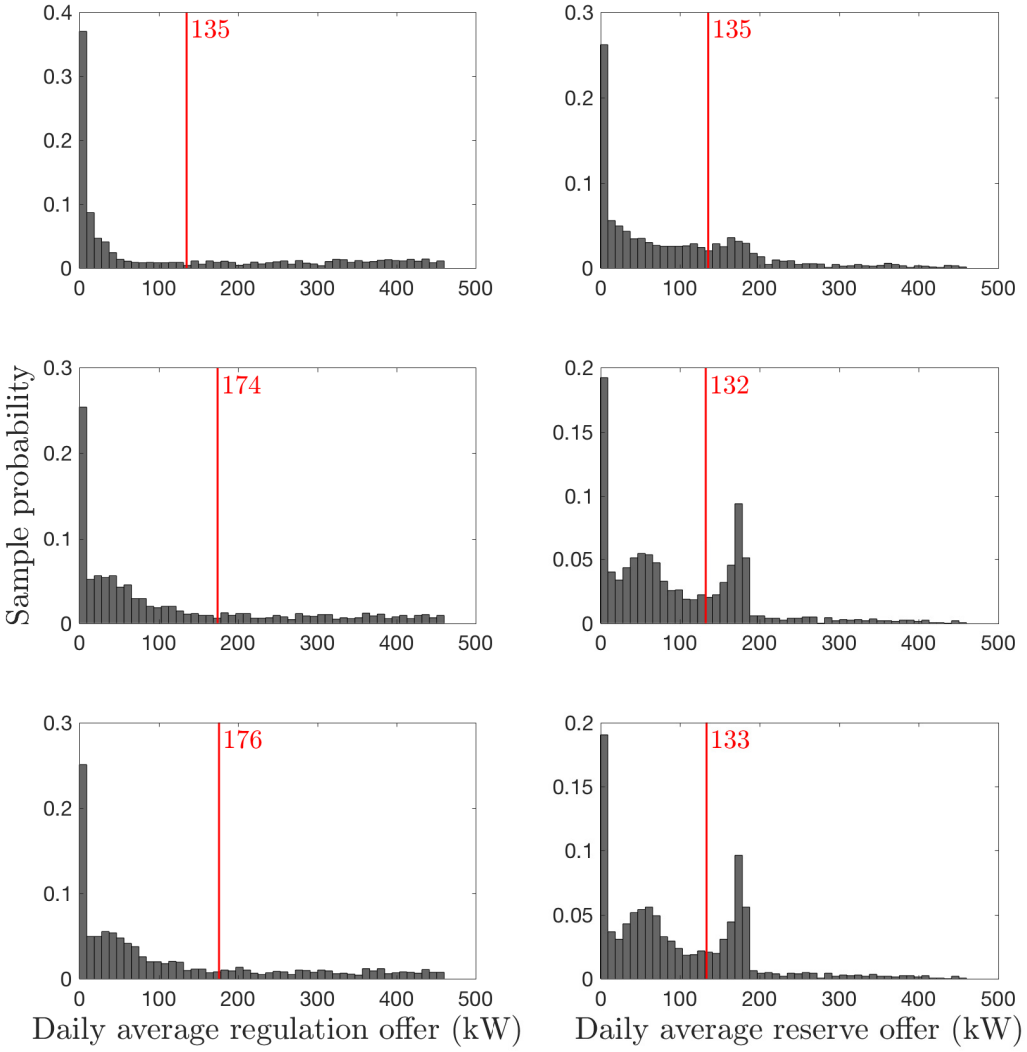

Figure 5.6: Histograms of daily average day-ahead capacity offers (left) and reserve offers (right) for $J = 1000$ heat pumps under local scenario optimization (top), central scenario optimization (middle), and central prescient optimization (bottom). Red lines represent sample means.

Figure 5.6 shows histograms of the daily average regulation and reserve capacity offers under the three decision methods. In all three methods, the daily average regulation and reserve capacities are comparable, and relatively small: 135 to 176 Watts per heat pump. We note that these averages include many hours of zero capacity during mild weather when no heating or cooling is needed. As expected, more regulation and reserve capacity is offered under central scenario optimization than local scenario optimization. Surprisingly, central scenario optimization offers almost as much capacity as central prescient optimization. We attribute this effect to the attenuation of variability that naturally occurs when summing weakly correlated random variables across a large number ($J = 1000$) of heat pumps.

Figure 5.7 show histograms of the daily regulation and reserve capacity revenues under the three decision methods. In all three methods, regulation revenues exceed reserve revenues by a factor of four to six. This is because regulation prices are almost always higher than reserve prices. Revenues are fairly small: \$25 to \$75 per heat pump per year from providing both regulation and reserve. Central scenario optimization increases regulation revenue by about 29% relative to local scenario optimization. Reserve revenue is similar across all decision methods. As with capacity, the revenue gap between central scenario optimization and central prescient optimization is quite small.

With a sample size of $N = 200$, scenario optimization results in high levels of robustness. We quantify the level of robustness in terms of a *violation*, *i.e.*, the event that the true regulation capacity in any hour is smaller than the decided regulation capacity offer in that hour. Violations represent cases where the aggregator is unable to meet their regulation commitment. In $KM = 52560$ simulated hours, no violations were observed for the local scenario decision method. For the central scenario decision method, the violation sample frequency was 0.35%.

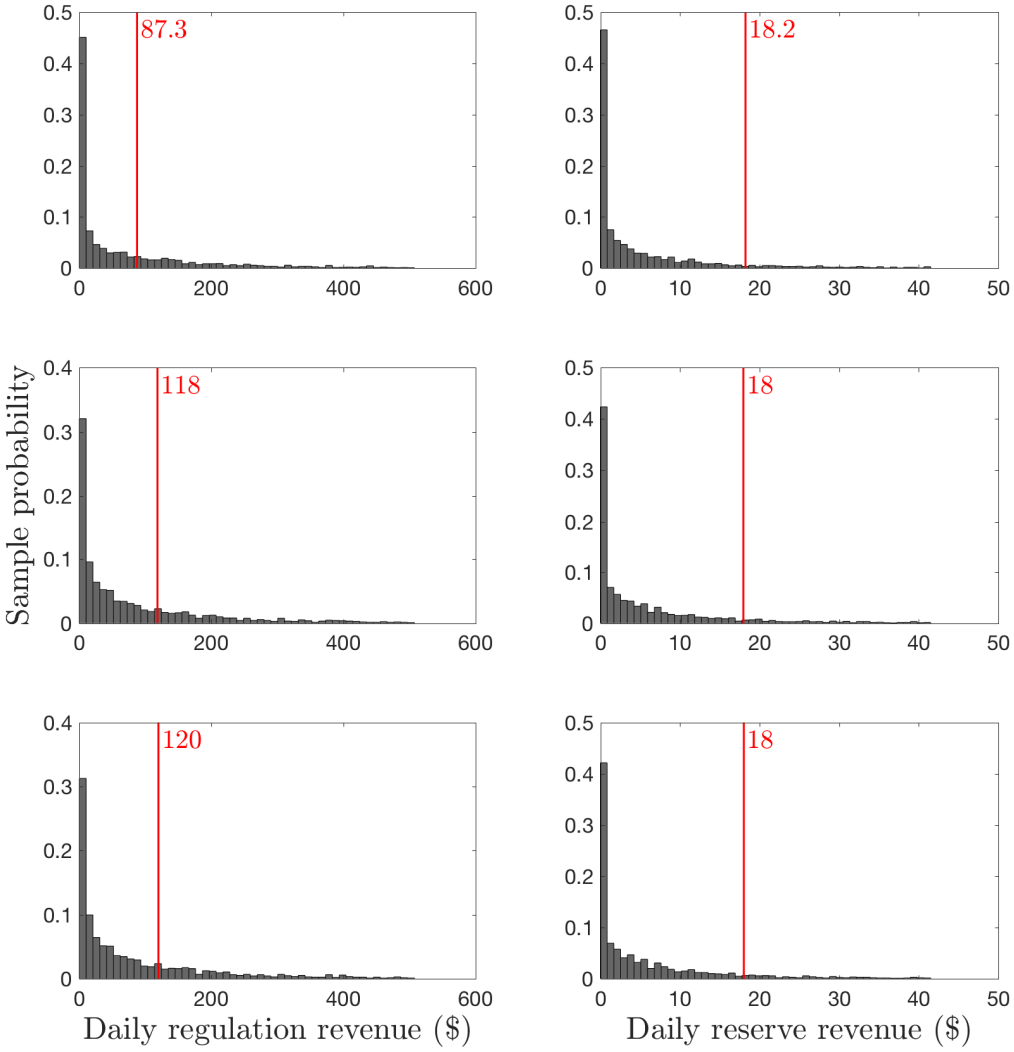

Figure 5.7: Histograms of daily day-ahead capacity revenues (left) and reserve revenues (right) for $J = 1000$ heat pumps under local scenario optimization (top), central scenario optimization (middle), and central prescient optimization (bottom). Red lines represent sample means.

Table 5.3: Per-heat-pump value of aggregation and cost of uncertainty.

	Annual average capacity	Annual revenue
Value of aggregation	36 ± 1 W (13%)	$\$11.2 \pm 5.4$ (29%)
Cost of uncertainty	2.71 ± 0.06 W (1%)	$\$0.54 \pm 0.25$ (1%)

5.3.6 Discussion

Table 5.3 shows the estimated value of aggregation and cost of uncertainty. The estimates are reported in terms of annual average capacity per heat pump and annual revenue per heat pump. The capacity and revenue estimates include both regulation and reserve. Each estimate includes the sample mean $\pm$ one sample standard deviation. The percent values of aggregation in Table 5.3 are relative to local scenario optimization. The percent costs of uncertainty are relative to central prescient optimization. We now discuss two conclusions that can be drawn from Table 5.3.

Cost of uncertainty

The first conclusion that can be drawn from Table 5.3 is that the cost of uncertainty is not too large. At least in this example, central scenario optimization delivers capacity offers and revenues that are close to the limiting case of perfect information (central prescient optimization). As discussed above, we attribute this to the attenuation of uncertainty caused by adding many weakly correlated random variables. This is similar in spirit to the Central Limit Theorem. Loosely, it is easier to predict the aggregate behavior of a large number of heat pumps than it is to predict the behavior of any particular individual, because random variations across heat pumps tend to cancel out.

Value of aggregation

The second conclusion that can be drawn from Table 5.3 is that aggregation substantially increases both the ancillary service capacities that can be offered and the associated revenues. We attribute this to two effects. The first effect is the attenuation of uncertainty described above. The second effect is an artefact of PJM's requirement that regulation capacity offers be *symmetric*.

For clarity, we illustrate the second effect in the simple case of maximizing the regulation capacity offer for one time step under perfect information. In this case, the largest symmetric capacity that can be offered individually by heat pump j is the smaller of its upward and downward flexibilities:

$$\min\left\{P_j^{\text{cap}} - P_j, P_j - P_j^{\text{mod}}\right\}.$$

The optimal aggregate regulation offer under local optimization is the sum of the maximum individual symmetric capacities:

$$\sum_{j=1}^{J} \min\left\{P_j^{\text{cap}} - P_j, P_j - P_j^{\text{mod}}\right\}.$$

Under central optimization, by contrast, individual flexibilities are first summed, then made symmetric, resulting in an offer

$$\min\left\{\sum_{j=1}^{J} P_j^{\text{cap}} - P_j, \sum_{j=1}^{J} P_j - P_j^{\text{mod}}\right\}.$$

It is straightforward to show that for any $P^{\text{mod}} \preceq P \preceq P^{\text{cap}}$,

$$\min\left\{\sum_{j=1}^{J} P_j^{\text{cap}} - P_j, \sum_{j=1}^{J} P_j - P_j^{\text{mod}}\right\} \geq \sum_{j=1}^{J} \min\left\{P_j^{\text{cap}} - P_j, P_j - P_j^{\text{mod}}\right\}.$$

In other words, central optimization yields at least as much symmetric capacity as local optimization. This result can be extended to multiple time steps, but not to asymmetric regulation markets, which allow separate offers for upward and downward regulation capacity. We note, however, that the value of aggregation may still be significant in asymmetric regulation markets due to attenuation of uncertainty.

Influence of assumptions

In this section, we restrict our attention to deciding ancillary service *capacity* offers. This restriction is consistent with other recent work in the research literature; see, *e.g.*, [72, 100–102, 180, 181]. In practice, however, most power system operators require ancillary service market participants to append a *price* offer to each of their capacity offers. This is the case in PJM. [169] The power system operator then clears each market by accepting offers in (roughly) ascending order of price until the required capacity is procured. The last (*i.e.*, highest-priced) offer accepted sets the market clearing price.

Generators typically decide their ancillary service price offers based on the opportunity cost of withholding capacity from the energy market. [33] For a heat pump aggregator that provides ancillary services but not energy, however, this opportunity cost is zero. Furthermore, providing ancillary services has negligible impact on the thermal comfort of building occupants (see §5.1.3 and §5.2.5), so incurs negligible opportunity cost in that respect. Therefore, such a heat pump aggregator could reasonably append a zero-price offer to each of their capacity offers. On the other hand, if the heat pump aggregator also participated in wholesale energy markets, *cf.* [69], then their opportunity costs of providing ancillary services would be nonzero. Deciding ancillary service price offers in this setting is an interesting direction for future research.

When calculating revenues, we assume that all of the aggregator's regulation and reserve offers are accepted. This assumption is optimistic, as the power system operator may not

need or accept the aggregator's capacity offers at some times. However, as discussed above, the aggregator's capacity offers would likely be paired with low, or even zero, price offers. As discussed above, low-priced offers are likely to be accepted.

When computing ancillary service capacities, we assume zero capacity is available from any heat pump that is (in the simulated time step) cycling off and on rather than modulating continuously. This assumption biases aggregate capacity and revenue estimates downward; in reality, an aggregator could perhaps extract some value out of cycling heat pumps. While pessimistic, this bias is likely small for appropriately-sized heat pumps, which should spend most of their time modulating.

We also assume that the aggregator is a price-taker. In other words, the aggregator exerts negligible influence over PJM's process of clearing the day-ahead ancillary service markets. This assumption is likely good if the aggregator's offers are small relative to the total market size. On the other hand, an aggregator offering many MW of capacity at relatively high prices might at times set market clearing prices. These market interactions are nontrivial to model, and could alter the aggregator's offer decision process. For example, the aggregator might strategically withhold capacity in some hours, or offer capacity at an artificially inflated price, in order to promote higher market clearing prices and increase their ancillary service revenue.

How many heat pumps would an aggregator require to exert significant influence on PJM's regulation market clearing process? In our 1000-heat-pump simulations, aggregate capacity offers are on the order of 100 kW. For comparison, federal rules require PJM to procure 800 MW of regulation capacity during hours when substantial load ramping is expected and 525 MW during non-ramping hours. [169] Assuming ~150 W of regulation capacity per heat pump, providing 1% of PJM's 525 MW capacity procurement during non-ramping hours would require ~3.5 million heat pumps. Heat pump adoption rates on the eastern seaboard are on the order of 10^5 units per year. [139] Assuming no heat pumps currently participate

in PJM's regulation market, and that all newly-installed heat pumps were aggregated to provide regulation, it would take ~35 years for heat pumps to provide 1% of PJM's 525 MW procurement. Therefore, the price-taker assumption will likely remain valid for heat pumps in PJM over the coming decades. In smaller power systems, however, strategic market interactions could be significant. Analyzing these interactions is another interesting direction for future research.

Finally, we note that some power system operators allow ancillary service providers to submit multiple price/capacity offers at each market time step. For example, an aggregator might offer the first 100 kW of regulation capacity at zero price, the second 100 kW at a moderate price, and a final 100 kW at a high price. This market structure would alter the aggregator's decision problem. We do not model this market structure in this section because PJM markets require a single price/capacity offer at each hour. [169] It could be an important consideration in other power systems, however.

Revenue magnitudes

Perhaps the most important message to take away from this section is that ancillary service revenues are small: $25–75 per heat pump per year. This finding is specific to PJM, but is similar to the annual per-heat-pump California estimates of $29–53 based on [68] and of $18–75 based on [67].

Assuming uniformly-distributed heat pump lifetimes of 8–20 years and annual cash flow discount rates of 5–15%, the net present value of $25–75 annual revenues is $210–470 (25th–75th percentile); see Figure 5.8. This range can be interpreted as the largest investment in sensing, communication and control capabilities for the purpose of providing regulation and spinning reserve that an aggregator can justify on economic grounds. If the aggregator can outfit the heat pumps with these capabilities for less than $210–470, then they can expect the resulting ancillary service revenues to yield an attractive return on that investment. In

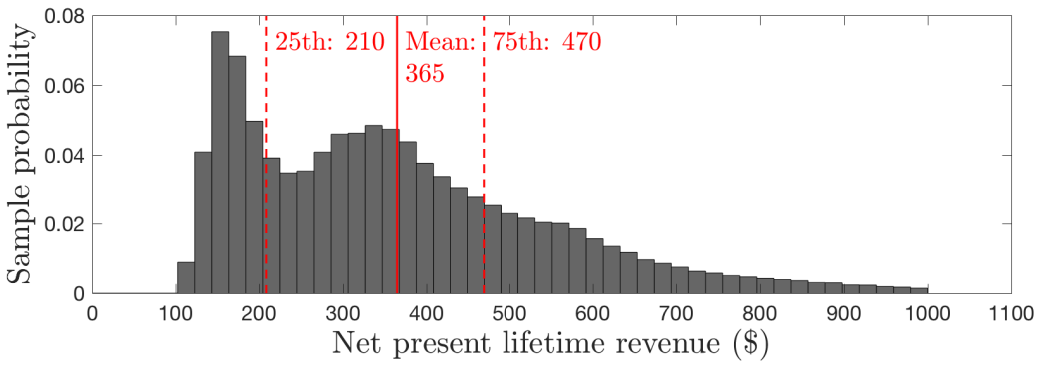

Figure 5.8: Histogram of the net present lifetime revenue per heat pump from providing regulation and spinning reserve. The solid red line is the sample mean; the dashed red lines are the 25th and 75th percentiles.

some situations, a heat pump might be outfitted with some or all of these capabilities for other purposes, such as fault detection, remote monitoring, or control via the Internet. In these situations, the incremental effort required to enter ancillary service markets could be relatively small. One such situation is the heat purchase agreement model of heat pump ownership discussed in §1.2 and §2.3, which requires sensing and communication for billing purposes. In other situations, the required hardware and software may be prohibitively expensive.

In any case, the findings in this section suggest that providing ancillary services is unlikely to generate significant net present profit under current market prices. It appears that a heat pump aggregator should view ancillary service provision primarily as a public service, rather than a money-making opportunity. This prognosis could change if ancillary service prices rise significantly due, *e.g.*, to increased integration of wind and solar generation. On the other hand, if battery costs continue to fall, batteries could supply more ancillary services and drive down market prices. Policies, incentives and market rules could also affect the outlook significantly.

5.3.7 Comparing scenario and distributionally-robust approaches

In §5.3.2, we formulated the aggregator's problem of deciding day-ahead regulation and reserve capacity offers as a randomized linear program. Indeed, Problem (5.5) can be reformulated as

$$\begin{array}{ll} \text{minimize} & c^\top x \\ \text{subject to} & Ax \preceq b_i, \ i = 1, \ldots, N \\ & x \succeq 0, \end{array} \tag{5.6}$$

where

$$x = \begin{bmatrix} P^{\text{reg}} \\ P^{\text{res}} \end{bmatrix}, \ c = -\Delta t \begin{bmatrix} \bar{\pi}^{\text{reg}} \\ \bar{\pi}^{\text{res}} \end{bmatrix}, \ A = \begin{bmatrix} I & \\ I & I \end{bmatrix}$$

and $b_1, \ldots, b_N \in \mathbf{R}^{2K}$ are independent, identically distributed samples from the distribution of the random vector

$$b = \begin{bmatrix} \min\left\{\sum_{j=1}^J P_j - P_j^{\text{mod}}, \sum_{j=1}^J P_j^{\text{cap}} - P_j\right\} \\ \sum_{j=1}^J P_j \end{bmatrix}. \tag{5.7}$$

Here we view $P_j, P_j^{\text{mod}}, P_j^{\text{cap}} \in \mathbf{R}^K$, $j = 1, \ldots, J$, as random vectors. The decision variable is $x \in \mathbf{R}^{2K}$, so Problem (5.6) has $2K$ variables and $4K$ inequality constraints.

Problem (5.6) is consistent with the scenario approach to convex programming under uncertainty developed by Campi, Garatti and Calafiore in [183–186]. Applied to Problem (5.6), the scenario approach guarantees (at a user-specified confidence level $\beta \in (0, 1)$) satisfaction of the chance constraint

$$\mathbf{Prob}\left\{Ax \preceq b\right\} \geq 1 - \alpha, \tag{5.8}$$

where $\alpha \in (0, 1)$ represents an acceptable probability of constraint violation. The constraint

(5.8) is referred to as a *joint* chance constraint, as it applies jointly to the $2K$ scalar inequality constraints contained in the vector inequality $Ax \preceq b$.

There are other approaches to chance-constrained linear programming; see, *e.g.*, [187–191]. Of particular interest is [192], wherein Calafiore and El Ghaoui consider the case where only the mean and covariance of b are known. Calafiore and El Ghaoui develop a method that guarantees

$$\inf_{\mathbf{P} \in \mathcal{P}_\ell} \mathbf{P}\left\{a_\ell^\top x \leq b_\ell\right\} \geq 1 - \alpha_\ell, \tag{5.9}$$

where $a_\ell^\top$ is the ℓth row of A:

$$A = \begin{bmatrix} a_1^\top \\ \vdots \\ a_{2K}^\top \end{bmatrix}.$$

The set $\mathcal{P}_\ell$ contains all distributions on $\mathbf{R}$ with mean mean $\bar{b}_\ell$ and variance σ_ℓ^2.

In words, the method in [192] guarantees that the chance constraint

$$\mathbf{P}\left\{a_\ell^\top x \leq b_\ell\right\} \geq 1 - \alpha_\ell$$

will be satisfied for any distribution $\mathbf{P}$ that is consistent with the known mean and variance of b_ℓ. For this reason, Calafiore and El Ghaoui refer to the method in [192] as *distributionally-robust*. Distributionally-robust optimization is a broader subject with a growing body of results; see, *e.g.*, [193–196]. We note that while Inequality (5.8) is a joint chance constraint, Inequality (5.9) is an individual (distributionally-robust) chance constraint. Even for linear programs, optimization with distributionally-robust joint chance constraints is strongly NP-hard for most ambiguity sets[3] [196], though tractable conservative approximations exist in some special cases [193–195]. The conservative approximations typically promote the un-

[3]In the context of distributionally-robust optimization, an ambiguity set is a set of probability measures on a given space that satisfy certain properties, such as having known moments or other statistics.

derlying linear program to a second-order cone program or semidefinite program, increasing computational complexity. For our current purposes, we prefer the exact individual chance constraint reformulation in [192] to the approximate joint chance constraint reformulations in [193–195].

In Theorem 3.1[4] of [192], Calafiore and El Ghaoui provide an exact reformulation of the distributionally-robust chance constraint (5.9):

$$\inf_{\mathbf{P}\in\mathcal{P}_\ell} \mathbf{P}\left\{a_\ell^\top x \le b_\ell\right\} \ge 1-\alpha_\ell \iff a_\ell^\top x + \kappa_\ell \sigma_\ell \le \bar{b}_\ell,$$

where $\kappa_\ell = \sqrt{(1-\alpha_\ell)/\alpha_\ell}$. Therefore, a solution to the distributionally-robust linear program

$$\begin{array}{ll} \text{minimize} & c^\top x \\ \text{subject to} & \inf_{\mathbf{P}\in\mathcal{P}_\ell} \mathbf{P}\left\{a_\ell^\top x \le b_\ell\right\} \ge 1-\alpha_\ell,\ \ell = 1,\ldots,2K \\ & x \succeq 0 \end{array}$$

can be generated by solving the deterministic linear program

$$\begin{array}{ll} \text{minimize} & c^\top x \\ \text{subject to} & Ax + s \preceq \bar{b} \\ & x \succeq 0, \end{array} \tag{5.10}$$

where

$$s = \begin{bmatrix} \kappa_1\sigma_1 \\ \vdots \\ \kappa_{2K}\sigma_{2K} \end{bmatrix}.$$

Problem (5.10) has $2K$ decision variables and $4K$ inequality constraints. Like Problem (5.6),

[4] Theorem 3.1 of [192] applies to the more general case where a_ℓ is also random, but we do not need that generality here.

the dimensions of Problem (5.10) are independent of J, the number of heat pumps.

Simulation

We now compare the scenario and distributionally-robust approaches outlined above through 1000 Monte Carlo simulations of deciding day-ahead hourly ancillary service capacity offers for an aggregation of 1000 heat pumps. We generate price, weather and load data as discussed in §5.3.3. Each simulation involves two stages. In the first stage, we generate sample input data and solve the scenario and distributionally-robust problems, (5.6) and (5.10). In keeping with the simulations earlier in this section, we use $N = 200$ training scenarios in the scenario problem and use the sample mean and covariance in the distributionally-robust problem. In earlier simulations, we observed that this sample size yielded individual constraint violation frequencies under 1%, so we set $\alpha_1 = \cdots = \alpha_{2K} = 0.01$ in the distributionally-robust problem.

In the second simulation stage, we generate a new validation scenario and record for each approach the realized ancillary service revenue and whether any constraints are violated under the validation scenario. To explore the value of distributional robustness, we draw the validation scenario from a 'true' distribution whose mean and covariance match the sample mean and covariance in the training set, but that is Gaussian. This introduces small but nontrivial distributional mismatch, as the distribution from which the training samples are drawn is not Gaussian. While the random vector b involves sums of many random variables (see Equation (5.7)), and so might be expected to be approximately Gaussian due to the Central Limit Theorem, the first K components of b also involve nonlinear transformations (specifically, pointwise minima) of those sums.

Results and discussion

In 1000 Monte Carlo simulations, both the scenario and distributionally-robust approaches satisfied constraints in the validation data with high frequency. In the scenario approach, all individual constraint violation frequencies in the validation data were below 0.6%. In the distributionally-robust approach, no constraint violations were observed. These results suggest that the distributionally-robust approach is more robust than the scenario approach in this setting. This aligns with our expectations, since in these simulations the distributions differ between the training and validation stages, and handling such distributional mismatch is the key feature of distributionally-robust optimization.

The increased frequency of constraint satisfaction of the distributionally-robust approach comes at a cost, as shown in Figure 5.9. On average over the sample, the daily ancillary service revenue earned under the distributionally-robust approach is about 88% of the revenue earned under the scenario approach. This result can be interpreted as evidence of a trade-off between the competing objectives of maximizing revenue and of robustly meeting ancillary service commitments. The scenario and distributionally-robust approaches strike different balances between these competing objectives: the scenario approach earns somewhat more revenue than the distributionally-robust approach, but is somewhat less robust.

We note that the conservatism of the distributionally-robust approach can be controlled via the parameters $\alpha_1, \ldots, \alpha_{2K}$, which are the acceptable probabilities of constraint violations. Indeed, raising the α_ℓ from 0.01 to 0.05 and re-running the Monte Carlo simulations increases the sample-average revenue earned under the distributionally-robust approach to 95% of the revenue earned under the scenario approach (up from 88% with $\alpha_\ell = 0.01$). This change also decreases robustness somewhat, causing a constraint violation frequency of 0.4% in the validation data, compared to the 0% violation frequency with $\alpha_\ell = 0.01$.

It is also worth noting that for this problem the distributionally-robust approach is more

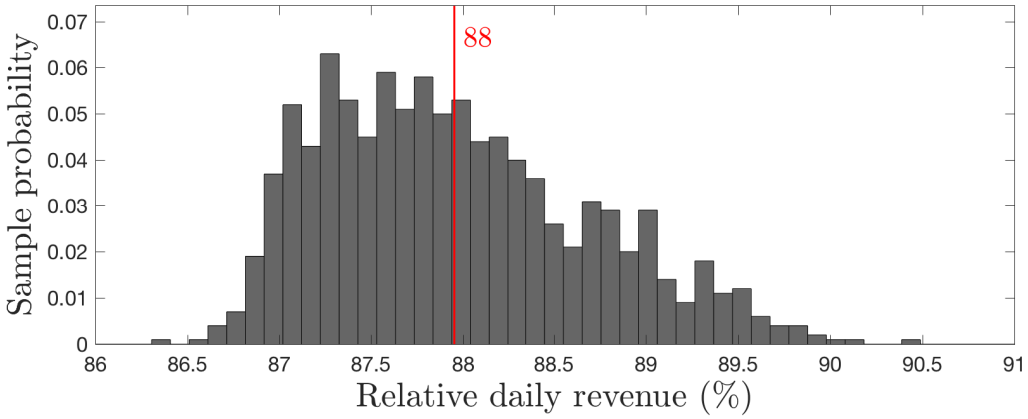

Figure 5.9: Histogram of the daily ancillary service revenue under the distributionally-robust approach, as a percentage of the daily revenue under the scenario approach, over 1000 Monte Carlo simulations. The red line indicates the sample mean.

computationally-efficient than the scenario approach. This is because the distributionally-robust problem has $4K$ constraints, while the scenario problem has $2K(N+1)$ constraints. In 1000 Monte Carlo simulations, the sample-average time required to solve the distributionally-robust problem was about 85% of that of the scenario problem. The difference in computation time is modest in these simulations because the number of scenarios, $N = 200$, is relatively small. In cases where very high robustness levels are required – necessitating very large values of N – the distributionally-robust approach is likely to require substantially less processing time than the scenario approach.

In conclusion, both the scenario approach and the distributionally-robust approach of [192] appear to be reasonable methods for deciding day-ahead ancillary service capacity offers for an aggregation of heat pumps. The distributionally-robust approach might be preferable to more risk-averse decision makers, or in situations where computational resources are limited.

Chapter 6

Conclusion

6.1 Summary

The goal of this thesis was to reduce greenhouse gas emissions by lowering barriers to adopting efficient electric heat pumps. To that end, we analyzed the HPA model of third-party heat pump ownership. We argued that an HPA aggregator could lower barriers to heat pump adoption by

- eliminating users' capital costs,
- taking on many of the risks associated with heat pump ownership,
- reducing net present costs by buying heat pumps in bulk, improving the heat pump selection process, and unlocking ancillary service revenues, and
- reducing users' 'hassle factors' associated with finding skilled installers, identifying and applying for incentives, *etc.*

We also developed solution methods for numerous problems that arise in the HPA model. In Chapter 2, we derived necessary and sufficient conditions for an HPA to mutually benefit

the aggregator and the user, and provided a method for fairly pricing heating and cooling. In Chapter 4, we developed a data-driven method for heat pump selection that provides probabilistic feasibility and optimality guarantees. In Chapter 5, we verified the feasibility of providing regulation and spinning reserve from an aggregation of reversible, variable-speed heat pumps. We also developed a method for co-optimizing day-ahead regulation and spinning reserve capacity offers under uncertainty. We estimated that providing these services could earn \$25–75 of revenue per heat pump per year.

The potential impact of this thesis is a self-reinforcing cycle: HPAs could accelerate heat pump adoption, providing more ancillary services, facilitating the integration of more wind and solar power, lowering electricity costs, and further accelerating heat pump adoption. This cycle could reduce emissions both directly, by replacing fossil-fueled heaters and inefficient air conditioners with efficient electric heat pumps, and indirectly, by replacing fossil-fueled generators with wind and solar power plants.

6.2 Extensions

There are many opportunities to extend this work. We now discuss a few.

Experiments. When gathering data for this thesis, we noted several important, open questions that could be answered through laboratory experiments.

1. Do temperature setbacks overnight or during unoccupied periods save energy with variable-speed heat pumps? Reducing the temperature difference between the indoor and outdoor air reduces thermal load, but heat pumps' efficiencies degrade when they work near maximum capacity to recover from setbacks. Field studies indicate that setbacks tend to increase energy use [79, 94], but the answer must depend on the setback depth and duration. Demonstrating controls that smooth out the recovery

from setbacks is another area of practical importance.

2. How does cycling off and on, rather than modulating continuously, affect variable-speed heat pump efficiency? To our knowledge, only a handful of experimental results in this area have been published. [93] This question is particularly important in cold (or hot) climates, where a reversible heat pump that is sized appropriately for heating (or cooling) will likely be oversized for cooling (or heating). As discussed in §4.4, oversizing leads to cycling and COP degradation, but there is significant uncertainty in the magnitude of these effects.

Thermal power estimation. For monitoring, fault detection and billing purposes, an HPA aggregator should be able to accurately estimate the thermal power output of each of their heat pumps. This task is nontrivial, as it generally requires measuring or estimating supply and return air temperatures and mass flow rates at the indoor unit. Appendix A of the field study [80] discusses related implementation issues. We note, however, that good mathematical models of heat pumps can be developed via system identification techniques if empirical performance data are available. Could such models be combined with low-cost sensors and nonlinear filtering techniques to produce accurate, low-cost thermal power estimates?

Other hardware. Our hardware scope was intentionally narrow; our simulations focused on one manufacturer's popular line of air-to-air heat pumps. We maintained this narrow focus for concreteness, and because an unusual amount of empirical performance data was available for these heat pumps. The hardware scope could be expanded to include, *e.g.*, other air-to-air heat pump manufacturers, ground-source heat pumps, or heat pump water heaters. The HPA model could be particularly attractive for ground-source heat pumps, whose high capital costs are a major barrier to adoption. Heat pump water heaters could

provide energy-intensive power system services due to their large thermal storage capacities.

Other power system services. In this thesis, we considered the two ancillary services that typically have the highest prices: regulation and spinning reserve. A heat pump aggregator could provide other power system services, such as limiting peak demand, supplying reactive power in distribution networks, or shifting load based on real-time energy prices or greenhouse gas intensities. In this thesis, we observed trade-offs between allocating flexible capacity for regulation and for reserve. A similar tension was observed between limiting peak demand and price-based load shifting in [197]. The revenues from multiple services are generally not additive, as the services compete for flexibility. How should an aggregator allocate flexibility between services, and what are the associated costs and benefits?

Other power system operators. The simulations in this thesis used price and signal data from PJM's ancillary service markets. Similar work has been done in the context of California's power system operator [68], but there are five other system operators in the United States and many more worldwide. Different system operators define different ancillary services, use different market rules, and deploy flexible resources in different ways. What value could a heat pump aggregator earn in other power systems?

Appendix A

A scenario approach to constrained ranking and selection

In this appendix, we consider the problem of selecting one of a finite number of systems. System performance is evaluated via cost and constraint functions that depend on uncertain parameters. The distribution of the uncertain parameters need not have any particular structure, but we assume that a number of independent, identically distributed scenarios drawn from this distribution are available. We develop a selection procedure based on simulation under these scenarios. The procedure probabilistically guarantees that the selection is feasible and approximately optimal. The selection and suboptimality threshold are computed by solving an optimization problem with constraints enforced for each scenario. The robustness level of the probabilistic guarantee is computed after solving this problem, and depends on the observed structure of the feasible region. Most of the computation involved in solving the optimization problem can be done in parallel. The proof of the probabilistic guarantee is a straightforward application of the recent theory in [150]. The guarantee holds distribution-free.

Problem statement

We consider the problem of selecting one of a finite number of systems indexed by $j = 1, \ldots, J$. We suppose that the selected system will be subject to uncertain influences represented by $\delta \in \Delta$, where Δ is a probability space equipped with a σ-algebra $\mathcal{D}$ and a probability measure $\mathbf{P}$. We do not assume that the distribution of δ is known or has any particular structure, but we do assume that an independent, identically distributed sample $(\delta^1, \ldots, \delta^N)$ from the distribution of δ is available. We refer to the δ^i as *scenarios*. Formally, we view $(\delta^1, \ldots, \delta^N)$ as an element of the probability space Δ^N equipped with the product σ-algebra $\mathcal{D}^N$ and the probability measure $\mathbf{P}^N = \mathbf{P} \times \cdots \times \mathbf{P}$ (N times).

If we knew with perfect foresight that the realized value of δ would be some $\hat{\delta}$, we would select a system $j \in \{1, \ldots, J\}$ to

$$\begin{array}{ll} \text{minimize} & f_0(j, \hat{\delta}) \\ \text{subject to} & f_\ell(j, \hat{\delta}) \leq 0, \ \ell = 1, \ldots, L, \end{array} \tag{A.1}$$

where $f_\ell : \{1, \ldots, J\} \times \Delta \to \mathbf{R}$, $\ell = 0, \ldots, L$, are given cost and constraint functions. Because δ is random, however, the goals of minimizing $f_0(j, \delta)$ and satisfying $f_\ell(j, \delta) \leq 0$ are ambiguous.

One approach to resolving this ambiguity is to search for a system that is optimal in the strictest sense:

$$\begin{array}{ll} \text{find} & j \in \{1, \ldots, N\} \\ \text{subject to} & \left\{ \begin{array}{l} f_0(j, \delta) = f_0^\star(\delta) \\ f_\ell(j, \delta) \leq 0, \ \ell = 1, \ldots, L \end{array} \right\} \text{ for all } \delta \in \Delta. \end{array} \tag{A.2}$$

Here $f_0^\star : \Delta \to \mathbf{R} \cup \{\infty\}$ gives the optimal value under δ,

$$f_0^\star(\delta) = \min_{j=1,\ldots,J} \{f_0(j,\delta) \mid f_\ell(j,\delta) \leq 0,\ \ell = 1,\ldots,L\}.$$

We assume that for all $\delta \in \Delta$, there exists a $j \in \{1,\ldots,J\}$ such that $f_\ell(j,\delta) \leq 0$, $\ell = 1,\ldots,L$ (so $f_0^\star(\delta) < \infty$).

Problem (A.2) is feasible only if one system is *robustly optimal*, *i.e.*, optimal under all possible uncertain influences. As a robustly optimal system is unlikely to exist in most applications, we consider the alternative of searching for a system that minimizes the worst-case optimality gap:

$$\begin{array}{ll} \text{minimize} & \tau \\ \text{subject to} & \left\{ \begin{array}{l} f_0(j,\delta) \leq f_0^\star(\delta) + \tau \\ f_\ell(j,\delta) \leq 0,\ \ell = 1,\ldots,L \end{array} \right\} \text{ for all } \delta \in \Delta. \end{array} \tag{A.3}$$

The decision variable in Problem (A.3) is $(j,\tau) \in \{1,\ldots,J\} \times \mathbf{R}$. Given a solution $(j^\star,\tau^\star)$, we say that $j^\star$ is *robustly $\tau^\star$-approximately optimal:* for any $\delta \in \Delta$, system $j^\star$ is guaranteed to be feasible and to cost at most $\tau^\star$ more than the system that is optimal under δ. If it happens that $\tau^\star = 0$, then $j^\star$ is in fact a solution to Problem (A.2), *i.e.*, $j^\star$ is robustly optimal.

Unfortunately, Problem (A.3) is intractable in general. A tractable approximation is the analogous scenario problem:

$$\begin{array}{lll} \text{minimize} & \tau & \\ \text{subject to} & f_0(j,\delta^i) \leq f_0^\star(\delta^i) + \tau,\ i = 1,\ldots,N & \\ & f_\ell(j,\delta^i) \leq 0,\ \ell = 1,\ldots,L,\ i = 1,\ldots,N. & \end{array} \tag{A.4}$$

By assumption, Problem (A.4) is feasible. We denote a solution to Problem (A.4) by $(j_N^\star, \tau_N^\star)$. Our main result is that $j_N^\star$ is $\alpha_N^\star$-*probably* $\tau_N^\star$-*approximately optimal:* with $100(1-\beta)\%$ confidence,

$$\mathbf{P}\left\{\delta \in \Delta \;\middle|\; \begin{array}{l} f_0(j_N^\star, \delta) - f_0^\star(\delta) \leq \tau_N^\star \\ f_\ell(j_N^\star, \delta) \leq 0,\ \ell = 1, \ldots, L \end{array}\right\} \geq 1 - \alpha_N^\star. \tag{A.5}$$

Here $\beta \in (0,1)$ is a user-specified confidence level. The robustness level $\alpha_N^\star$ is computed *a posteriori* and depends on the (random) structure of the feasible region of Problem (A.4). The smaller $\tau_N^\star$ and $\alpha_N^\star$, the stronger the guarantee. If it turns out that $\tau_N^\star = 0$, then we conclude with $100(1-\beta)\%$ confidence that $j_N^\star$ is $\alpha_N^\star$-*probably optimal*. The guarantee (A.5) is based on the recent theory in [150], and holds distribution-free.

Solving the scenario problem

Given $(\delta^1, \ldots, \delta^N)$, a solution $(j_N^\star, \tau_N^\star)$ to Problem (A.4) can be computed by exhaustive search as follows.

1. Feasibility screening:
   (a) Compute $f_\ell(j, \delta^i)$ for each $j = 1, \ldots, J$, $\ell = 1, \ldots, L$ and $i = 1, \ldots, N$.
   (b) Set $\mathcal{J} = \{j \in \{1, \ldots, J\} \mid f_\ell(j, \delta^i) \leq 0,\ \ell = 1, \ldots, L,\ i = 1, \ldots, N\}$.
2. Minimization:
   (a) Compute $f_0(j, \delta^i)$ for each $j \in \mathcal{J}$ and $i = 1, \ldots, N$.
   (b) Compute $f_0^\star(\delta^i) = \min_j \{f_0(j, \delta^i) \mid j \in \mathcal{J}\}$ for each $i = 1, \ldots, N$.
   (c) Compute $\tau_j = \max_i \{f_0(j, \delta^i) - f_0^\star(\delta^i) \mid i = 1, \ldots, N\}$ for each $j \in \mathcal{J}$.
   (d) Compute $\tau_N^\star = \min_j \{\tau_j \mid j \in \mathcal{J}\}$ and set $j_N^\star$ to a corresponding minimizer, using a tie-break rule if there are multiple minimizers.

This procedure is a function that takes a sample $(\delta^1, \ldots, \delta^N)$ as its input and outputs a selection $j_N^\star$ and suboptimality threshold $\tau_N^\star$. We denote this function by $\mathcal{A}_N : \Delta^N \to \{1, \ldots, J\} \times \mathbf{R}$ and write

$$(j_N^\star, \tau_N^\star) = \mathcal{A}_N(\delta^1, \ldots, \delta^N).$$

We also define functions $\mathcal{A}_m : \Delta^m \to \{1, \ldots, J\} \times \mathbf{R}$ for $m = 1, \ldots, N$. Each $\mathcal{A}_m$ implements the above procedure on a sample of cardinality m. We note that this procedure lends itself to parallel computation: only steps 1(b) and 2(c) involve coupling across scenarios.

Computing the robustness level

To compute the robustness level $\alpha_N^\star$, we must find a *support subsample*. A support subsample is a sequence of scenarios $(\delta^{i_1}, \ldots, \delta^{i_k})$ with $i_1 < \cdots < i_k$ such that $\{i_1, \ldots, i_k\} \subseteq \{1, \ldots, N\}$ and

$$\mathcal{A}_k(\delta^{i_1}, \ldots, \delta^{i_k}) = \mathcal{A}_N(\delta^1, \ldots, \delta^N).$$

In words, optimizing over a support subsample yields the same selection and suboptimality threshold as optimizing over the full sample. Given a confidence level $\beta \in (0, 1)$ and a support subsample of cardinality $s_N^\star$, a robustness level $\alpha_N^\star$ for which the guarantee (A.5) holds is given by

$$\alpha_N^\star = \begin{cases} 1 & \text{if } s_N^\star = N \\ 1 - \left[\beta \Big/ N\binom{N}{s_N^\star}\right]^{1/(N-s_N^\star)} & \text{otherwise.} \end{cases} \tag{A.6}$$

The right-hand side of (A.6) is an increasing function of $s_N^\star$. To strengthen the guarantee (A.5), therefore, we would like to find a small support subsample. The following procedure, adapted from [150], can be shown to yield an irreducible subsample (though not necessarily one of minimal cardinality).

1. Initialize $S \leftarrow (\delta^1, \ldots, \delta^N)$.

2. For $i = 1, \ldots, N$,

   (a) Set $S_i = S \setminus \delta^i$.

   (b) If $\mathcal{A}_{|S_i|}(S_i) = A_N(\delta^1, \ldots, \delta^N)$, set $S \leftarrow S_i$.

When this procedure terminates, the final sample S is an irreducible support subsample. Its cardinality $s_N^\star$ can be used in (A.6) to compute a robustness level $\alpha_N^\star$ valid in the probabilistic guarantee (A.5).

Proof of robustness guarantee

To prove that a solution $(j_N^\star, \tau_N^\star)$ to the scenario problem (A.4) comes with the probabilistic guarantee (A.5), we reduce our problem to the case studied in [150]. This involves identifying terms in [150] with corresponding terms in our problem, and verifying that the assumptions in [150] hold in our setting.

Our decision space is

$$\Theta = \{1, \ldots, J\} \times \mathbf{R}.$$

A decision $\theta \in \Theta$ is a selection and suboptimality threshold pair (j, τ). Assumption 1 of [150] associates with each $\delta \in \Delta$ a constraint set Θ_δ that contains the admissible decisions under δ. In our problem,

$$\Theta_\delta = \{\theta \in \Theta \mid f_0(\theta_1, \delta) - f_0^\star(\delta) \leq \theta_2,\ f_\ell(\theta_1, \delta) \leq 0,\ \ell = 1, \ldots, L\}.$$

It is straightforward to show that Assumption 1 of [150] holds, *i.e.*, that for $m = 1, 2, \ldots,$ applying algorithm $\mathcal{A}_m$ to a sample $(\delta^1, \ldots, \delta^m)$ returns a unique decision $\theta_m = \mathcal{A}_m(\delta^1, \ldots, \delta^m)$ such that $\theta_m \in \Theta_{\delta^i}$ for all $i = 1, \ldots, m$.

The main result in [150] involves the *violation probability*

$$V(\theta) = \mathbf{P}\left\{\delta \in \Delta \mid \theta \notin \Theta_\delta\right\}.$$

In our setting, the violation probability is the probability that $f_0(\theta_1, \delta) - f_0^\star(\delta) > \theta_2$ or $f_\ell(\theta_1, \delta) > 0$ for some $\ell \in \{1, \ldots, L\}$. The main result in [150] is that under assumption 1,

$$\mathbf{P}^N\left\{V(\theta_N^\star) > \varepsilon(s_N^\star)\right\} \leq \beta \tag{A.7}$$

for any confidence level $\beta \in (0, 1)$ and any function $\varepsilon : \{0, \ldots, N\} \to [0, 1]$ satisfying

$$\begin{aligned} &\varepsilon(N) = 1 \\ &\sum_{k=0}^{N} \binom{N}{k} (1 - \varepsilon(k))^{N-k} = \beta. \end{aligned}$$

As discussed in [150], the right-hand side of Equation (A.6) (viewed as a function of k rather than $s_N^\star$) satisfies this condition. Therefore, the general guarantee (A.7) holds in our setting. Expanding this guarantee, we conclude with $100(1-\beta)\%$ confidence (with respect to $\mathbf{P}^N$) that

$$\mathbf{P}\left\{\delta \in \Delta \mid \theta_N^\star \notin \Theta_\delta\right\} < \alpha_N^\star,$$

or, equivalently, that

$$\mathbf{P}\left\{\delta \in \Delta \;\middle|\; \begin{array}{l} f_0((\theta_N^\star)_1, \delta) - f_0^\star(\delta) \leq (\theta_N^\star)_2 \\ f_\ell((\theta_N^\star)_1, \delta) \leq 0, \;\; \ell = 1, \ldots, L \end{array}\right\} \geq 1 - \alpha_N^\star.$$

This is our robustness guarantee (A.5).

Appendix B

Discussion of input data and sources

In this appendix, we qualitatively assess the fidelity of the input data used in this thesis. We also discuss the distributional assumptions and their potential influence on our results.

Data fidelity

To support the simulations and model-fitting in this thesis, we tried to use datasets that were as large and as high-fidelity as possible. Relative to studies on similar topics in competitive, peer-reviewed journals such as *IEEE Transactions on Power Systems* and *IEEE Transactions on Smart Grid*, we believe our datasets were of high quality. That's not to say there weren't data limitations – there were, as we discuss below – just that the overall data quality were high relative to the research state of the art.

We used data from five of tiers of sources, in descending order of fidelity:

1. real data from independent sources,
2. real data from potentially biased sources (e.g. manufacturer-reported heat pump data),
3. simulated data,
4. conversations with industry experts, and

5. comments from homeowners and practitioners on various websites (primarily the forums on greenbuildingadvisor.com).

The input data used in this thesis can be broadly categorized as follows.

- Weather: Tier 1.
- Energy and ancillary service prices: Tier 1.
- Thermal load: Tier 3 (with simulation inputs based on a Tier 1 source).
- Heat pump performance: a mix of Tiers 1 and 2.
- Heat pump capital and maintenance costs: limited Tier 1, mostly Tiers 4-5.

To capture statistical dependencies between weather and prices, we needed those datasets to be coincident in both space and time. The limiting factor was PJM's ancillary service prices, for which six years of hourly data were available. This limitation fixed the size of the weather and thermal load datasets at $6 \times 8760 = 52560$ hours. When we needed more than six years of data, we resampled with replacement from the six-year dataset. We chose the location of Philadelphia because its electricity and gas prices and heating/cooling degree days are close to the national averages, because historical weather data from a reputable source (the meteorology department of Pennsylvania State University) were available, and because Philadelphia is in PJM. We focused on PJM because PJM is the biggest Independent Service Operator in the United States and has demand-friendly ancillary service market rules.

We generated hourly thermal load data by propagating weather data through RC network models. We tuned the RC parameters to annual thermal load intensity ($\mathrm{kWh/m^2/year}$) data from the United States Department of Energy's Residential Energy Consumption Survey (Tier 1). The tuning process is described in §3.2.6. Because this survey specified only population means, and provided no further distributional information, we assumed uniform

distributions over plausible ranges of values around the means (*e.g.*, ±20%). We also randomized the floor area of the simulated space loads using a uniform distribution. The annual load (kWh/year) was the product of the annual load intensity (kWh/m^2/year) and the floor area (m^2), so was not uniformly distributed. Samples drawn from that distribution were used as inputs to the RC parameter tuning. The tuning involved nonlinear transformations, so the distributions of the RC parameters were highly nonuniform, as were the hourly thermal load data.

The heat pump performance data were based on a mix of third-party laboratory data and manufacturer-reported lab data for a popular line of cold-climate air-source heat pumps. We would have preferred to use only third-party heat pump performance data, but that data is extremely limited. In our opinion, the only currently feasible way to fit a good heat pump model to empirical data that does not come from a manufacturer is to buy a heat pump, instrument it, and measure its capacity and COP under a wide variety of boundary conditions in one's own lab. We did, however, draw on a 2011 NREL report of lab testing of the same heat pump line. That study found good agreement between their independent laboratory measurements and the manufacturer-reported data.

The heat pump costs were the weakest input data. We had a hard time pinning these data down with any precision, as costs vary from market to market, year to year, and installer to installer. Installers appear to charge what the market will bear, rather than (say) their internal costs plus a fixed profit margin. Also, contractors seem reluctant to share those data, presumably for reasons related to competition and profit. We modeled the uncertainty in these parameters through uniform distributions with wide support (*e.g.*, $4-6000 for the all-in installed cost of a one-ton mini-split). We based those ranges on Internet sources (Tier 5), on installers' quotes (Tier 2), and on conversations with industry experts (Tier 4). We freely acknowledge that there was a lot of uncertainty in the cost data, and that the distributions essentially represent our (and the industry experts') prior beliefs, rather than

empirical data.

Distributional assumptions

In the stochastic simulations in this thesis, we tried to use historical data wherever possible. When we had insufficient historical data, at times we resampled with replacement from the historical data.

We assumed uniform distributions on numerous parameters in the numerical examples in Chapter 2. We don't claim that those examples accurately reflect reality; we included them mainly to illustrate the analytical results in that chapter. Compared to Chapters 3–5, the analysis in Chapter 2 was simplified; our intention in Chapter 2 was to introduce the basic parameters and relationships without too much notational or conceptual overhead. The other places we used uniform distributions were mentioned above: annual load intensities, floor areas and heat pump costs. Uniform distributions are a common modeling instrument in situations where full distributional information is not available, but plausible supports are.

The load data used in scenario optimization in Chapters 4–5 were not uniformly distributed. While the load data were based on primal uncertain parameters drawn from uniform distributions, those data were propagated through many transformations, generally nonlinear. The only uniformly-distributed parameters used directly in scenario optimization were the heat pump capital and maintenance costs in Chapter 4.

Mis-specified cost distributions could influence net present value estimates and bias heat pump selection decisions. In practice, however, the scenario-based selection algorithm in Chapter 4 would most likely be implemented by a heat pump installer, who should have a clear idea of their relevant cost parameters. They could likely use historical data from their past installations, either directly or by way of a statistical model. For this reason,

we do not currently see a clear role for distributionally-robust optimization in the selection problem. Also, that problem is nonconvex and chance-constrained, and we are not aware of any distributionally-robust methods for such problems. Distributionally-robust optimization does appear to be an appropriate solution method for the day-ahead capacity offer decision problem that we formulated in Chapter 5, however. We discuss this in detail in §5.3.7.

Bibliography

1. Edenhofer, O. *et al. Climate Change 2014: Mitigation of Climate Change. Working Group III Contribution to the Fifth Assessment Report of the Intergovernmental Panel on Climate Change* tech. rep. (Cambridge University Press, 2014).

2. Dean, B., Dulac, J., Petrichenko, K. & Graham, P. *Towards zero-emission efficient and resilient buildings: Global Status Report* tech. rep. (United Nations Environment Programme Global Alliance for Buildings and Construction, 2016).

3. *International Energy Outlook* tech. rep. (U.S. Energy Information Agency, 2017).

4. Urge-Vorsatz, D., Cabeza, L., Serrano, S., Barreneche, C. & Petrichenko, K. Heating and cooling energy trends and drivers in buildings. *Renewable and Sustainable Energy Reviews* **41** (2015).

5. Williams, J. *et al. Pathways to deep decarbonization in the United States* tech. rep. (Sustainable Development Solutions Network and the Institute for Sustainable Development and International Relations, 2014).

6. Steinberg, D. *et al. Electrification and Decarbonization: Exploring US Energy Use and Greenhouse Gas Emissions in Scenarios with Widespread Electrification and Power Sector Decarbonization* tech. rep. NREL/TP-6A20-68214 (National Renewable Energy Laboratory, 2017).

7. Chua, K., Chou, S. & Yang, W. Advances in heat pump systems: A review. *Applied energy* **87,** 3611–3624 (2010).

8. Fischer, D. & Madani, H. On heat pumps in smart grids: A review. *Renewable and Sustainable Energy Reviews* **70,** 342–357 (2017).

9. Northeast Energy Efficiency Partnerships. *Cold climate air-source heat pump specification & product list*

10. Ang, B. & Su, B. Carbon emission intensity in electricity production: A global analysis. *Energy Policy,* 56–63 (2016).

11. Billimoria, S., Guccione, L., Henchen, M. & Louis-Prescott, L. *The Economics of Electrifying Buildings* tech. rep. (Rocky Mountain Institute, 2018).

12. Brockway, A. & Delforge, P. Emissions reduction potential from electric heat pumps in California homes. *The Electricity Journal* **31,** 44–53 (2018).

13. Bergman, N. Why is renewable heat in the UK underperforming? A socio-technical perspective. *Proceedings of the Institution of Mechanical Engineers, Part A: Journal of Power and Energy* **227,** 124–131 (2013).

14. *Energy Measurement and Verification: Ductless Heat Pumps* tech. rep. (Northeast Energy Efficiency Partnerships, 2014).

15. Snape, J., Boait, P. & Rylatt, R. Will domestic consumers take up the renewable heat incentive? An analysis of the barriers to heat pump adoption using agent-based modelling. *Energy Policy* **85,** 32–38 (2015).

16. Hlavinka, A., Mjelde, J., Dharmasena, S. & Holland, C. Forecasting the adoption of residential ductless heat pumps. *Energy Economics* **54,** 60–67 (2016).

17. Lee, H., Wang, J., Walker, R. & Horkitz, K. *Northwest Ductless Heat Pump Initiative: Market Progress Evaluation* tech. rep. E18-374 (Northwest Energy Efficiency Alliance, 2018).

18. *Tigi Solar: Heat Purchase Agreements* July 2018. http://www.tigisolar.com/heat-purchase-agreement.html.

19. *Aqualor Energi: Heat Purchase Agreements* July 2018.

20. *SHARC Energy: Wastewater Heat Recovery* July 2018. http://www.sewageheatrecovery.com/wp-content/uploads/2016/04/IWS-corp-pres.-april-15-public.pdf.

21. Agrell, P. & Bogetoft, P. Economic and environmental efficiency of district heating plants. *Energy Policy* **33,** 1351–1362 (2005).

22. Henning, D., Amiri, S. & Holmgren, K. Modelling and optimisation of electricity, steam and district heating production for a local Swedish utility. *European Journal of Operational Research* **175,** 1224–1247 (2006).

23. Davidson, C., Steinberg, D. & Margolis, R. Exploring the market for third-party-owned residential photovoltaic systems: insights from lease and power-purchase agreement contract structures and costs in California. *Environmental Research Letters* **10** (2015).

24. Rai, V., Reeves, D. & Margolis, R. Overcoming barriers and uncertainties in the adoption of residential solar PV. *Renewable Energy* **89,** 498–505 (2016).

25. Goldberg, M., Cliburn, J. & Coughlin, J. *Economic impacts from the Boulder County, Colorado, ClimateSmart Loan program: using property-assessed clean energy (PACE) financing.* tech. rep. NREL/TP-7A20-52231 (National Renewable Energy Laboratory, 2011).

26. Kirkpatrick, A. & Bennear, L. Promoting clean energy investment: An empirical analysis of property assessed clean energy. *Journal of Environmental Economics and Management* **68,** 357–375 (2014).

27. Ameli, N., Pisu, M. & Kammen, D. Can the US keep the PACE? A natural experiment in accelerating the growth of solar electricity. *Applied Energy* **191,** 163–169 (2017).

28. 2019. https://www.solartompkins.org/overview.html.

29. Sorensen, P. *et al.* Power fluctuations from large wind farms. *IEEE Transactions on Power Systems* **22,** 958–965 (2007).

30. Makarov, Y., Loutan, C., Ma, J. & De Mello, P. Operational impacts of wind generation on California power systems. *IEEE Transactions on Power Systems* **24,** 1039–1050 (2009).

31. Halamay, D., Brekken, T., Simmons, A. & McArthur, S. Reserve requirement impacts of large-scale integration of wind, solar, and ocean wave power generation. *IEEE Transactions on Sustainable Energy* **2,** 321–328 (2011).

32. Lund, P., Lindgren, J., Mikkola, J. & Salpakari, J. Review of energy system flexibility measures to enable high levels of variable renewable electricity. *Renewable and Sustainable Energy Reviews* **45,** 785–807 (2015).

33. Kirby, B. *Ancillary Services: Technical and Commercial Insights* tech. rep. (2007).

34. Zhou, Z., Levin, T. & Conzelmann, G. *Survey of US ancillary services markets* tech. rep. ANL/ESD-16/1 (Argonne National Lab, Argonne, IL, 2016).

35. Huang, K. & Huang, Y. Integrating direct load control with interruptible load management to provide instantaneous reserves for ancillary services. *IEEE Transactions on Power Systems* **19,** 1626–1634 (2004).

36. Callaway, D. & Hiskens, I. Achieving controllability of electric loads. *Proceedings of the IEEE* **99,** 184–199 (2011).

37. Mathieu, J., Koch, S. & Callaway, D. State estimation and control of electric loads to manage real-time energy imbalance. *IEEE Transactions on Power Systems* **28.1,** 430–440 (2013).

38. Hao, H., Lin, Y., Kowli, A., Barooah, P. & Meyn, S. Ancillary service to the grid through control of fans in commercial building HVAC systems. *IEEE Transactions on Smart Grid* **5,** 2066–2074 (2014).

39. Lin, Y., Barooah, P., Meyn, S. & Middelkoop, T. Experimental evaluation of frequency regulation from commercial building HVAC systems. *IEEE Transactions on Smart Grid* **6,** 776–783 (2015).

40. Vrettos, E., Kara, E., MacDonald, J., Andersson, G. & Callaway, D. Experimental demonstration of frequency regulation by commercial buildings—Part I: Modeling and hierarchical control design. *IEEE Transactions on Smart Grid* **9,** 3213–23 (2018).

41. Vrettos, E., Kara, E., MacDonald, J., Andersson, G. & Callaway, D. Experimental demonstration of frequency regulation by commercial buildings—Part II: results and performance evaluation. *IEEE Transactions on Smart Grid* **9,** 3224–34 (2018).

42. Su, L. & Norford, L. Demonstration of HVAC chiller control for power grid frequency regulation—Part 1: Controller development and experimental results. *Science and Technology for the Built Environment* **21,** 1134–1142 (2015).

43. Su, L. & Norford, L. Demonstration of HVAC chiller control for power grid frequency regulation—Part 2: Discussion of results and considerations for broader deployment. *Science and Technology for the Built Environment* **21,** 1143–1153 (2015).

44. Kim, Y., Norford, L. & Kirtley, J. Modeling and analysis of a variable speed heat pump for frequency regulation through direct load control. *IEEE Transactions on Power Systems* **30,** 397–408 (2015).

45. Kim, Y., Fuentes, E. & Norford, L. Experimental study of grid frequency regulation ancillary service of a variable speed heat pump. *IEEE Transactions on Power Systems* **31,** 3090–3099 (2016).

46. Cai, J. & Braun, J. Laboratory-based assessment of HVAC equipment for power grid frequency regulation: Methods, regulation performance, economics, indoor comfort and energy efficiency. *Energy and Buildings* **185,** 148–161 (2019).

47. Cai, J. & Braun, J. A regulation capacity reset strategy for HVAC frequency regulation control. *Energy and Buildings* **185,** 272–286 (2019).

48. *Efficient electric use* tech. rep. (Electric Power Research Institute, Apr. 1976).

49. Isaksen, L., Ma, F., Simons, N. & Gellings, C. Bibliography on load management. *IEEE Transactions on Power Apparatus and Systems* **100,** 2597–2601 (1981).

50. Gellings, C. Demand-side load management. *IEEE spectrum* **18,** 49–52 (1981).

51. Fiske, G., Law, E. & Seeto, D. The economic analysis of load management: the case of cycling residential air conditioners. *IEEE Transactions on Power Apparatus and Systems* **12,** 4725–4732 (1981).

52. Gellings, C. The concept of demand-side management for electric utilities. *Proceedings of the IEEE* **73,** 1468–1470 (1985).

53. Runnels, J. & Whyte, M. Evaluation of demand-side management. *Proceedings of the IEEE* **73,** 1489–1495 (1985).

54. Eto, J. *The past, present, and future of US utility demand-side management programs* tech. rep. LBNL-39931 (Lawrence Berkeley National Laboratory, 1996).

55. Albadi, M. & El-Saadany, E. *Demand response in electricity markets: An overview* in *IEEE Power Engineering Society General Meeting* (2007), 1–5.

56. Strbac, G. Demand side management: Benefits and challenges. *Energy policy* **36,** 4419–4426 (2008).

57. Shariatzadeh, F., Mandal, P. & Srivastava, A. Demand response for sustainable energy systems: A review, application and implementation strategy. *Renewable and Sustainable Energy Reviews* **45,** 343–350 (2015).

58. Hirsh, R. *Power loss: The origins of deregulation and restructuring in the American electric utility system* (MIT Press, 1999).

59. 102nd Congress of the United States of America. *Energy Policy Act* 1992.

60. Federal Energy Regulatory Commission. *Promoting Wholesale Competition Through Open Access Non-discriminatory Transmission Services by Public Utilities: Recovery of Stranded Costs by Public Utilities and Transmitting Utilities* Order No. 888. 1996.

61. Boisvert, R., Cappers, P. & Neenan, B. The benefits of customer participation in wholesale electricity markets. *The Electricity Journal* **15,** 41–51 (2002).

62. Kirschen, D. Demand-side view of electricity markets. *IEEE Transactions on Power Systems* **18,** 520–527 (2003).

63. Kirby, B. *Load response fundamentally matches power system reliability requirements* in *IEEE Power Engineering Society General Meeting* (2007).

64. Ramanathan, B. & Vittal, V. A framework for evaluation of advanced direct load control with minimum disruption. *IEEE Transactions on Power Systems* **23,** 1681–1688 (2008).

65. Callaway, D. Tapping the energy storage potential in electric loads to deliver load following and regulation, with application to wind energy. *Energy Conversion and Management* **50,** 1389–1400 (2009).

66. Zhang, W., Lian, J., Chang, C. & Kalsi, K. Aggregated Modeling and Control of Air Conditioning Loads for Demand Response. *IEEE Transactions on Power Systems* **28,** 4655–4664 (2013).

67. Hao, H., Sanandaji, B., Poolla, K. & Vincent, T. Aggregate flexibility of thermostatically controlled loads. *IEEE Transactions on Power Systems* **30,** 189–198 (2015).

68. Mathieu, J., Dyson, M. & Callaway, D. Resource and revenue potential of California residential load participation in ancillary services. *Energy Policy,* 76–87 (2015).

69. Mathieu, J., Kamgarpour, M., Lygeros, J., Andersson, G. & Callaway, D. Arbitraging intraday wholesale energy market prices with aggregations of thermostatic loads. *IEEE Transactions on Power Systems* **30,** 763–772 (2015).

70. Tindemans, S., Trovato, V. & Strbac, G. Decentralized control of thermostatic loads for flexible demand response. *IEEE Transactions on Control Systems Technology* **23,** 1685–1700 (2015).

71. Zhao, P., Henze, G., Plamp, S. & Cushing, V. Zhao, P., Henze, G.P., Plamp, S. and Cushing, V.J., 2013. Evaluation of commercial building HVAC systems as frequency regulation providers. *Energy and Buildings* (2013).

72. Pavlak, G., Henze, G. & Cushing, V. Optimizing commercial building participation in energy and ancillary service markets. *Energy and Buildings* **81,** 115–126 (2014).

73. Beil, I., Hiskens, I. & Backhaus, S. Frequency regulation from commercial building HVAC demand response. *Proceedings of the IEEE* **104,** 745–757 (2016).

74. Fabietti, L. *et al.* Experimental implementation of frequency regulation services using commercial buildings. *IEEE Transactions on Smart Grid* **9,** 1657–1666 (2017).

75. Nicolosi, M. Wind power integration and power system flexibility–An empirical analysis of extreme events in Germany under the new negative price regime. *Energy Policy* **38,** 7257–7268 (2010).

76. Cludius, J., Hermann, H., Matthes, F. & Graichen, V. The merit order effect of wind and photovoltaic electricity generation in Germany 2008–2016: Estimation and distributional implications. *Energy Economics* **44,** 302–313 (2014).

77. Potomac Economics. *State of the Market report for the ERCOT Electricity Markets* tech. rep. (Electric Reliability Council of Texas, 2016).

78. Harley, B. *Performance of Ductless Heat Pumps in the Northeast* tech. rep. (Northeast Sustainable Energy Association, 2014).

79. Ueno, K. & Loomis, H. *Long-Term Monitoring of Mini-Split Ductless Heat Pumps in the Northeast* tech. rep. DOE/GO-102015-4529 (National Renewable Energy Laboratory, 2015).

80. Korn, D. *et al. Ductless Mini-Split Heat Pump Impact Evaluation* tech. rep. (Electric, Gas Program Administrators of Massachusetts, and Rhode Island, 2016).

81. Hendron, R. & Engebrecht, C. *Building America house simulation protocols* tech. rep. DOE/GO-102010-3141 (U.S. Department of Energy Office of Energy Efficiency and Renewable Energy, 2010).

82. Jump, D., Walker, I. & Modera, M. *Field measurements of efficiency and duct retrofit effectiveness in residential forced air distribution systems* in *ACEEE Summer Study on Energy Efficiency in Buildings* (Pacific Grove, CA, 1996).

83. *How much carbon dioxide is produced when different fuels are burned?* tech. rep. (U.S. Energy Information Agency, 2018). https://www.eia.gov/tools/faqs/faq.php?id=73&t=11.

84. *Inventory of U.S. Greenhouse Gas Emissions and Sinks: 1990-2016* tech. rep. (U.S. Environmental Protection Agency, 2018).

85. Energy Information Administration. *Residential Energy Consumption Survey* tech. rep. (U.S. Department of Energy, 2015).

86. *Electric Power Annual* tech. rep. (U.S. Energy Information Agency, 2016).

87. *State Electricity Profiles* tech. rep. (U.S. Energy Information Agency, 2018).

88. *State Residential Fuel Prices* tech. rep. (U.S. Energy Information Agency, 2018).

89. Morgan M.G.and Henrion, M. & Small, M. *Uncertainty: a guide to dealing with uncertainty in quantitative risk and policy analysis* (Cambridge University Press, 1992).

90. Baechler, M. *et al. Building America Best Practices Series: Guide to Determining Climate Regions by County* tech. rep. PNNL-17211 (Pacific Northwest National Laboratory, 2010).

91. Grassi, W. *Heat Pumps: Fundamentals and Applications.* (Springer, 2017).

92. Mitsubishi Electric Cooling & Heating. *FH Hyper-Heat Series specifications, mylinkdrive.com* (2019).

93. Winkler, J. *Laboratory test report for Fujitsu 12RLS and Mitsubishi FE12NA mini-split heat pumps* tech. rep. (National Renewable Energy Laboratory, 2011).

94. Williamson, J. & Aldrich, R. *Field Performance of Inverter-Driven Heat Pumps in Cold Climates* tech. rep. DOE/GO-102015-4642 (National Renewable Energy Laboratory, 2015).

95. Bukac, H. *Modeling Capacity and Coefficient of Performance of a Refrigeration Compressor* in *International Compressor Engineering Conference* (2004).

96. Verhelst, C., Logist, F., Van Impe, J. & Helsen, L. Study of the optimal control problem formulation for modulating air-to-water heat pumps connected to a residential floor heating system. *Energy and Buildings* **45,** 43–53 (2012).

97. Bloess, A., Schill, W. & Zerrahn, A. Power-to-heat for renewable energy integration: A review of technologies, modeling approaches, and flexibility potentials. *Applied Energy* **212,** 1611–1626 (2018).

98. Lee, Z., Gupta, K., Kircher, K. & Zhang, K. Mixed-integer model predictive control of variable-speed heat pumps. *Energy and Buildings* **198,** 75–83 (2019).

99. Hao, H., Sanandaji, B., Poolla, K. & Vincent, T. Potentials and economics of residential thermal loads providing regulation reserve. *Energy Policy* **79,** 115–126 (2015).

100. Vrettos, E., Oldewurtel, F. & Andersson, G. Robust energy-constrained frequency reserves from aggregations of commercial buildings. *IEEE Transactions on Power Systems* **31,** 4272–4285 (2016).

101. Vrettos, E. & Andersson, G. Scheduling and provision of secondary frequency reserves by aggregations of commercial buildings. *IEEE Transactions on Sustainable Energy* **7,** 850–864 (2016).

102. Rey, F. *et al.* Strengthening the group: Aggregated frequency reserve bidding with ADMM. *IEEE Transactions on Smart Grid* **10,** 850–864 (2019).

103. Zakula, T., Armstrong, P. & Norford, L. Modeling environment for model predictive control of buildings. *Energy and Buildings* **85,** 549–559 (2014).

104. Shao, S., Shi, W., Li, X. & Chen, H. Performance representation of variable-speed compressor for inverter air conditioners based on experimental data. *International Journal of Refrigeration* **27,** 805–815 (2004).

105. Rencher, A. & Schaalje, G. *Linear models in statistics.* (John Wiley & Sons, Inc., 2008).

106. Davies, M. *Building heat transfer* (Wiley, 2004).

107. Underwood, C. P. & Yik, F. W. H. *Modeling Methods for Energy in Buildings* (Blackwell Publishing, 2004).

108. Li, X. & Wen, J. Review of building energy modeling for control and operation. *Renewable and Sustainable Energy Reviews* **37,** 517–537 (2014).

109. Harish, V. & Kumar, A. A review on modeling and simulation of building energy systems. *Renewable and Sustainable Energy Reviews* **56,** 1272–1292 (2016).

110. Crawley, D. *et al.* EnergyPlus: creating a new-generation building energy simulation program. *Energy and Buildings* **33,** 319–331 (2001).

111. Klein, S. *et al. TRNSYS 16 - A TRaNsient system simulation program, user manual* Solar Energy Laboratory, University of Wisconsin-Madison (Madison, Wisconsin, 2004).

112. Radecki, P. & Hencey, B. *Online building thermal parameter estimation via unscented Kalman filtering* in *American Control Conference* (2012), 3056–3062.

113. Lin, Y., Middelkoop, T. & Barooah, P. *Issues in identification of control-oriented thermal models of zones in multi-zone buildings* in *Conference on Decision and Control* (2012).

114. Oldewurtel, F. *et al.* Use of model predictive control and weather forecasts for energy efficient building climate control. *Energy and Buildings* **45,** 15–27 (2012).

115. Sturzenegger, D. *et al. Model Predictive Control of a Swiss Office Building* in *11th RHEVA World Congress Clima* (2013).

116. Radecki, P. & Hencey, B. *Online thermal estimation, control, and self-excitation of buildings* in *Conference on Decision and Control* (2013), 4802–4807.

117. Dobbs, J. & Hencey, B. Model Predictive HVAC Control with Online Occupancy Model. *Energy and Buildings* **82,** 675–684 (2014).

118. Laret, L. *Etude du regime transitoire de locaux d'habitation. Modelisation par des systemes d'equations differentielles ordinaires* PhD thesis (L'Universite de Liege, Belgium, 1975).

119. Hachem, B., Laret, L. & Nusgens, P. *Heat exchange under non steady state conditions - application to intermittent heating* in *6th International Congress CLIMA 2000, Milan, Italy.* (1975).

120. Sonderegger, R. *Dynamic models of house heating based on equivalent thermal parameters* PhD thesis (Princeton University, Princeton, NJ, 1978).

121. Laret, L. *Modelisation du comportement transitoire de locaux climatises, par des systemes differentiels lineaires* in *3rd Symposium International sur L'Informatique Appliquee au Batiment, Banff, Canada* (1978), 10–12.

122. Lebrun, J. Etudes experimentales des regimes transitoires en chambres climatiques - ajustment des modeles de calcul. *Journees Bilan et Perspective Genie Civil,* 18–19 (1978).

123. Laret, L. *Use of general models with a small number of parameters* in *7th International Congress CLIMA 2000, Budapest, Hungary* (1980), 263–275.

124. Lorenz, F. & Masy, G. *Methode d'evaluation de l'economie d'energie apportee par l'intermittence de chauffage dans les batiments* Traitement par differences finies d'un model a deux constantes de temps GM820130-01 (University de Liege, Liege, Belgium, 1982).

125. Crabb, J., Murdoch, N. & Penman, J. M. A simplified thermal response model. *Building Services Engineering Research & Technology* **8.1,** 13–19 (1987).

126. Penman, J. M. Second order system identification in the thermal response of a working school. *Building and Environment* **25,** 105–110 (1990).

127. Coley, D. & Penman, J. Second order system identification in the thermal response of real buildings. Paper II: recursive formulation for on-line building energy management and control. *Building and Environment* **27,** 269–277 (1992).

128. Dewson, T., Day, B. & Irving, A. Least squares parameter estimation of a reduced order thermal model of an experimental building. *Building and Environment* **28,** 127–137 (1993).

129. Coley, D. & Penman, J. M. Simplified thermal response modelling in building energy management. Paper III: demonstration of a working controller. *Building and Environment* **31,** 93–97 (1996).

130. Balan, R., Cooper, J., Chao, K., Stan, S. & Donca, R. Parameter identification and model based predictive control of temperature inside a house. *Energy and Buildings* **43,** 748–758 (2011).

131. Lee, D., Lee, S., Karava, P. & Hu, J. *Simulation-Based Approximate Policy Gradient and Its Building Control Application* tech. rep. (Purdue University, 2018).

132. Liu, M. & Shi, Y. Model predictive control of aggregated heterogeneous second-order thermostatically controlled loads for ancillary services. *IEEE Transactions on Power Systems* **31,** 1963–1971 (2016).

133. Kramer, R., van Schijndel, J. & Schellen, H. Simplified thermal and hygric building models: a literature review. *Frontiers of Architectural Research* **1,** 318–325 (2012).

134. Dorsett, D. *Out with the old, in with the new: A 15-minute way to calculate design heating load when sizing replacement equipment* (2016).

135. Kneifel, J. *Prototype Residential Building Designs for Energy and Sustainability Assessment* tech. rep. (National Institute of Standards and Technology, 2012).

136. Mariethoz, S. & Morari, M. *Modelling and hierarchical hybrid optimal control of prosumers for improved integration of renewable energy sources into the grid* in *American Control Conference* (2012), 3114–3119.

137. Kim, Y., Blum, D., Xu, N., Su, L. & Norford, L. Technologies and magnitude of ancillary services provided by commercial buildings. *Proceedings of the IEEE* **104,** 758–779 (2016).

138. *Guide to Sizing & Selecting Air-Source Heat Pumps in Cold Climates* tech. rep. (Northeast Energy Efficiency Partnerships, 2018).

139. *Air Source Heat Pump & Smart Controls Initiative Overview* tech. rep. (Northeast Energy Efficiency Partnerships, 2019).

140. Rutkowski, H. *Manual J: Residential Load Calculation* 8th ed. Air Conditioning Contractors of America (2016).

141. *Manual S: Residential Equipment Selection* 2nd ed. Air Conditioning Contractors of America (2015).

142. Hedegaard, K. & Balyk, O. Energy system investment model incorporating heat pumps with thermal storage in buildings and buffer tanks. *Energy* **63,** 356–365 (2013).

143. Bagarella, G., Lazzarin, R. & Noro, M. Sizing strategy of on–off and modulating heat pump systems based on annual energy analysis. *International Journal of Refrigeration* **65,** 183–193 (2016).

144. Fischer, D., Lindberg, K., Madani, H. & Wittwer, C. Impact of PV and variable prices on optimal system sizing for heat pumps and thermal storage. *Energy and Buildings* **128,** 723–733 (2016).

145. Patteeuw, D. & Helsen, L. Combined design and control optimization of residential heating systems in a smart-grid context. *Energy and Buildings* **133,** 640–657 (2016).

146. Beck, T., Kondziella, H., Huard, G. & Bruckner, T. Optimal operation, configuration and sizing of generation and storage technologies for residential heat pump systems in the spotlight of self-consumption of photovoltaic electricity. *Applied Energy* **188,** 604–619 (2017).

147. Dongellini, M., Naldi, C. & Morini, G. Sizing effects on the energy performance of reversible air-source heat pumps for office buildings. *Applied Thermal Engineering* **114,** 1073–1081 (2017).

148. Zhang, Q., Zhang, L., Nie, J. & Li, Y. Techno-economic analysis of air source heat pump applied for space heating in northern China. *Applied Energy* **207,** 533–542 (2017).

149. Kim, S. & Nelson, B. *Recent advances in ranking and selection* in *Winter Simulation Conference* (2007), 162–172.

150. Campi, M., Garatti, S. & Ramponi, F. A General Scenario Theory for Nonconvex Optimization and Decision Making. *IEEE Transactions on Automatic Control* **63,** 4067–4078 (2018).

151. Bechhofer, R. A single-sample multiple decision procedure for ranking means of normal populations with known variances. *The Annals of Mathematical Statistics,* 16–39 (1954).

152. Gupta, S. *On a decision rule for a problem in ranking means* PhD thesis (University of North Carolina, Chapel Hill, NC, 1956).

153. Rinott, Y. On two-stage selection procedures and related probability-inequalities. *Communications in Statistics – Theory and methods* **7,** 799–811 (1978).

154. Chen, C. A lower bound for the correct subset-selection probability and its application to discrete-event system simulations. *IEEE Transactions on Automatic Control* **41,** 1227–1231 (1996).

155. Nelson, B., Swann, J., Goldsman, D. & Song, W. Simple procedures for selecting the best simulated system when the number of alternatives is large. *Operations Research* **49,** 950–963 (2001).

156. Chick, S. & Inoue, K. New two-stage and sequential procedures for selecting the best simulated system. *Operations Research* **49,** 732–743 (2001).

157. Boesel, J., Nelson, B. & Kim, S. Using ranking and selection to "clean up" after simulation optimization. *Operations Research* **51,** 814–825 (2003).

158. Kim, S. & Nelson, B. On the asymptotic validity of fully sequential selection procedures for steady-state simulation. *Operations Research* **54,** 475–488 (2006).

159. Andradottir, S. & Kim, S. Fully sequential procedures for comparing constrained systems via simulation. *Naval Research Logistics* **57,** 403–421 (2010).

160. Healey, C., Andradottir, S. & Kim, S. Selection Procedures for Simulations with Multiple Constraints under Independent and Correlated Sampling. *ACM Transactions on Modeling and Computer Simulation* **24,** 14 (2014).

161. Hong, L., Luo, J. & Nelson, B. Chance Constrained Selection of the Best. *INFORMS Journal on Computing* **27,** 317–334 (2015).

162. Monks, T. & Currie, C. *Practical considerations in selecting the best set of simulated systems* in *Proceedings of the 2018 Winter Simulation Conference* (2018), 2191–2200.

163. Szechtman, R. in (eds Henderson, S. G. & Nelson, B.) chap. A Hilbert space approach to variance reduction (Elsevier, 2006).

164. Eckman, D. *Reconsidering ranking-and-selection guarantees* PhD thesis (Cornell University, Ithaca, NY, 2019).

165. *International Building Code* International Code Council, Inc. (Washington, DC, 2012).

166. *International Energy Conservation Code* International Code Council, Inc. (Washington, DC, 2018).

167. *The Pennsylvania State Climatologist* (2019).

168. *Electric Service Tarriff* PECO Energy Company (2301 Market Street, Philadelphia, PA, 2019).

169. Forward Market Operations. *Energy & Ancillary Services Market Operations* PJM (Apr. 2019).

170. PJM Interconnection. *PJM Data Miner 2* (2019).

171. Burdick, A. *Strategy Guideline. Accurate Heating and Cooling Load Calculations* tech. rep. (U.S. Department of Energy Office of Energy Efficiency and Renewable Energy, 2011).

172. Kirby, B., Kueck, J., Laughner, T. & Morris, K. Spinning reserve from hotel load response. *The Electricity Journal* **21,** 59–66 (2008).

173. Kinjyo, Y., Palmer, M., Yona, A. & Senjyu, T. *Autonomous power system control by decentralized controllable loads* in *IEEE Conference on Power Electronics and Drive Systems* (2013), 881–886.

174. Bhattarai, B., Bak-Jensen, B., Pillai, J. & Maier, M. *Demand flexibility from residential heat pump* in *IEEE PES General Meeting* (2014), 1–5.

175. Palacio, S., Kircher, K. J. & Zhang, K. M. On the feasibility of providing power system spinning reserves from thermal storage. *Energy and Buildings* **104,** 131–138 (2015).

176. Ledva, G., Vrettos, E., Mastellone, S., Andersson, G. & Mathieu, J. *Applying networked estimation and control algorithms to address communication bandwidth limitations and latencies in demand response* in *48th Hawaii International Conference on System Sciences* (2015), 2645–2654.

177. Douglass, P., Garcia-Valle, R., Nyeng, P., Ostergaard, J. & Togeby, M. Smart demand for frequency regulation: Experimental results. *Smart Grid, IEEE Transactions on* **4,** 1713–1720 (2013).

178. Lakshmanan, V., Marinelli, M., Hu, J. & Bindner, H. Provision of secondary frequency control via demand response activation on thermostatically controlled loads: Solutions and experiences from Denmark. *Applied Energy* **173,** 470–480 (2016).

179. PJM Interconnection. *Markets & Operations: Ancillary Services* (2019).

180. Maasoumy, M., Rosenberg, C., Sangiovanni-Vincentelli, A. & Callaway, D. *Model predictive control approach to online computation of demand-side flexibility of commercial buildings HVAC systems for supply following* in *American Control Conference (ACC)* (2014), 1082–1089.

181. Lin, Y., Barooah, P. & Mathieu, J. Ancillary Services Through Demand Scheduling and Control of Commercial Buildings. *IEEE Transactions on Power Systems* **32,** 186–197 (2017).

182. Boyd, S., Parikh, N., Chu, E., Peleato, B. & Eckstein, J. Distributed optimization and statistical learning via the alternating direction method of multipliers. *Foundations and Trends in Machine Learning* **3,** 1–122 (2011).

183. Campi, M. & Garatti, S. The exact feasibility of randomized solutions of uncertain convex programs. *SIAM Journal on Optimization* **19,** 1211–1230 (2008).

184. Calafiore, G. Random convex programs. *SIAM Journal on Optimization* **20,** 3427–3464 (2010).

185. Campi, M. & Garatti, S. Wait-and-judge scenario optimization. *Mathematical Programming* **167,** 155–189 (2018).

186. Calafiore, G. & Campi, M. Uncertain convex programs: Randomized solutions and confidence levels. *Mathematical Programming* **102,** 25–46 (2005).

187. Charnes, A. & Cooper, W. Chance-constrained programming. *Management science* **6,** 73–79 (1959).

188. Vajda, S. *Probabilistic Programming* (Academic Press, New York, NY, 1972).

189. Prekopa, A. *Stochastic Programming* (Kluwer Academic Publishers, 1995).

190. Uryasev, S. *Probabilistic Constrained Optimization* (Kluwer Academic Publishers, Dodrecht, Netherlands, 2000).

191. Nemirovski, A. & Shapiro, A. Convex approximations of chance constrained programs. *SIAM Journal on Optimization* **17,** 969–996 (2006).

192. Calafiore, G. & El Ghaoui, L. On distributionally robust chance-constrained linear programs. *Journal of Optimization Theory and Applications* **130,** 1–22 (2006).

193. Chen, W., Sim, M., Sun, J. & Teo, C. From CVaR to uncertainty set: Implications in joint chance-constrained optimization. *Operations Research* **58,** 470–485 (2010).

194. Zymler, S., Kuhn, D. & Rustem, B. Distributionally robust joint chance constraints with second-order moment information. *Mathematical Programming* **137,** 167–198 (2013).

195. Wiesemann, W., Kuhn, D. & Sim, M. Distributionally robust convex optimization. *Operations Research* **62,** 1358–1376 (2014).

196. Hanasusanto, G., Roitch, V., Kuhn, D. & Wiesemann, W. A distributionally robust perspective on uncertainty quantification and chance constrained programming. *Mathematical Programming* **151,** 35–62 (2015).

197. Kircher, K. J. & Zhang, K. M. *Model predictive control of thermal storage for demand response* in *American Control Conference (ACC)* (2015), 956–961.